STUDY OF TRAPPED MODES IN TWO- AND THREE-LAYER FLUIDS

by

Sunanda Saha

DEPARTMENT OF MATHEMATICS

INDIAN INSTITUTE OF TECHNOLOGY GUWAHATI

GUWAHATI-781039, INDIA

October, 2014

STUDY OF TRAPPED MODES IN TWO- AND THREE-LAYER FLUIDS

A Thesis submitted

in partial fulfillment of the requirements

for the degree of

DOCTOR OF PHILOSOPHY

by

Sunanda Saha

(Roll Number: 10612304)

to the

DEPARTMENT OF MATHEMATICS

INDIAN INSTITUTE OF TECHNOLOGY GUWAHATI

October, 2014

CERTIFICATE

It is certified that the work contained in the thesis titled **"Study of trapped modes in two- and three-layer fluids"** by **Sunanda Saha**, a student in the Department of Mathematics, Indian Institute of Technology Guwahati for the award of the degree of Doctor of Philosophy has been carried out under my supervision and this work has not been submitted elsewhere for a degree.

October, 2014

Dr. Swaroop Nandan Bora
Professor
Department of Mathematics
Indian Institute of Technology Guwahati, India

Dedicated

to

My Parents ..

Acknowledgement

There are a number of people without whose cooperation and goodwill this thesis might not have seen the light of the day, and to whom I am greatly indebted.

First of all, I would like to express my deepest gratitude to my supervisor, Prof. Swaroop Nandan Bora, for his excellent guidance, caring attitude, patience, and providing me with an excellent atmosphere for carrying out research. This thesis would not have been possible without the help and support of him, not to mention his advice and unsurpassed knowledge in water wave theory and other allied branches of applied mathematics. The impeccable advice, support and friendship of my supervisor has been invaluable at both academic and personal fronts, for which I am extremely grateful. I must also acknowledge his confidence in me and the amount of freedom I was given in carrying out my research.

I owe my gratefulness to my doctoral committee members, Prof. D. C. Dalal, Prof. Rajen Kumar Sinha and Prof. Natesan Srinivasan, for their valuable suggestions and meaningful comments. I would like to acknowledge the financial and academic support of Indian Institute of Technology Guwahati and its staff, and particularly to the Ministry of Human Resource Development, Govt. of India for providing the necessary financial support for carrying out this research. The library and computer facilities of the institute have been indispensable. I also thank the Department of Mathematics, IIT Guwahati for its support and assistance since the start of my research work in 2010, especially the head of department, Prof. Bhaba Kumar Sarma.

I also take this opportunity to thank my parents for giving me full freedom to work on my choice. I am grateful to them for the sacrifices that they have made while allowing me to continue my Ph.D. Their devotion, not only for my research work but also for my life till date, will be treasured in my memory forever.

Many special thanks are also due to Mrs. Swapnali Bora for her love and affection throughout my stay in IIT Guwahati. I also thank my senior colleague, Santu Das, for his help and fruitful discussion throughout my research work. Last, but by no moment the least, I thank my friends Mohar Dey, Tanvi Joshi, Manasi Kulkarni and my other friends at IIT Guwahati for their support and encouragement throughout.

For any errors or inadequacies that may remain in this work, the responsibility, of course, is entirely my own.

October, 2014 **(Sunanda Saha)**

Abstract

Trapped waves are of considerable interest in providing examples of discrete wave frequencies in the presence of a continuous spectrum. In this thesis, we first investigate the existence of trapped modes in a two-layer fluid of finite depth subject to different conditions: (i) upper surface bounded above by a rigid lid; (ii) upper surface bounded above by a thin ice-cover; (iii) fluid flowing over an elastic bottom at a finite depth. In all these problems, a submerged horizontal circular cylinder is placed in either of the layers. The effect of surface tension at the surface of separation is neglected and each fluid layer is considered to be immiscible. Furthermore, the assumptions of linear and time harmonic motions are followed. To solve the ice-cover problem, the standard idealization of ice as a thin elastic plate, which responds to only flexural changes, is followed. In the elastic bottom problem, the flexural bottom is considered as a thin elastic plate and is based on the Euler-Bernoulli beam equation.

Later on, trapped mode frequencies are computed for a submerged horizontal circular cylinder with the hydrodynamic set-up involving an infinite depth three-layer incompressible fluid with layer-wise different densities. The impermeable horizontal cylinder is fully immersed in either the bottom layer or the uppermost layer. In this problem we restrict the uppermost layer to be covered by a free surface only.

In all these problems mentioned above, trapped mode frequencies are computed below a cut-off value. In one of the later parts of the thesis, we compute trapped modes which are embedded in a continuous spectrum due to the presence of a pair of identical cylinders submerged in either layer of a two-layer fluid which is covered by a thin ice-cover. In this case we assume the lower layer to be of infinite depth. Though numerical computation is carried out for a pair of cylinders only, we additionally provide the theoretical development for the case of a specific arrangement of multiple cylinders.

We have excluded the presence of surface tension at the free surface and interfaces for all the problems considered here. Its exclusion is justified by presenting some numerical results in the last problem of the thesis.

In this study of trapped waves, mixed boundary value problems are set up for the determination of velocity potentials corresponding to each layer where the governing partial differential equation happens to be modified Helmholtz equation in two-dimensions for oblique incidence within the fluid. The governing equation is accompanied by boundary conditions near the upper rigid boundary or the ice-cover surface or the free surface, at the interface between two fluids and at the bottom boundary, if any, depending on the problem considered. The trapped mode condition arises which ensures that wave propagation to infinity does not take place at the interface(s) or at the upper surface.

In order to examine the existence of trapped modes, multipole expansion method, along with the properties of an infinite system of linear equations, is used. A number of observations are made on the trapped modes with regard to different submergence depths and depths of all the layers. For the frequencies below a cut-off value, there exist two modes (except for the rigid lid problem) for which trapped wave exists. For low density ratios, the motion of the

first mode is concentrated about the upper surface while for the second mode the motion is concentrated about the interface. As the density ratio increases, the motion for the first mode is transferred from the upper surface to the interface, and the upper surface elevation becomes very small. The dispersion relation is also analyzed for various water depths and for different submergence depths of the cylinder placed in either of the layers. In a separate instance, we also observe the existence of trapped modes above a cut-off frequency. This occurs for the case of a pair of circular cylinders in a two-layer fluid with an ice-cover. The trapped mode frequencies in this case are embedded in a continuous spectrum.

For the case of the rigid lid problem, it is observed that if we move the cylinder away from the interface towards the upper surface, the trapped mode frequency increases and the trapped mode ceases to exist as the cylinder comes closer to the rigid lid. By varying the submergence depth and fixing all the parameters, it is observed that the trapped mode increases as density ratio decreases. When the rigid lid is replaced by a thin ice-cover, there exists two wavenumbers each of which has two trapped modes. For both the wavenumbers, the second mode gets more affected due to the presence of the ice-cover. With an increase in flexural rigidity of the ice-cover, the second mode for both the wavenumbers ceases to exist. Trapped mode wavenumbers increase due to the consideration of the elasticity of the sea-bed, which is more realistic as compared to a flat and rigid bed.

For the case of a three-layer fluid, we observe the effect of the depth of the middle layer having constant density which basically acts as a crude representation of a smooth pycnocline between the upper and lower layers. In this case there exist two trapped modes. For both the modes, as the depth of the middle layer increases, the wavenumbers interchange their properties at near crossing points. Further, as the density ratio increases to 1.0, one of them tends to zero and other tends to some finite value. For the case when a pair of cylinders is placed entirely in the lower layer of a two-layer fluid bounded above by a thin ice-cover, we present numerical evidence that trapped modes do exist above the cut-off frequency for oblique waves for such a geometry. For the parameter values chosen, the number of trapped modes embedded in the continuous spectrum decreases with an increase in the flexural rigidity of the ice-cover. The trapped mode frequency decreases when either the depth of the upper layer or the submergence depth increases.

For the case when the effect of surface tension is included, we observe that out of the two modes of the dispersion curves, the higher mode gets more affected with the variation of the surface tension parameters. Variation of the trapped mode against density ratio does not get affected by the presence of surface tension either at the free surface or the interface. Therefore, we make the observation that in this type of problems, the inclusion of surface tension in the formulation does not lead to any significant difference. Though in this problem the upper layer is covered by a free surface, similar observation is expected when the free surface be replaced by a rigid lid or an ice-cover and hence it is justifiable to ignore surface tension altogether.

The existence of trapped modes show that, in general, a radiation condition for the waves at infinity is insufficient for the uniqueness of the scattering problem. The solutions are expected

to render a quantitative guidance to various types of water wave problems in two-layer and three-layer fluids. It is to be noted that the existence of trapped modes throughout the present work is based on numerical evidence only, i.e., the values of those frequencies are located numerically for which the truncated determinant vanishes. However, we feel that similar proofs for two-layer and three-layer fluids, as was done for a single-layer fluid in Ursell (1951), may be possible to be derived.

Contents

List of Figures **xvii**

List of Tables **xxiii**

1 Introduction **1**

1.1 Some important equations in water wave theory 3

1.2 Literature survey 7

1.3 Outline of the thesis 13

2 Trapped modes in a two-layer fluid of finite depth bounded above by a rigid lid **15**

2.1 Introduction 15

2.2 Mathematical formulation of the problem 15

2.3 Solutions by multipoles 17

2.3.1 Cylinder submerged in the lower layer 18

2.3.2 Cylinder submerged in the upper layer 22

2.4 Conclusions 26

3 Flexural gravity waves trapped in a two-layer fluid of finite depth **29**

3.1 Introduction 29

3.2 Mathematical formulation of the problem 29

3.3 Solutions by multipoles 32

3.3.1 Cylinder submerged in the upper layer 33

3.3.2 Cylinder submerged in the lower layer 34

3.4 Numerical Results 35

3.4.1 Dispersion curves 35

3.4.2 Cylinder submerged in the upper layer 36

3.4.3 Cylinder submerged in the lower layer 41

3.5 Conclusions 44

4 Elastic bottom effect on trapped waves in a two-layer fluid **46**

4.1 Introduction 46

4.2 Mathematical formulation of the problem 46

4.3 Solutions by multipoles . . . 48
4.3.1 Cylinder submerged in the lower layer . . . 49
4.3.2 Cylinder submerged in the upper layer . . . 52
4.4 Conclusions . . . 54

5 Trapped modes in a three-layer fluid 56
5.1 Introduction . . . 56
5.2 Mathematical formulation of the problem . . . 56
5.3 Solutions by multipoles . . . 59
5.3.1 Cylinder submerged in the lower layer . . . 59
5.3.2 Cylinder submerged in the upper layer . . . 63
5.3.3 Limiting values of the density ratios . . . 67
5.4 Conclusions . . . 69

6 Trapped waves supported by a pair of cylinders in an ice-covered two-layer fluid 71
6.1 Introduction . . . 71
6.2 Mathematical formulation of the problem . . . 71
6.3 Solutions by multipoles . . . 72
6.3.1 Cylinders submerged in the lower layer . . . 73
6.4 Numerical results and discussion for two identical cylinders submerged in either of the layers . . . 76
6.4.1 Cylinders submerged in the lower layer . . . 76
6.4.2 Cylinders submerged in the upper layer . . . 79
6.5 Conclusions . . . 85

7 Effects of surface tension on trapped modes in a two-layer fluid 87
7.1 Introduction . . . 87
7.2 Mathematical formulation of the problem . . . 87
7.3 Solutions by multipoles . . . 90
7.3.1 Cylinder submerged in the upper layer . . . 90
7.3.2 Cylinder submerged in the lower layer . . . 92
7.4 Conclusions . . . 95

8 Summary and future work 96
8.1 Summary . . . 96
8.2 Future work . . . 98

Bibliography 101

APPENDICES 105

A Euler–Bernoulli equation for a thin ice-cover **105**

B Coordinate shift **107**

List of published and communicated papers **111**

List of Figures

2.1 Cross-sectional view for a two-layer fluid covered by a rigid lid in the presence of a cylinder. 16

2.2 Trapped mode frequencies plotted against la for a cylinder of radius a in the lower fluid layer for different depths d/a of the upper layer; $\rho = 0.95$, $h/a = 6$ and $f/a = -1.01$. 20

2.3 Trapped mode frequencies plotted against ρ for a cylinder of radius a in the lower fluid layer for different depths d/a of the upper layer; $la = 2$, $h/a = 6$ and $f/a = -1.01$. 20

2.4 Trapped mode frequencies plotted against la for a cylinder of radius a in the lower fluid layer for different submergence depths f/a; $\rho = 0.95$, $d/a = 3$ and $h/a = 6$. 21

2.5 Trapped mode frequencies plotted against ρ for a cylinder in the lower fluid layer for different submergence depths f/a; $la = 2$, $d/a = 3$ and $h/a = 6$. 22

2.6 Trapped mode frequencies plotted against la for a cylinder in the upper fluid layer for different depths h/a of the lower layer; $\rho = 0.95$, $f/a = 1.01$ and $d/a = 3$. 23

2.7 Trapped mode frequencies plotted against ρ for a cylinder in the upper fluid layer for different depths h/a of the lower layer ; $la = 3$, $f/a = 1.01$ and $d/a = 3$. 24

2.8 Trapped mode frequencies plotted against la for a cylinder in the upper fluid layer for different submergence depths f/a; $\rho = 0.95$, $d/a = 3$ and $h/a = 6$. . . 24

2.9 Trapped mode frequencies plotted against ρ for a cylinder in the upper fluid layer for different submergence depths f/a ; $la = 2$, $d/a = 3$ and $h/a = 6$. . . . 25

3.1 Cross-sectional view for a two-layer fluid covered by an ice-cover in the presence of a cylinder. 30

3.2 Dispersion curves for a cylinder of radius a (a) in the lower layer for different depths d/a of the upper layer; $\rho = 0.95$, $f/a = -1.01$, $h/a = 6$, $D/a^4 = 0.001$ and $\varepsilon/a = 0.001$ (b) in the upper layer for different depths h/a of the lower layer; $\rho = 0.95$, $f/a = 1.01$, $d/a = 3$, $D/a^4 = 0.001$ and $\varepsilon/a = 0.001$. 36

3.3 Dispersion curves for a cylinder of radius a (a) in the lower layer for different submergence depths f/a; $\rho = 0.95$, $d/a = 3$, $h/a = 6$, $D/a^4 = 0.001$ and $\varepsilon/a = 0.001$ (b) in the upper layer for different submergence depths f/a; $\rho = 0.95$, $h/a = 6$, $d/a = 3$, $D/a^4 = 0.001$ and $\varepsilon/a = 0.001$. 37

3.4 Dispersion curves for a cylinder of radius a (a) in the lower layer for different depths h/a of the lower layer; $\rho = 0.95$, $d/a = 3$, $f/a = -1.01$, $D/a^4 = 0.001$ and $\varepsilon/a = 0.001$ (b) in the upper layer for different depths d/a of the upper layer; $\rho = 0.95$, $h/a = 6$, $f/a = 1.01$, $D/a^4 = 0.001$ and $\varepsilon/a = 0.001$. 37

3.5 Trapped mode wavenumbers plotted against ρ for a cylinder of radius a in the upper fluid layer for different submergence depths f/a; $la = 2$, $d/a = 2.1$, $h/a = 6$, $D/a^4 = 0.001$ and $\varepsilon/a = 0.001$. 38

3.6 Trapped mode wavenumbers plotted against ρ for a cylinder of radius a in the upper fluid layer for different submergence depths f/a, close-up of near crossing; $la = 2$, $d/a = 2.1$, $h/a = 6$, $D/a^4 = 0.001$ and $\varepsilon/a = 0.001$. 38

3.7 Trapped mode wavenumbers plotted against ρ for a cylinder of radius a in the upper fluid layer for different depths d/a of the upper layer; $la = 2$, $f/a = 1.01$, $h/a = 6$, $D/a^4 = 0.001$ and $\varepsilon/a = 0.001$. 39

3.8 Trapped mode wavenumbers plotted against ρ for a cylinder of radius a in the upper fluid layer for different depths h/a of the lower layer h/a; $la = 2$, $f/a = 1.01$, $d/a = 3$, $D/a^4 = 0.001$ and $\varepsilon/a = 0.001$. 39

3.9 Trapped mode wavenumbers plotted against ρ for a cylinder of radius a in the upper fluid layer for different depths h/a of the lower layer, close-up; $la = 2$, $f/a = 1.01$, $d/a = 3$, $D/a^4 = 0.001$ and $\varepsilon/a = 0.001$. 40

3.10 Trapped mode wavenumbers plotted against ρ for a cylinder of radius a in the upper fluid layer for different ice-parameters; $la = 2$, $f/a = 1.01$, $d/a = 2.1$ and $h/a = 6$. 40

3.11 Trapped mode wavenumbers in a single-layer fluid; $D/a^4 = 0.001$; $\varepsilon/a = 0.001$ and $h/a = 6$ (a) for different submergence depths f/a; $d/a = 2.1$ (b) for different depths of the layer d/a; $(d - f)/a = 1.01$. 41

3.12 Trapped mode wavenumbers plotted against ρ for a cylinder of radius a in the lower fluid layer for different depths d/a of the upper layer; $la = 2$, $h/a = 6$, $f/a = -1.01$, $D/a^4 = 0.001$ and $\varepsilon/a = 0.001$. 41

3.13 Trapped mode wavenumbers plotted against ρ for a cylinder of radius a in the lower fluid layer for different submergence depths f/a; $la = 2$, $h/a = 6$, $d/a = 3$, $D/a^4 = 0.001$ and $\varepsilon/a = 0.001$. 42

4.1 Schematic diagram for elastic bottom plate in finite water depth two-layer fluid. 47

4.2 Trapped mode wavenumbers versus ρ for a cylinder of radius a in the lower fluid layer for different (a) submergence depths f/a, (b) depths h/a of the lower layer, (c) depths d/a of the upper layer; $la = 2$, $D/a^4 = 0.001$ and $\varepsilon/a = 0.001$. . . . 50

4.3 Trapped mode wavenumbers versus ρ for a cylinder of radius a in the lower fluid layer for different values of D/a^4 and ε/a; $la = 2$, $h/a = 2.1$, $d/a = 1$ and $f/a = -1.01$. 51

4.4 Dispersion curves for a cylinder of radius a placed in the lower layer for different depths h/a of the lower layer; $D/a^4 = 0.001$, $\varepsilon/a = 0.001$, $\rho = 0$, $h/a = 3.0$ and $d/a = 1.0$. 52

4.5 Trapped mode wavenumbers versus ρ for a cylinder of radius a in the upper fluid layer for different submergence depths f/a; $D/a^4 = 0.001$, $\varepsilon/a = 0.001$, $la = 2$, $h/a = 3.0$ and $d/a = 2.1$. 53

4.6 Dispersion curves for a cylinder of radius a placed in the upper layer for different depths h/a of the lower layer; $D/a^4 = 0.001$, $\varepsilon/a = 0.001$, $\rho = 0.5$, $f/a = 1.01$ and $d/a = 3.0$. 53

4.7 Dispersion curves for a cylinder of radius a placed in the upper layer for different submergence depths f/a; $D/a^4 = 0.001$, $\varepsilon/a = 0.001$, $\rho = 0.5$, $h/a = 3.0$ and $d/a = 3.0$. 54

5.1 Cross-sectional view of a three-layer fluid of infinite depth. 57

5.2 Dispersion curves for a cylinder of radius a placed in the lower layer for different depths d/a of the middle layer; $f/a = -1.01$, $h/a = 3$, $\rho = 0.4$, $\rho^* = 0.5$. 61

5.3 Dispersion curves for a cylinder of radius a placed in the lower layer for different depths d/a of the middle layer; $f/a = -1.01$, $h/a = 3$, $\rho = 0$, $\rho^* = 0.5$. 61

5.4 Dispersion curves for a cylinder of radius a placed in the lower layer for different submergence depths f/a; $d/a = 1.5$, $h/a = 3$, $\rho = 0.4$, $\rho^* = 0.5$. 62

5.5 Trapped mode wavenumbers plotted against ρ^* for a cylinder of radius a in the lower fluid layer for different depths d/a of the middle layer; $f/a = -1.01$, $h/a = 3$, $\rho = 0$, $la = 2$. 63

5.6 Trapped mode wavenumbers plotted against ρ^* for a cylinder of radius a in the lower fluid layer for different depths d/a of the middle layer; $f/a = -1.01$, $h/a = 3$, $\rho = 0.4$, $la = 2$. 63

5.7 Trapped mode wavenumbers plotted against ρ^* for a cylinder of radius a in the lower fluid layer for different submergence depths f/a; $d/a = 2.0$, $h/a = 3$, $\rho = 0.4$, $la = 2$. 64

5.8 Dispersion curves for a cylinder of radius a placed in the upper layer; $(f-d)/a = 1.01$, $h/a = 4.0$, $\rho = 0.4$, $\rho^* = 0.5$. 65

5.9 Dispersion curves for a cylinder of radius a placed in the upper layer for different submergence depths f/a; $d/a = 1.0$, $h/a = 4$, $\rho = 0.4$, $\rho^* = 0.5$. 65

5.10 Trapped mode wavenumbers plotted against ρ^* for a cylinder of radius a in the upper fluid layer for different depths d/a of the middle layer; $f/a = 2.09$, $h/a = 3.1$, $\rho = 0.4$, $la = 2$. 66

5.11 Trapped mode wavenumbers plotted against ρ for a cylinder of radius a in the upper fluid layer for different submergence depths f/a; $d/a = 1.0$, $h/a = 3.1$, $\rho^* = 0$, $la = 2$. 66

5.12 Trapped mode wavenumbers plotted against ρ for a cylinder of radius a in the upper fluid layer for different submergence depths f/a; $d/a = 1.0$, $h/a = 3.1$, $\rho^* = 0.5$, $la = 2$. 67

5.13 Trapped mode wavenumbers plotted against ρ for a cylinder of radius a in the upper fluid layer for different depths d/a of the middle layer; $f/a = 2.09$, $h/a = 3.1$, $\rho^* = 0.5$, $la = 2$. 67

6.1 Cross-sectional view of a two-layer fluid covered by an ice-cover in the presence of two cylinders in the lower layer. 73

6.2 (a) Values of Ka at which the real part of the determinant vanishes and (b) the absolute values of the determinant of the complex matrix for two cylinders of equal radius a submerged in the lower layer; $d/a = 2$, $f/a = -1.1$, $\rho = 0.5$, $\alpha_{inc} = 0.34$, $D/a^4 = 0$ and $\varepsilon/a = 0$. 78

6.3 (a) Values of Ka at which the real part of the determinant vanishes and (b) the absolute values of the determinant of the complex matrix for two cylinders of equal radius a submerged in the lower layer; $d/a = 2$, $f/a = -1.1$, $\rho = 0.5$, $\alpha_{inc} = 0.34$, $D/a^4 = 0.001$ and $\varepsilon/a = 0.001$. 78

6.4 (a) Values of Ka at which the real part of the determinant vanishes and (b) the absolute values of the determinant of the complex matrix for two cylinders of equal radius a submerged in the lower layer; $d/a = 2$, $f/a = -1.1$, $\rho = 0.5$, $\alpha_{inc} = 0.34$, $D/a^4 = 0.01$ and $\varepsilon/a = 0.001$. 79

6.5 (a) Values of Ka at which the real part of the determinant vanishes and (b) the absolute values of the determinant of the complex matrix for three different values of upper layer depth d/a for two cylinders of equal radius a submerged in the lower layer; $f/a = -1.1$, $\rho = 0.5$, $\alpha_{inc} = 0.34$, $D/a^4 = 0.001$ and $\varepsilon/a = 0.001$. 80

6.6 Variation of third mode for three different values of upper layer depth d/a for two cylinders of equal radius a submerged in the lower layer; $f/a = -1.1$, $\rho = 0.5$, $\alpha_{inc} = 0.34$, $D/a^4 = 0.001$ and $\varepsilon/a = 0.001$. 81

6.7 (a) Values of Ka at which the real part of the determinant vanishes and (b) the absolute values of the determinant of the complex matrix for three different values of submergence depth f/a for two cylinders of equal radius a submerged in the lower layer; $d/a = 2.0$, $\rho = 0.5$, $\alpha_{inc} = 0.34$, $D/a^4 = 0.001$ and $\varepsilon/a = 0.001$. 82

6.8 Variation of third mode for three different values of submergence depth f/a for two cylinders of equal radius a submerged in the lower layer; $d/a = 2.0$, $\rho = 0.5$, $\alpha_{inc} = 0.34$, $D/a^4 = 0.001$ and $\varepsilon/a = 0.001$. 83

6.9 (a) Values of Ka at which the real part of the determinant vanishes and (b) the absolute values of the determinant of the complex matrix for two cylinders of equal radius a submerged in the upper layer; $d/a = 2.50$, $f/a = 1.25$, $\rho = 0.5$, $\alpha_{inc} = 0.34$, $D/a^4 = 0$ and $\varepsilon/a = 0$. 84

6.10 (a) Values of Ka at which the real part of the determinant vanishes and (b) the absolute values of the determinant of the complex matrix for two cylinders of equal radius a submerged in the upper layer; $d/a = 2.50$, $f/a = 1.25$, $\rho = 0.5$, $\alpha_{inc} = 0.34$, $D/a^4 = 0.0001$ and $\varepsilon/a = 0.0001$. 84

6.11 (a) Values of Ka at which the real part of the determinant vanishes and (b) the absolute values of the determinant of the complex matrix for two cylinders of equal radius a submerged in the upper layer; $d/a = 2.50$, $f/a = 1.25$, $\rho = 0.5$, $\alpha_{inc} = 0.34$, $D/a^4 = 0.001$ and $\varepsilon/a = 0.001$. 85

7.1 Schematic diagram for a two-layer fluid with surface tension at free surface and interface. 88

7.2 Dispersion curves for a cylinder of radius a in the upper layer for different values of M_2/a^2; $\rho = 0.5$, $d/a = 3$, $f/a = 1.01$, $h/a = 6$ and $M_1/a^2 = 0$. 92

7.3 Trapped mode wavenumbers plotted against ρ for a cylinder of radius a in the upper fluid layer for different values of M_1/a^2; $la = 2$, $d/a = 2.1$, $h/a = 6$, $f/a = 1.05$ and $M_2/a^2 = 0$. 92

7.4 Trapped mode wavenumbers plotted against ρ for a cylinder of radius a in the upper fluid layer for different values of M_2/a^2; $la = 2$, $d/a = 2.1$, $h/a = 6$, $f/a = 1.05$ and $M_1/a^2 = 0$. 93

7.5 Dispersion curves for a cylinder of radius a in the lower layer for different values of M_2/a^2; $\rho = 0.5$, $d/a = 3$, $f/a = -1.01$, $h/a = 6$ and $M_1/a^2 = 0$. 94

7.6 Trapped mode wavenumbers plotted against ρ for a cylinder of radius a in the lower fluid layer for different values of M_1/a^2; $la = 2$, $d/a = 3.0$, $h/a = 6.0$, $f/a = -1.01$ and $M_2/a^2 = 0$. 94

7.7 Trapped mode wavenumbers plotted against ρ for a cylinder of radius a in the lower fluid layer for different values of M_2/a^2; $la = 2$, $d/a = 3.0$, $h/a = 6.0$, $f/a = -1.01$ and $M_1/a^2 = 0$. 95

B.1 Coordinate shift for Graf's addition theorem 107

List of Tables

3.1 Values of wavenumber u_2a for different values of N with the cylinder placed in the lower layer; $la = 2$, $f/a = -1.01$, $h/a = 6$, $d/a = 1$, $D/a^4 = 0.001$ and $\varepsilon/a = 0.001$ 35

Nomenclature

ω : radian frequency of the incoming water waves

g : acceleration due to gravity

d : uniform finite depth of the upper layer fluid in two-layer fluid

h : uniform finite depth of the lower layer fluid in two-layer fluid

f : submergence depth of the cylinder

a : radius of the cylinder

$I_n(.)$: modified Bessel function of the first kind of order n

$K_n(.)$: modified Bessel function of the second kind of order n

ρ_0 : uniform mass density of thin elastic plate

h_0 : thickness of thin elastic plate

l : wavenumber along y-direction

$\nabla^2_{x,z}$: $\dfrac{\partial^2}{\partial x^2} + \dfrac{\partial^2}{\partial z^2}$

p_j : hydrodynamic pressure in the corresponding fluid region; $j = I, II$

K : $= \omega^2/g$

σ : $(1+\rho)/(1-\rho)$

k : root of the dispersion relation for rigid lid case

u_j : roots of the dispersion relation; $j = 1, 2$

$\mathfrak{D}$: $= E{h_0}^3/\{12(1-\nu^2)\}$, the flexural rigidity of the elastic plate

E : the effective (i.e., low strain rate) average Young's modulus of the elastic plate

ν : the Poisson's ratio

m : $= \rho_0 h_0$, the mass per unit surface area of the elastic plate

D : $= \mathfrak{D}/(\rho_j g); j = I$ for Chapter 3 and $j = II$ for Chapter 4

ε : $= \rho_0 h_0/\rho_j; j = I$ for Chapter 3 and $j = II$ for Chapter 4

Chapter 1

Introduction

A fluid is a substance that can flow. That is, the particles comprising a fluid continuously change their positions relative to one another. If the fluid is at rest, then no shear forces can exist in it, which is a different property from solids which can resist shear forces while at rest. Fluid mechanics is that branch of applied mechanics which is concerned with the statics and dynamics of liquids and gases. The analysis of the behaviour of fluids is based upon the fundamental laws of applied mechanics that relate to the conservation of mass, energy and momentum. The subject branches out into sub-disciplines such as aerodynamics, hydraulics, geophysical fluid dynamics, bio-fluid mechanics etc. It is known now, beyond any doubt, that a moving fluid in contact with a solid body does not have any velocity relative to the body at the contact surface. This condition of not slipping over a solid surface has to be satisfied by a moving fluid. This is known as the no-slip condition.

The most fundamental idea that we need in fluid mechanics is the continuum hypothesis. In simple terms this says that when dealing with fluids we can ignore the fact that they actually consist of billions of individual molecules (or atoms) in a rather small region, and instead treat the properties of that region as if it were a continuum. By appealing to this assumption, we may treat any fluid property as varying continuously from one point to the next within the fluid; this would clearly not be possible without this hypothesis. The continuum hypothesis enables us to use the simplest concept of local velocity of the fluid and the whole flow field may be specified as an aggregate of such local velocities. Two distinct alternative kinds of specifications are possible. The first, known as the Lagrangian type, involves observing the trajectory of each individual fluid parcel as it moves from some initial location. The alternative is the Eulerian type of specification. This corresponds to a coordinate system fixed in space, and in which fluid properties are studied as functions of time as the flow passes through fixed spatial locations. The Lagrangian type of specification is useful in certain special contexts, but it leads to rather cumbersome analysis and in general is at a disadvantage in not giving directly the spatial gradients of velocity in the fluid and hence an Eulerian specification is being employed in most of the cases.

If all properties of a flow are independent of time, then the flow is called steady; otherwise, it is called unsteady. A uniform flow is the one in which all velocity vectors are identical (in both direction and magnitude) at every point of the flow for any given instant of time. Flows for which this is not true are said to be nonuniform.

At an instant of time, there is a velocity vector with a definite direction at every point. The instantaneous curves that are everywhere tangent to the direction field are called the streamlines of the flow. For unsteady flows, the streamline pattern changes with time. The pathline is the trajectory of a fluid particle of fixed identity over a period of time. Pathlines and streamlines are identical in a steady flow, but not in an unsteady flow. A streakline is another concept in flow visualization experiments. It is defined as the current location of all fluid particles that have passed through a fixed spatial point at a succession of previous times. It is determined by injecting dye or smoke at a fixed point for an interval of time.

Viscosity is that fluid property by virtue of which a fluid offers resistance to shear stresses. Newton's law of viscosity states that for a given rate of angular deformation of a fluid, shear stress is directly proportional to viscosity. A fluid which obeys this law is known as Newtonian fluid. For example, water is a Newtonian fluid. A non-Newtonian fluid is a fluid whose flow properties differ in many ways from those of Newtonian fluids. For example, ketchup, custard, toothpaste, blood, and shampoo are non-Newtonian fluids. In a non-Newtonian fluid, the relation between the shear stress and the shear rate is different and can even be time-dependent. Therefore, a constant coefficient of viscosity cannot be defined.

The Navier-Stokes equations are the set of equations that describe the motion of fluid substances such as liquids and gases. These equations state that changes in momentum (force) of fluid particles depend only on the external pressure and internal viscous forces (similar to friction) acting on the fluid. Thus, the Navier-Stokes equations describe the balance of forces acting at any given region of the fluid.

A fluid is said to be incompressible when the density of an element of fluid is not affected by changes in the pressure. The density of the fluid in a mass element may also change as a consequence of molecular conduction of heat (or, rarely, of a solute) into the element. However, circumstances in which the effect of conduction of heat in the fluid is negligible are common, and a statement that a fluid is effectively incompressible is usually taken to imply, in the absence of any explicit qualification about heat conduction, that the density of each mass element of the fluid remains constant. The Navier-Stokes equations and mass conservation are then sufficient to determine the solution to a fluid mechanics problem. Actually, the absolute pressure in an incompressible fluid is indeterminate and only its gradient is relevant for the equations of motion. Taking the divergence of the Navier-Stokes equation and using the mass conservation equation in simplifying the result gives Poisson equation for the pressure.

A flow field with velocity vector $\mathbf{u}$ is said to be irrotational if *curl* $\mathbf{u} = 0$; otherwise, it is rotational. The condition of irrotationality guarantees the existence of another scalar function Φ, called the velocity potential. If the flow is both irrotational and incompressible, the Laplacian of the velocity potential must be zero – giving us the equation of continuity for a potential flow.

It is perhaps not an overstatement to say that wave motion is the most basic feature of all physical phenomena. Whenever we see or hear anything, we can do so because of the existence of waves. Electromagnetic waves cover a spectrum of waves from low frequency radio waves through visible light to X-ray and gamma ray. Sound propagates as a wave through the air. When someone sings or plays a musical instrument, the standing waves in their vocal chords, guitar strings or drumskins produce a pressure change or sound wave, which is audible.

Waves can propagate both on the surface of solid bodies (for example, as earthquakes) and through the bulk of a solid (for example, in seismic oil prospecting). The surface of a sea is perhaps the most obvious example of a wave bearing medium. Water waves vary in size from the small ripples caused by raindrops through shock waves such as the Severn Bore, to enormous ocean waves that can capsize large ships. Waves in different media can interact, often with devastating effects, for example, when an underwater earthquake causes a tsunami, a huge wall of water sets in a motion that can destroy coastal settlements, or when the waves generated by the wind blowing on a bridge produce a catastrophic resonance. These examples alone are sufficient to motivate researchers to study various aspects of wave propagation. Wave phenomena also occur in many other physical systems.

Real water waves propagate in viscous oceans over an irregular rough bottom of varying permeability. However, a striking feature of the water waves in the oceans is that in most cases the main body of the fluid motion is nearly irrotational such that the viscosity which causes the rotation may be negligible. Another remarkable fact is that water can be reasonably regarded as incompressible and, consequently, a velocity potential and a stream function exist for wave propagation in oceans. The problems associated with water wave propagation are difficult owing to the complex nature of the process. The difficulties arise from the irregularity of the wave motion, wave breaking and energy dissipation due to friction, turbulence etc. Any mathematical model that we attempt will require some simplifications or idealizations. The application of a mathematical description often depends on the number of space dimensions involved with the problem. In the case of a one-dimensional model, it is possible to introduce some nonlinear effects into the method of solution. However, in the case of two- and three-dimensional models, the mathematical formulations are often restricted to those solvable by linear harmonic wave theory.

The study of different kinds of water waves is of immense importance for various applications. For example, it is required for predicting the behaviour of floating structures (immersed totally or partially) such as ships, submarines and tension-leg platforms, and for describing flows over bottom topography. Furthermore, the investigation of wave patterns of ships and other vessels in forward motion is closely related to the calculation of the wave-making resistance and the other hydrodynamic characteristics that are used in marine design. Another area of application is the mathematical modeling of unsteady waves resulting from phenomena such as underwater earthquakes, blasts, etc.

1.1 Some important equations in water wave theory

For the treatment of wave motion as discussed here, a Cartesian coordinate system is adopted with the z-axis directed vertically upwards and $z = 0$ in the plane of the undisturbed free surface. For a purely two-dimensional motion, the dependence on y is omitted and time is denoted by t throughout.

The equations for conservation of mass and momentum for an inviscid and incompressible

fluid are

$$\nabla \cdot \mathbf{u} = 0, \tag{1.1}$$

$$\frac{\partial \mathbf{u}}{\partial t} + \mathbf{u} \cdot \nabla \mathbf{u} = -\frac{1}{\rho}\nabla p + \mathbf{g}, \tag{1.2}$$

where ρ is the fluid density, $\mathbf{g}$ is the acceleration due to gravity and p is the pressure in the fluid relative to atmospheric pressure. We also make the simplifying assumptions that the flow is irrotational and hence the velocity field $\mathbf{u}$ can be written as the gradient of a scalar velocity potential $\Phi(x, y, z, t)$, that is $\mathbf{u} = \nabla\Phi$. Principle of conservation of mass requires that the divergence of the velocity is zero so that Φ satisfies Laplace's equation

$$\nabla^2\Phi = 0 \qquad \text{throughout the fluid.} \tag{1.3}$$

Using the identity

$$\mathbf{u} \times (\nabla \times \mathbf{u}) = \nabla\big(\frac{1}{2}\mathbf{u} \cdot \mathbf{u}\big) - \mathbf{u} \cdot \nabla\mathbf{u}, \tag{1.4}$$

we can write the convective acceleration as

$$\mathbf{u} \cdot \nabla\mathbf{u} = \nabla\big(\frac{1}{2}\nabla\Phi \cdot \nabla\Phi\big), \tag{1.5}$$

with $\nabla \times \mathbf{u} = 0$ since the flow is irrotational. If the gravity acts in the negative z-direction, we can write

$$\mathbf{g} = \nabla(-gz). \tag{1.6}$$

The momentum equation therefore becomes

$$\frac{\partial}{\partial t}(\nabla\Phi) + \nabla\big(\frac{1}{2}\nabla\Phi \cdot \nabla\Phi\big) = -\frac{1}{\rho}\nabla p - \nabla(gz), \tag{1.7}$$

so that, with usual assumptions of smoothness in $\Phi = \Phi(x, y, z, t)$,

$$\nabla\left\{\frac{\partial\Phi}{\partial t} + \frac{1}{2}\nabla\Phi \cdot \nabla\Phi + \frac{p}{\rho} + gz\right\} = 0, \tag{1.8}$$

and hence

$$\frac{\partial\Phi}{\partial t} + \frac{1}{2}\nabla\Phi \cdot \nabla\Phi + \frac{p}{\rho} + gz = C(t), \tag{1.9}$$

for some function $C(t)$. However, we can take $C(t) = 0$ by using the simple transformation

$$\Phi \mapsto \Phi + \int_0^t C(s)ds, \tag{1.10}$$

which does not affect the velocity field. For this type of flow, we obtain **Bernoulli's equation**,

$$\frac{\partial\Phi}{\partial t} + \frac{1}{2}\nabla\Phi \cdot \nabla\Phi + \frac{p}{\rho} + gz = 0. \tag{1.11}$$

Once we determine Φ, the pressure field p can be obtained from Bernoulli's equation.

We now turn our attention to the surface of the fluid. We assume that the flow is two dimensional, so that the surface lies at $z = \eta(x, t)$, where the coordinate x measures distance along the surface. For the moment we will neglect the effect of surface tension so that the

pressure at this free surface is atmospheric, $p = p_{atm}$. We can take $p = 0$ at the free surface using the simple transformation $p \mapsto p - p_{atm}$, which does not change the basic Euler equations which depend upon ∇p. Bernoulli's equation (1.11) at the free surface then gives us the boundary condition

$$\frac{\partial \Phi}{\partial t} + \frac{1}{2}\nabla\Phi \cdot \nabla\Phi + g\eta = 0 \qquad \text{at} \qquad z = \eta(x,t). \tag{1.12}$$

This is also known as the **dynamic boundary condition at the free surface**. To obtain the other boundary condition that we need here, we note that the fluid particles cannot cross the air-water interface and is obtained by equating the vertical speed of the free surface itself to that of a fluid particle at the free surface, which gives

$$\frac{\partial \Phi}{\partial z} = \frac{\partial \eta}{\partial t} + \frac{\partial \Phi}{\partial x}\frac{\partial \eta}{\partial x} \qquad \text{at} \qquad z = \eta(x,t). \tag{1.13}$$

This is known as **kinematic boundary condition at the free surface**. When there is an impermeable sea-bed so that the local fluid depth is $h(x)$, then there will be no flow normal to the bed and hence

$$\frac{\partial \Phi}{\partial \mathbf{n}} = 0 \qquad \text{on} \qquad z = -h(x), \tag{1.14}$$

where $\mathbf{n}$ is an outward unit normal to the bed. For sufficiently small motions relative to the wavelength, the above nonlinear free surface conditions (1.12) and (1.13) may be linearized about the undisturbed state. The linearized theory requires the amplitude of the fluid motion to be small compared to the wavelength throughout the fluid domain including the vicinity of any structure, and hence the amplitude of any structural motion must also be small relative to other length scales. It is consistent with the linearization to apply the free surface boundary conditions on $z = 0$, in which case the kinematic condition (1.13) becomes

$$\frac{\partial \Phi}{\partial z} = \frac{\partial \eta}{\partial t} \qquad \text{on} \qquad z = 0 \tag{1.15}$$

and the dynamic condition (1.12) becomes

$$\frac{\partial \Phi}{\partial t} + g\eta = 0 \qquad \text{on} \qquad z = 0. \tag{1.16}$$

These two conditions may be combined by differentiation of (1.16) with respect to t and substitution for $\partial\eta/\partial t$ from (1.15) to get the linearized free surface condition

$$\frac{\partial^2 \Phi}{\partial t^2} + g\frac{\partial \Phi}{\partial z} = 0 \qquad \text{on} \qquad z = 0. \tag{1.17}$$

All the results, here and in the subsequent chapters, are based on the linearized theory and relate to time-harmonic motion with a specified frequency. For time-harmonic motions of radian frequency ω, time may be removed from the problem by writing

$$\Phi(x,z,t) = Re[\phi(x,z)e^{-i\omega t}], \tag{1.18}$$

where ϕ is a complex-valued potential and Re denotes the real part. From Eq. (1.3) it follows that ϕ satisfies Laplace's equation

$$\nabla^2\phi = 0 \tag{1.19}$$

throughout the fluid domain. In terms of ϕ, the linearized free surface condition (1.17) becomes

$$\frac{\partial \phi}{\partial z} - K\phi = 0 \qquad \text{on} \qquad z = 0, \tag{1.20}$$

and the bed condition (1.14) becomes

$$\frac{\partial \phi}{\partial \mathbf{n}} = 0 \qquad \text{on} \qquad z = -h(x). \tag{1.21}$$

For deep water, characterized by the limit $h(x) \to \infty$ for all x, the condition (1.21) is replaced by

$$|\nabla \phi| \to 0 \qquad \text{as} \qquad z \to -\infty. \tag{1.22}$$

On the equilibrium surface of the structure which is denoted by S_B, the normal component must be equal to the velocity component in the same direction of an adjacent fluid particle. For a stationary structure, this condition in terms of the velocity potential Φ is expressed as

$$\frac{\partial \Phi}{\partial \mathbf{n}} = 0 \qquad \text{on} \qquad S_B. \tag{1.23}$$

In linearized theory this condition is applied on the equilibrium surface of the structure. A wave train incident upon a fixed structure will be diffracted to produce a diffracted wave field. By linear superposition, the velocity potential may be decomposed into two parts as

$$\Phi = \Phi_{diff} + \Phi_{inc}, \tag{1.24}$$

where Φ_{inc} represents the incident wave train and Φ_{diff} the diffracted waves. Because the structure is held fixed, the appropriate boundary condition is

$$\frac{\partial \Phi_{diff}}{\partial \mathbf{n}} = -\frac{\partial \Phi_{inc}}{\partial \mathbf{n}} \qquad \text{on} \qquad S_B. \tag{1.25}$$

To obtain a unique solution, the diffracted potential Φ_{diff} must satisfy a radiation condition specifying that the waves corresponding to this potential propagate away from the structure. The radiation condition can be written as

$$\lim_{kx \to \pm\infty} \left(\frac{\partial \Phi_{diff}}{\partial x} \mp ik\Phi_{diff} \right) = 0 \qquad \text{in two dimensions,} \tag{1.26}$$

and

$$\lim_{kr \to \infty} r^{1/2} \left(\frac{\partial \Phi_{diff}}{\partial r} - ik\Phi_{diff} \right) = 0 \qquad \text{in three dimensions,} \tag{1.27}$$

where k is the wavenumber and r represents a polar coordinate. In three dimensions, a radially spreading cylindrical wave of decreasing amplitude is obtained and energy conservation arguments require the factor $r^{1/2}$ in (1.27).

Conventionally, this problem is solved by first taking a Fourier transform in time, and then decomposing the resulting frequency domain problem into the so-called scattering and radiation problems. In the *scattering problem*, the structure is held fixed in incident waves of a prescribed frequency. When a train of surface (or internal) waves travelling from a large distance is incident on an obstacle submerged or partially immersed in water, some parts of the wave is reflected back by the obstacle and some part is transmitted over or below it. The

wave which is reflected back is known as *reflected wave* and the wave which is transmitted is known as *transmitted wave*. The reflected waves and the transmitted waves are called outgoing waves as they go away from the obstacle after striking. In scattering theory, the reflected wave is accompanied by a constant, known as the *reflection coefficient* and the transmitted wave is accompanied by another constant, known as the *transmission coefficient*. In the *radiation problem*, the incident waves are removed and the structure is forced to oscillate at a prescribed frequency. The scattering and radiation problems are closely related and differ only by the "forcing" boundary condition imposed at the surface of the structure. These two problems are linked through the equations of motion for the freely-floating structure.

The uniqueness of solutions in the frequency domain to the scattering and radiation problems has been a subject of research since at least the early 1950's. Many (probably most) researchers working in this area believed that it was only a matter of time before a general uniqueness proof would be obtained that was valid for any structural geometry and for all frequencies. For a specified geometry, uniqueness of the solution to a forcing problem at a particular frequency is equivalent to the non-existence of a trapped mode at that frequency.

A trapped mode is a solution of the corresponding homogeneous boundary value problem and represents a free oscillation with finite energy of the fluid surrounding the fixed structure. These modes persist in some localized region including the free surface whilst decaying rapidly to zero as the free surface extends to infinity. Their existence means that large amplitude motions of the fluid and structures are possible when the system is forced at a frequency close to that of the trapped mode. For a given structure, trapped modes may exist only at discrete frequencies. Mathematically, a trapped mode corresponds to an eigenvalue embedded in a continuous spectrum of the relevant operator.

1.2 Literature survey

For a homogenous (single-layer) fluid, the topic of uniqueness and the existence of trapped modes has been receiving a plenty of attention over several decades. Earlier proofs of uniqueness were presented by John (1950) for a single non-bulbous body of different types that intersects the free surface, and by Ursell (1950) for a submerged horizontal cylinder, lying in an infinitely deep fluid, immersed to any depth for all frequencies. Simon and Ursell (1984) provided a uniqueness proof for any two-dimensional system of submerged obstacles, contained between two lines intersecting at a point on the free surface, inclined at an angle $\pi/4$ to the horizontal direction.

The existence of trapped modes was first established by Ursell (1951) who showed that such a mode could exist in the vicinity of a submerged horizontal circular cylinder with its axis normal to the sides of a deep tank extending to infinity in both directions provided that the cylinder was sufficiently small. McIver and Evans (1985) showed numerically that this restriction on the size of the cylinder was not necessary. In this work, they further went on to prove that at least one mode above a cylinder of arbitrary size did exist and that further modes were possible as the top of the cylinder approached the free surface. This was consistent with the general theory of Jones (1953) who had earlier proved the existence of trapped modes in a tank of finite or infinite depth containing a submerged horizontal cylinder of arbitrary but

symmetric cross-section. Later on Ursell (1987) provided a simplified proof by using minimum-energy arguments.

The existence of trapped modes in the presence of a single rigid vertical circular cylinder placed on the centreline and extended throughout the depth of a long narrow wave channel was first demonstrated by Callan et al. (1991) for sufficiently small cylinders. The trapped modes took the form of a persistent local oscillation near the cylinder at a unique frequency below the first cut-off frequency for the channel, and were antisymmetric with respect to the centreplane of the channel and symmetric with respect to a plane through the axis of the cylinder perpendicular to the sides of the channel. Computation of trapped modes by Evans and Linton (1991) in the case of a cylinder of rectangular cross-section indicated that additional trapped modes arose only if the dimension of the rectangle in the direction of the sides of the channel exceeded the width of the channel. Linton and Evans (1992a) presented a numerical method by using an appropriate Green's function for determining trapped modes for more general cylinders in terms of homogeneous solutions of a Fredholm integral equation. In particular the results presented by them found good agreement with those by Callan et al. (1991) for the circular cylinder case. Using a standard variational approach, Evans et al. (1994) proved the existence of trapped modes in channels of constant depth containing a vertical, surface-piercing cylinder of uniform cross-section which extended throughout the depth and was symmetrically placed with respect to the centreline of the channel. Evans and Porter (1997) considered the case of a circular cylinder on the centreplane and generalized the results of Callan et al. (1991) to the case of any number of circular cylinders of arbitrary size, all positioned on the centreplane. The work of Evans et al. (1994) was extended by Davies and Parnovski (1998) to include, for example, a pair of identical cylinders being reflections of each other in the centreplane. They provided both existence and non-existence results for trapped modes depending on the shape, size and position of the obstacle(s) in the channel or acoustic waveguide. Porter (2002) provided strong numerical evidence in support of the existence of two-dimensional trapped waves supported by a symmetrically arranged pair of horizontal submerged cylinders for a particular form of cross-section.

The importance of trapped modes in the offshore industry was brought into prominence by Maniar and Newman (1997) who came upon with extremely large wave diffraction forces and corresponding large amplitudes of free surface elevations between the adjacent elements of an array consisting of a large number of identical bottom-mounted circular cylinders. These effects occurred at frequencies extremely close to the trapped mode frequencies predicted by the theory of Callan et al. (1991) and tabulated in Linton and Evans (1992a). According to Maniar and Newman (1997), such periodic arrays have applications to structures such as floating bridges or proposed designs for floating airports. In practice, however, it is clear that at least a double array of supporting cylinders is required so that it is important to predict the corresponding trapped mode frequencies for more than a single cylinder on the centreplane.

For a long time it was anticipated that trapped modes would not exist if the discrete spectrum was empty as like in the two-dimensional case. This idea was based on the uniqueness condition (non-existence of non-trivial solutions) proved by John (1950) who stated that the solution was unique if any vertical line drawn downward from the free surface did not intersect the surface-piercing or any other submerged body. However, McIver (1996) disproved this

conjecture by showing the existence of trapped modes for a pair of surface-piercing bodies. She found trapped mode solutions for the two-dimensional water wave problem in which any finite periodicity in a horizontal direction no longer existed. The fluid motion was essentially confined to the neighbourhood of a tandem structure giving a free oscillation of finite energy within a fluid of infinite extent. The solution was constructed from two equal-strength wave sources placed on the free surface and positioned in such a way that the waves radiating to infinity from each source were canceled by those from the other source, thus giving a local oscillation of the fluid. She showed that there did exist families of streamline pairs surrounding the sources that could be interpreted as two surface-piercing structures. A three-dimensional analogue of the solution obtained by McIver (1996) followed soon with McIver and McIver (1997) showing that a family of surface-piercing tori supported localized oscillations. The first example of a trapped mode involving only submerged bodies was presented by McIver (2000). These investigations proclaim the existence of a new type of trapped modes which are embedded in a continuous spectrum. Harter et al. (2007, 2008) incorporated the effect of surface tension on trapped modes. They showed that its exclusion from the problem was not always justifiable, as its inclusion in a particular submerged body example changed the topological nature of the streamline pattern.

McIver et al. (2003) showed how sloshing trapped modes may be excited in the time domain by the forced motion of a trapping structure, i.e., when the velocity of the structure was specified. When the structure was forced to oscillate at the trapped mode frequency, the energy in the trapped mode could not escape to infinity and resonant growth of the fluid motion was observed. When the structure was forced to oscillate at a frequency that differed from the trapped mode frequency, the initial motion of the structure excited a trapped mode so that the long time behaviour was a combination of oscillations at the forcing frequency and the trapped mode frequency. Subsequently, McIver (2005) proved that sloshing trapped modes could not be excited by any free motion of a sloshing trapping structure. Thus, if such a trapping structure was displaced and released from rest, or was subject to incident waves, the trapped mode was not observed. He pointed out that the study of the individual scattering and radiation problems did not provide direct information about the uniqueness of a solution to the problem for a freely-floating structure. In general, there is a unique solution for the problem of a freely-floating structure even at frequencies corresponding to the existence of sloshing trapped modes supported by the fixed structure. Conversely, it was shown by McIver and McIver (2006) and McIver and McIver (2007) that the freely-floating structure could support trapped modes at frequencies for which the scattering and radiation problems had a unique solution. This latter type of trapped mode is a coupled motion of the fluid and structure that possesses finite energy known as “motion modes”.

In recent years, the increase of human activities in the polar regions has amplified the necessity of investigations in the domain of ice cover dynamics. In order to understand the mechanism and the effects of wave propagation through the marginal ice zone in the polar regions, the ice-cover is modeled as a thin ice-sheet of which a very small part is immersed in water and is composed of materials having elastic properties. Unlike the case of plane gravity waves, the upper surface boundary condition associated with the boundary value problem is of fifth order in the presence of a thin ice-cover. The governing equation of the BVP is Laplace’s

equation which is not of the standard Sturm-Liouville type. Fox and Squire (1994) developed a precise linearized model for the reflection and transmission processes due to oblique waves at the margin of a sheet of shore-fast sea ice. Chung and Fox (2002) considered the interaction between the propagating waves and a semi-infinite ice sheet. They laid emphasis on the calculation of the reflection of incident waves. Evans and Porter (2003) analyzed the problem of scattering of obliquely incident waves by a narrow crack in an ice-sheet floating in water of finite depth. They also used Green's function approach to solve the same problem. Another important reason for investigation of water wave problems in which water is covered by a thin ice-sheet is due to their application in the construction of very large floating structures, like floating oil storage bases, floating runways etc.

Undertaking of projects such as construction of underwater tubular bridges across several fjords and straits as a viable mean of improving/increasing modes of transportation (Friis et al. (1991)) requires the investigation of various hydrodynamic phenomena that may arise. One such phenomenon is the occurrence of trapped waves: such waves have modes which are the finite-energy solution of the unforced problem. Since straits and fjords rarely contain a fluid of constant density, it seems that a more appropriate model for the study of existence of properties of trapped waves should perhaps include more than one fluid layer because the number and frequencies of such waves, if they exist in multi-layer cases, may depend on the number of such fluid layers and their densities. Since a two-layer fluid is the simplest representation of a multi-layer fluid, scattering and radiation problems in a two-layer fluid have been attempted to a reasonable extent but not much work has been accomplished with regard to the existence of trapped waves in such cases. Some notable works **on** scattering and radiation problems in a two-layer fluid worth mentioning are: (i) Cadby and Linton (2000) solved the three-dimensional wave/structure interaction problem involving a submerged sphere in a two-layer fluid with one of the layers being of infinite depth; (ii) Linton and Cadby (2002) solved the scattering of oblique waves by a horizontal circular cylinder in an infinitely deep two-layer fluid, and calculated the amount of energy that was converted from one wavenumber to the other for the case of the cylinder placed in either of the upper or lower fluid layers by employing a multipole expansion method; (iii) Mohapatra and Bora (2009a) solved a three-dimensional problem involving the interaction of waves with a sphere in a fluid consisting of two layers with the upper layer bounded above by a rigid lid, which was taken to be the approximation of the free surface, and the lower layer bounded below by a horizontal surface.

In the case of gravity wave propagation in a two-layer fluid having a thin ice-cover and an interface, two progressive waves exist which are generated at the upper surface and the interface. For example, (i) Bhattacharjee and Sahoo (2008) obtained Fourier type expansion formulas and the related orthogonal mode-coupling relations for flexural gravity wave problems in a two-layer fluid; (ii) Mohapatra and Bora (2009b), by using linear water wave theory, investigated the scattering of oblique incident waves by small bottom undulations in a two-layer fluid where the upper surface was a thin ice-cover. Modified Helmholtz equation was solved, and the reflection and transmission coefficients were evaluated; (iii) Mohapatra and Bora (2012) solved the scattering problem for a submerged sphere placed in one of the layers of the two-layer fluid and computed the exciting forces for both horizontal and vertical directions; (iv) Mondal and Sahoo (2012) analyzed the effect of compressive force on flexural gravity waves

in two-layer fluids. Wave characteristics for surface and interfacial modes in the cases of deep and shallow water were studied and generalized expansion formulas, along with associated orthogonal mode-coupling relations, were derived for the velocity potentials to deal with wave-structure interaction problems in three dimensions for both cases of finite and infinite water depths in channels of finite and semi-infinite widths.

The first result about trapped modes in a two-layer fluid was obtained by Kuznetsov (1993) when he examined and proved the existence of trapped modes above a submerged cylinder in the lower layer of infinite depth. Using the density difference as a small parameter in a formal perturbation analysis and reducing the equations to a problem in the lower layer, he studied the existence of trapped modes at the free surface as well as at the interface between the two liquid layers. Later, Linton and Cadby (2003) computed the trapped mode frequencies for a horizontal circular cylinder submerged either in the upper layer or in the lower layer. They also considered the case of a pair of submerged identical circular cylinders in the lower layer and predicted the existence of trapped modes embedded in the continuous spectrum. By using Maz'ya's identity, Kuznetsov et al. (2003) also provided examples of bodies which supported trapped modes in a two-layer fluid. Nazarov and Videman (2009) derived the general sufficient condition for wave trapping in a two-layer fluid in which it was shown in particular that a trapped mode always exists when the submerged body intersects neither the free surface nor the interface. Nazarov et al. (2012) investigated the trapping of oblique water waves by horizontal cylinders in a two-layer fluid. They studied two cases dependent on a small parameter: first, the liquid densities were considered close to each other, and secondly, the density of the upper layer was much less in comparison to that of the lower layer. They also presented the sufficient conditions for wave trapping for appropriate limit problems.

The sharp interface between the layers in all of the above two-layer models is basically a crude representation of the smooth pycnocline that exists between fresh and salt water. However, a better and effective model would perhaps involve replacing the sharp interface in the two-layer model by a layer of finite width in which the density either varies linearly between the upper and lower values, or remains constant representing some sort of mean density of the middle layer. Even though the former case is possibly a better and more realistic model, the latter case is simpler and it serves to improve upon the two-layer model. Sturova (1999) considered the first case and solved the diffraction and radiation problem when a circular cylinder was located beneath the middle layer in which the density was constant. Chakrabarti et al. (2005) considered the latter case and showed the existence of trapped mode supported by a submerged cylinder placed in the bottom layer of infinite depth by using perturbation method. They showed that this problem reduced to the ones involving a homogenous fluid of infinite depth and the two-layer fluid (Kuznetsov (1993)) in the limiting cases.

In all these problems described above, the sea-bed is assumed to be either of infinite depth or of finite depth with a flat and rigid bottom. But the flexibility of the bed is also a very important aspect of study which has not been accounted for in these previous investigations. Mallard and Dalrymple (1977) studied wave propagation over a deformable bottom and found that the wave characteristic was significantly affected in the presence of an elastic bed. Bauer (1981) obtained the coupled frequencies of the structure-liquid system by considering the bottom as a flexible membrane or as a thin elastic plate in a rectangular tank. Later, Bauer (1993) estimated the

natural frequencies of an elastic rectangular container partially filled with liquid. Chiba et al. (2002) analyzed the hydroelastic vibration of a frictionless liquid in a cylindrical tank having a free surface and a flexible membrane bottom. Mohapatra and Sahoo (2011) studied surface gravity wave propagation over an elastic bed based on small amplitude wave theory. They analyzed the wave characteristics for both cases of deep and shallow water waves.

All these works motivate us to investigate trapped modes in two- and three-layer fluids. We begin with a three-dimensional problem where trapped waves exist due to the presence of a horizontal circular cylinder placed in either layer of a two-layer fluid with the upper layer and the lower layer bounded above and below, respectively, by rigid horizontal walls, which are taken to be the approximations of the free surface and the bottom surface. This problem is the extension of the works of Kuznetsov (1993) and Linton and Cadby (2003). In both the above works, lower layer of infinite depth was considered but in our problem it is considered to be of finite depth and we also examine its effect on trapped modes. Multipole expansion method is used to evaluate the frequencies for which trapped mode exists. We then extend the previous physical problem by replacing the rigid lid at the upper surface by a thin ice-cover. The effect of variation of ice-parameters on the trapped mode is observed. Trapped mode for a single-layer fluid bounded by a thin ice-cover is also recovered by considering the density ratio tend to zero. The understanding of the free vibration characteristics of the fluid-structure interaction plays a significant role in various branches of engineering, for example, the propellant in space vehicles can be free from resonance, large-capacity oil containers in the petrochemical industry can survive earthquakes, very large floating oil storage tanks, ships and submarines can avoid or be subjected to reduced localized vibrations. Realizing the importance of vibration as stated above, we replace the horizontal bottom boundary by a thin elastic plate and consider the upper layer as the free surface and observe the variation of trapped mode. Along with other investigations, in this problem we look into the effect of the variation of elastic plate parameters on the trapped modes when a horizontal circular submerged cylinder is placed in either layer. Again, we know that the consideration of a two-layer fluid is the simplest representation of a sharp pycnocline between two layers. However, a better model will be the one with the consideration of a middle layer of constant density additionally. Consideration of this fact and the same hydrodynamic set up as considered by Chakrabarti et al. (2005), we investigate the existence of trapped mode by using multipole expansion method. We also extend their work to the case of the cylinder placed in the uppermost layer of the three-layer fluid. Trapped mode frequencies discussed in all the works mentioned above are considered below a cut-off value. However, some works show that trapped mode also occurs at discrete frequencies which are embedded in a continuous spectrum. The work of Evans and Porter (1997) shows us the direction to consider the case of horizontal multiple cylinders placed in either layer of a two-layer fluid with an ice-cover at the upper surface. For this set-up we discuss the trapped modes which are embedded in the continuous spectrum and for which propagating waves exist at the interface but not near the ice-cover. We present the theoretical platform for the case of multiple cylinders and numerical results for the case of a pair of cylinders. We observe how the distance between the two cylinders affects the trapped modes. For most of the works in water wave problems, the effect of surface tension is neglected. In the last problem in the thesis, we include the surface tension at the free surface and the interface of a two-layer fluid of finite

depth and observe its effect on trapped modes.

1.3 Outline of the thesis

In this thesis we investigate the existence of trapped modes supported by submerged horizontal circular cylinder(s) placed in a two-layer or a three-layer fluid (immiscible always) with different upper surface and bottom boundary conditions. As a first step towards the formulation of our problems, the incident potential of the progressive oblique waves is obtained in subsequent chapters by applying the governing equation and related boundary conditions. Afterwards, we introduce an obstacle into the wave to examine the trapped waves by the obstacle. Because of the presence of the obstacle, in addition to the incident potential, a diffracted potential also enters into the picture. The existence of trapped modes show that, in general, a radiation condition for the waves at infinity is insufficient for the uniqueness of the scattering problem. The mathematical tools utilized in this thesis are (a) Multipole expansion method, (b) Contour integration and applications of Residue theorem, (c) Zeros and poles of complex-valued functions and application of Rouche's theorem.

We feel it pertinent to throw some light on multipole expansion method. The multipole expansion method expresses the potential far from the localized source as a power series of multipoles. The multipoles are constructed to satisfy the field equation, the free surface and the interface, the bottom boundary and the trapped mode conditions. The potentials are made to satisfy the appropriate body boundary condition. This leads to an infinite system of homogenous linear algebraic equations for the unknown coefficients in the multipole sum which can be solved numerically by truncation. The system of equations that result from using a multipole expansion method possesses excellent convergence characteristics and only a few equations are needed to obtain accurate numerical values. The application of this method is restricted to a certain class of obstacles only because in order to apply body boundary condition in certain coordinate system, the multipoles are also needed to be expanded in that system.

In Chapter 2, we consider the trapped mode problem in a two-layer fluid of finite depth and bounded above by a rigid lid. The effect of surface tension at the surface of separation is neglected. Under such a situation time-harmonic waves propagate with one wavenumber only, unlike the case where the upper layer has a free surface and the waves propagate with two wavenumbers. Using multipole expansion method, we obtain an infinite system of homogeneous linear equations. For a fixed geometrical configuration, we numerically compute the values of those frequencies for which the values of the truncated determinant become approximately zero, which confirms the existence of trapped modes. We plot the dispersion curves and observe those trapped mode frequencies which exist below a cut-off value. Trapped mode frequencies are plotted against various values of the density ratios for different geometrical configurations.

Chapter 3 deals with the trapped mode problem in a two-layer fluid where the upper layer has a thin ice-cover, which obeys elastic properties, while the lower layer is bounded by a rigid horizontal bottom surface. The effect of different values of ice-cover parameters on trapped mode is investigated along with the other investigations carried out in Chapter 2.

In Chapter 4, a hydrodynamic model is developed to examine the trapped modes supported by a submerged horizontal circular cylinder placed in either layer of a two-layer fluid flowing

over an elastic bottom at a finite depth. Along with other investigations, we also look into the effect of the variations of elastic plate parameters on the existence of trapped modes. Significant difference is observed with respect to the existence and also in the pattern of the trapped modes between the present case and the one when the cylinder is placed in an infinite depth lower layer in a two-layer fluid.

In Chapter 5 the problem of existence of trapped waves in a three-layer fluid due to the presence of a cylinder is investigated for the hydrodynamic model containing three layers of incompressible fluid of different constant densities. An impermeable cylinder is considered to be fully immersed in either the uppermost layer or the lowermost layer of infinite depth. The top layer consists of fresh water, the middle layer of salt and the lower layer of mud. Here we observe the effect of the width of the middle layer on the trapped modes. This model can also be compared with the presence of a smooth pycnocline of constant density between two layers. However, a more realistic situation is probably the linear variation of the density of the pycnocline with respect its depth.

In Chapter 6 we study the trapped waves supported by a pair of cylinders placed in either layer of a two-layer fluid. The upper layer is covered by a thin ice-cover and the lower layer is of infinite depth. By using multipole expansion method and the method of contour integration, we numerically locate the distance between these cylinders for which trapped wave exists. We also observe the variation of this separation parameter by varying geometrical configuration such as submergence depth, depth of the layers etc.

Except for some notable works (Harter et al. (2007, 2008)), all other works on radiation or scattering or trapped mode, researchers have usually excluded the effect of surface tension at the free surface and the interface. We have also carried out all our problems by excluding the effect of surface tension at the free surface or the interfaces. But to examine whether its inclusion changes the value or pattern of trapped modes, in Chapter 7 we consider a the set-up of a two-layer fluid of finite depth bounded above by a free surface along with the presence of surface tension at the free surface and the interface. Then we observe numerically the variation of surface tension parameters on trapped modes.

Finally, Chapter 8 consists of a brief summary of results highlighting the contribution made by this thesis and the scope of future investigations.

Chapter 2

Trapped modes in a two-layer fluid of finite depth bounded above by a rigid lid

2.1 Introduction

The objective of the present work is to investigate whether a submerged horizontal circular cylinder in a two-layer fluid of finite depth bounded above by a rigid lid and below by an impermeable horizontal bottom supports trapped mode. In order to examine the existence of trapped modes, the multipole expansion method of Thorne (1953), along with the properties of infinite system of homogenous linear equations, is used. For a fixed geometrical configuration, we numerically estimate the values of those frequencies for which trapped modes exist. We examine the effects of density, depth of each layer, distance of the cylinder from the interface etc. on the existence of trapped modes.

2.2 Mathematical formulation of the problem

As the first step towards the formulation of our problem, the incident potential of the progressive wave is to be obtained by applying the governing equation and the related boundary conditions. Cartesian coordinates are chosen such that the xy-plane coincides with the undisturbed interface between the two fluids. Each fluid is assumed to be of infinite horizontal extent in the x- and y-directions while the depth is along the z-direction which is considered positive vertically upwards as shown in Fig. 2.1. We consider the irrotational motion of a two-layer inviscid, incompressible and immiscible fluid of small amplitude under the action of gravity, flowing between two rigid infinite horizontal walls, which are approximations of the free surface and the bottom surface, placed at $z = d$ and $z = -h$, respectively. The origin O is considered at the interface and hence $z = 0$ is the mean position of the interface of the layers. The effect due to surface tension at the interface between the two fluids is neglected. We further assume that all the motions are time harmonic along the body in the y-direction. Under these assumptions of linear water wave theory, velocity potentials in the upper and lower layers can, respectively, be defined for oblique waves in the form (Evans and McIver (1984))

$$\Phi^{I}(x,y,z,t) = \mathrm{Re}[\phi^{I}(x,z)e^{ily}e^{-i\omega t}],$$
$$\Phi^{II}(x,y,z,t) = \mathrm{Re}[\phi^{II}(x,z)e^{ily}e^{-i\omega t}],$$

where $\phi^{I}(x,z)$ and $\phi^{II}(x,z)$, respectively, are complex-valued potential functions for the upper layer fluid $(-\infty < x < \infty;\ -\infty < y < \infty;\ 0 < z < d)$ of density ρ_{I} and the lower layer fluid $(-\infty < x < \infty;\ -\infty < y < \infty;\ -h < z < 0)$ of density $\rho_{II} > \rho_{I}$ and Re denotes the real part. Both the radian frequency ω and the wavenumber l are taken to be real and positive so that the solution stays bounded for all y and t. This assumption for ω and l will hold for all the subsequent problems throughout the thesis.

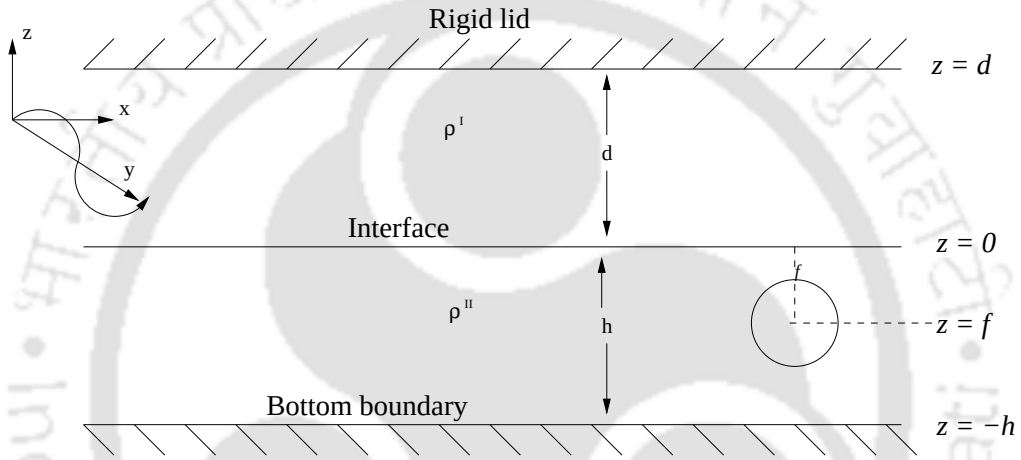

Figure 2.1: Cross-sectional view for a two-layer fluid covered by a rigid lid in the presence of a cylinder.

The governing equation for the boundary value problems involving these potentials $\phi^{I}(x,z)$ and $\phi^{II}(x,z)$ is the modified Helmholtz equation

$$\left(\nabla^2_{x,z} - l^2\right)\phi^{I} = 0 \qquad \text{in} \qquad -\infty < x < \infty,\ 0 < z < d, \tag{2.1}$$
$$\left(\nabla^2_{x,z} - l^2\right)\phi^{II} = 0 \qquad \text{in} \qquad -\infty < x < \infty,\ -h < z < 0. \tag{2.2}$$

Denoting the small displacement at the interface by $\zeta(x,y,t)$, the linearized kinematic condition at the mean interface is given by (Kassem (1982))

$$\frac{\partial \zeta}{\partial t} = \frac{\partial \Phi^{I}}{\partial z} = \frac{\partial \Phi^{II}}{\partial z} \qquad \text{on} \qquad z = 0. \tag{2.3}$$

According to linearized theory of water waves, the hydrodynamic pressure $p_j;\ j = I, II$, in the corresponding fluid region is given by (Kassem (1982))

$$p_j = -\rho_j g\left(z + \frac{1}{g}\frac{\partial \Phi^{j}}{\partial t}\right). \tag{2.4}$$

Denoting the ratio $\rho_I/\rho_{II}(< 1)$ of the densities of the two fluids by ρ and using Eqs. (2.3) and (2.4), the interface matching conditions due to the continuity of velocity and pressure are,

respectively, given by

$$\frac{\partial \phi^{I}}{\partial z} = \frac{\partial \phi^{II}}{\partial z} \qquad \text{on} \qquad z = 0, \tag{2.5}$$

$$\rho\Big(\frac{\partial \phi^{I}}{\partial z} - K\phi^{I}\Big) = \frac{\partial \phi^{II}}{\partial z} - K\phi^{II} \qquad \text{on} \qquad z = 0. \tag{2.6}$$

The linearized impermeable boundary conditions at the upper surface and lower surface are, respectively, given by

$$\frac{\partial \phi^{I}}{\partial z} = 0 \qquad \text{on} \qquad z = d, \tag{2.7}$$

$$\frac{\partial \phi^{II}}{\partial z} = 0 \qquad \text{on} \qquad z = -h. \tag{2.8}$$

Within this framework, progressive waves take the form (up to an arbitrary multiplicative constant)

$$\phi^{I} = \exp(\pm ix\sqrt{u^2 - l^2})\Big(e^{u(z-d)} + e^{-u(z-d)}\Big), \tag{2.9}$$

$$\phi^{II} = \exp(\pm ix\sqrt{u^2 - l^2})\cosh u(z+h)F(u), \tag{2.10}$$

where

$$F(u) = \frac{e^{-ud} - e^{ud}}{\sinh uh}, \tag{2.11}$$

with u satisfying the relation

$$(u - K\coth uh) = \rho(u + K\coth ud). \tag{2.12}$$

This equation has exactly one positive real root, say $u = k$. If $\rho = 0$, then either $u = 0$ or $u = K\coth uh$. In the case of deep water, the fact that $uh \gg 1$ yields $\coth kh \to 1$. Therefore, the dispersion relation reduces to $K(\sigma - e^{-2ud}) = u(1 - e^{-2ud})$ in which $\sigma = (1+\rho)/(1-\rho)$.

For the existence of trapped modes we require

$$\phi, |\nabla\phi| \to 0 \qquad \text{as} \qquad |x| \to \infty, \tag{2.13}$$

and hence we restrict $l > k$ which ensures that no wave propagation to infinity takes place at the interface.

2.3 Solutions by multipoles

A horizontal circular cylinder of radius a, having its axis along $z = f$ and its generator running parallel to the y-axis, is placed in the two-layer fluid. If $f > 0$, the cylinder is in the upper fluid, whereas for $f < 0$ the cylinder is in the lower fluid. Polar coordinates (r, θ) are defined in the xz-plane centred on $(0, f)$ as

$$x = r\sin\theta \text{ and } z = f - r\cos\theta.$$

In both upper and lower layer fluids, the total potential ϕ can be decomposed into the sum of two potentials:

$$\phi = \phi_{inc} + \phi_{diff}, \tag{2.14}$$

where ϕ_{inc} is the velocity potential due to the incident waves and ϕ_{diff} the one due to the diffracted waves. The total potential ϕ satisfies Eqs. (2.5)–(2.8), trapped mode condition (2.13) and the boundary condition

$$\frac{\partial \phi}{\partial \mathbf{n}} = 0 \qquad \text{on the surface of the cylinder.} \tag{2.15}$$

Therefore ϕ_{diff} must satisfy Eqs. (2.5)–(2.8), condition (2.13) and the body boundary condition which, due to Eqs. (2.14) and (2.15), is of the form

$$\frac{\partial \phi_{diff}}{\partial r} = -\frac{\partial \phi_{inc}}{\partial r} \qquad \text{on} \qquad r = a. \tag{2.16}$$

Multipole potentials are constructed which, for frequencies less than the cut-off value, do not radiate energy away from the submerged body. These potentials, each of which satisfies all conditions except Eq. (2.16), are singular on the axis of the cylinder but not in the fluid region. According to Kassem (1982, 1986), different types of multipoles describing the velocity potentials can be elaborated when each layer of a two-layer fluid is of finite constant depth. Taking this into consideration, the trapped mode potential is then constructed from a linear combination of all possible multipoles. Application of the body boundary condition (2.16) results in an infinite system of homogenous linear equations.

2.3.1 Cylinder submerged in the lower layer

Symmetric multipoles, $\phi_n (n \geq 0)$, are defined by (Taylor and Hu (1991))

$$\phi_n^I = \int\!\!\!\!\!\!-_0^\infty \cosh nu \cos(lx \sinh u) \Big[A_L(v) e^{vz} + B_L(v) e^{-vz} \Big] du, \tag{2.17}$$

$$\phi_n^{II} = K_n(lr) \cos n\theta + \int\!\!\!\!\!\!-_0^\infty \cosh nu \cos(lx \sinh u) \Big[C_L(v) e^{vz} + D_L(v) e^{-vz} \Big] du, \tag{2.18}$$

where $v = l \cosh u$, $K_n(.)$ is modified Bessel function of the second kind of order n and the integrals are Cauchy Principal Value integrals.

$K_n(lr) \cos n\theta$ has the following integral representation (Ursell (1951)):

$$K_n(lr) \cos n\theta = \begin{cases} \displaystyle\int\!\!\!\!\!\!-_0^\infty \cosh nu \cos(lx \sinh u) e^{v(z-f)} du & \text{for} \quad z < f, \\ \displaystyle (-1)^n \int\!\!\!\!\!\!-_0^\infty \cosh nu \cos(lx \sinh u) e^{v(f-z)} du & \text{for} \quad z > f. \end{cases}$$

With the help of the boundary conditions at the rigid lid, the interface and the bottom, the coefficients $A_L(v)$, $B_L(v)$, $C_L(v)$ and $D_L(v)$ appearing in Eqs. (2.17) and (2.18) are obtained

as

$$\begin{aligned} A_L(v) &= \frac{K(1+\sigma)}{G(v)}\Big((-1)^{n+1}e^{vf} - e^{-v(f+2h)}\Big), \\ B_L(v) &= \frac{K(1+\sigma)}{G(v)}\Big((-1)^{n+1}e^{vf} - e^{-v(f+2h)}\Big), \\ C_L(v) &= \frac{\Big((-1)^{n+1}e^{vf} - e^{-v(f+2h)}\Big)\Big((v+K\sigma)e^{-2vd} - (v+K)\Big)}{G(v)}, \\ D_L(v) &= \Big(C_L(v) + e^{-vf}\Big)e^{-2vh}, \end{aligned}$$

where

$$G(v) = (v+K\sigma)e^{-2v(d+h)} + (v-K\sigma) - (v+K)e^{-2vh} - (v-K)e^{-2vd}. \tag{2.19}$$

The total velocity potential can now be written as (Linton and Cadby (2002))

$$\phi = \sum_{n=0}^{\infty} \alpha_n \phi_n^{II}, \tag{2.20}$$

with

$$\phi_n^{II} = K_n(lr)\cos n\theta + \sum_{m=0}^{\infty} A_{mn} I_m(lr)\cos m\theta, \tag{2.21}$$

where $I_m(.)$ is modified Bessel function of the first kind of order m and

$$A_{mn} = \epsilon_n \int_0^{\infty} \cosh mu \cosh nu \Big[(-1)^n C_L(v)e^{vf} + D_L(v)e^{-vf}\Big] du, \tag{2.22}$$

with $\epsilon_0 = 1, \epsilon_n = 2, n \geq 1$.

We note that there are no singularities of the integrand on the real axis since we know that $v > l > k$. Applying the body boundary condition (2.15), we obtain an infinite system of homogenous linear equations in the unknowns α_m:

$$\alpha_n + \frac{I_n'(la)}{K_n'(la)} \sum_{m=0}^{\infty} \alpha_m A_{mn} = 0, \qquad n = 0, 1, 2, \ldots \tag{2.23}$$

For a fixed geometrical configuration, the problem of finding the trapped mode frequencies is completely specified by the two non-dimensional parameters ka and la: one of the parameters may be fixed and the other varied until the value of the determinant becomes approximately zero. This is, in fact, the most crucial stage of the investigation. The largest computational expense occurs while computing the integrals in (2.22) the values of which are used in evaluating the determinant of the matrix in Eq. (2.23). Thus it seems appropriate to keep la fixed while ka is varied up to la. For numerical evaluation of the zeros of the determinant, we truncate the system to a 32×32 system and the result presented next are obtained correct up to three decimal places.

Numerical results

Figures 2.2–2.5 show the results obtained for trapped modes above a horizontal circular cylinder of radius a submerged in the lower layer of a two-layer fluid bounded above by a rigid lid. For all the cases, the depth h/a of the lower layer is taken as 6.0 while that d/a of the upper layer is taken as 3.0 for Figs. 2.4 and 2.5. Submergence depth f/a of the cylinder is considered as -1.01 for Figs. 2.2 and 2.3 which means that the cylinder is very close to the interface. For a two-layer fluid consisting of fresh water and salt water, the value of ρ would ideally be around 0.97. The same qualitative features are observed for such a density ratio, but the effects of the interface are not very distinct. Hence, throughout our numerical results, the density ratio of the fluid is chosen as 0.95, wherever applicable, for clear observation of the features of the dispersion curves: for Figs. 2.2 and 2.4 and later for Figs. 2.6 and 2.8, to be precise. Trapped modes require $l > k$ so that $l = k$ (thin dashed line) is an upper bound for the figures in which frequencies are plotted against la.

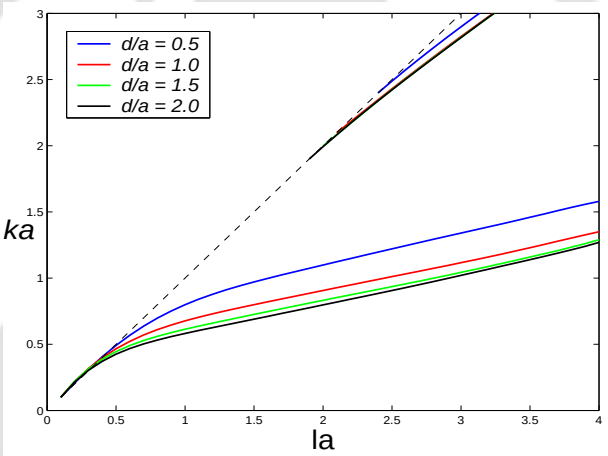

Figure 2.2: Trapped mode frequencies plotted against la for a cylinder of radius a in the lower fluid layer for different depths d/a of the upper layer; $\rho = 0.95$, $h/a = 6$ and $f/a = -1.01$.

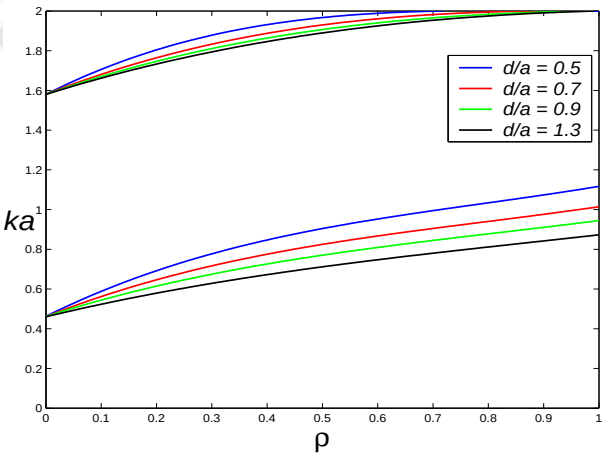

Figure 2.3: Trapped mode frequencies plotted against ρ for a cylinder of radius a in the lower fluid layer for different depths d/a of the upper layer; $la = 2$, $h/a = 6$ and $f/a = -1.01$.

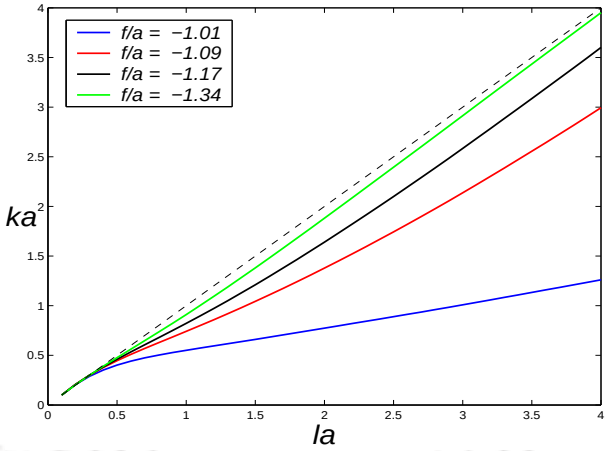

Figure 2.4: Trapped mode frequencies plotted against la for a cylinder of radius a in the lower fluid layer for different submergence depths f/a; $\rho = 0.95$, $d/a = 3$ and $h/a = 6$.

Figure 2.2 shows the plots of trapped mode frequencies where the different curves correspond to the four different depths of the upper fluid layer: $d/a = 0.5$, 1.0, 1.5 and 2.0. Corresponding to each value of d/a, there are two curves showing the first and second modes. With an increase in the depth of the upper fluid layer, these trapped mode frequencies decrease.

Figure 2.3 shows the plot of trapped mode frequencies against ρ when $la = 2$. Corresponding to different depths of the upper fluid layer: $d/a = 0.5$, 0.7, 0.9 and 1.3, we observe two modes. For the limiting case $\rho \to 1$, the wavenumber ka tends to some limit for each mode. However for the second mode, the wavenumber $ka \to la = 2$. In the far-field form of the potential, we have an $\exp(-\sqrt{l^2 - k^2}|x|)$ term. Thus the rate of decay of the exponential term decreases as ρ takes values closer to unity and in this case no trapped mode exists. The single-layer finite depth results for depth h/a and cylinder submergence f/a are recovered when $\rho = 0$ (with the interface now playing the role of the free surface) which are discussed in Linton and Cadby (2003).

In Fig. 2.4, the different curves correspond to different submergence depths of the cylinder: $f/a = -1.01$, -1.09, -1.17 and -1.34. From this figure we observe that with an increase in submergence depth, frequency of the trapped mode increases and almost coincides with the upper bound $k = l$ for some particular value of f/a. In other words, if the depth of submergence increases beyond a particular value, then trapped mode frequencies cease to exist. As the cylinder approaches the interface, i.e., $|f/a| \to 1$, the curve folds out from the upper bound.

Figure 2.5 shows the plot of trapped mode frequencies against ρ with $la = 2$ for different submergence depths: $f/a = -1.01$, -1.02, -1.03, -1.05, -1.10, -1.30 and -1.50. From Fig. 2.5(a) it is observed that when the cylinder is submerged near the interface, there exist two modes. With an increase in submergence depth, trapped mode frequency corresponding to the second mode increases to $la = 2$ and the trapped modes disappear. For submergence depth approximately greater than or equal to 1.05, there exists only one mode, as observed from Fig. 2.5(b), which also ceases to exist as we further move the cylinder downwards. Furthermore, for a fixed submergence depth, the trapped mode frequency increases steadily as the density

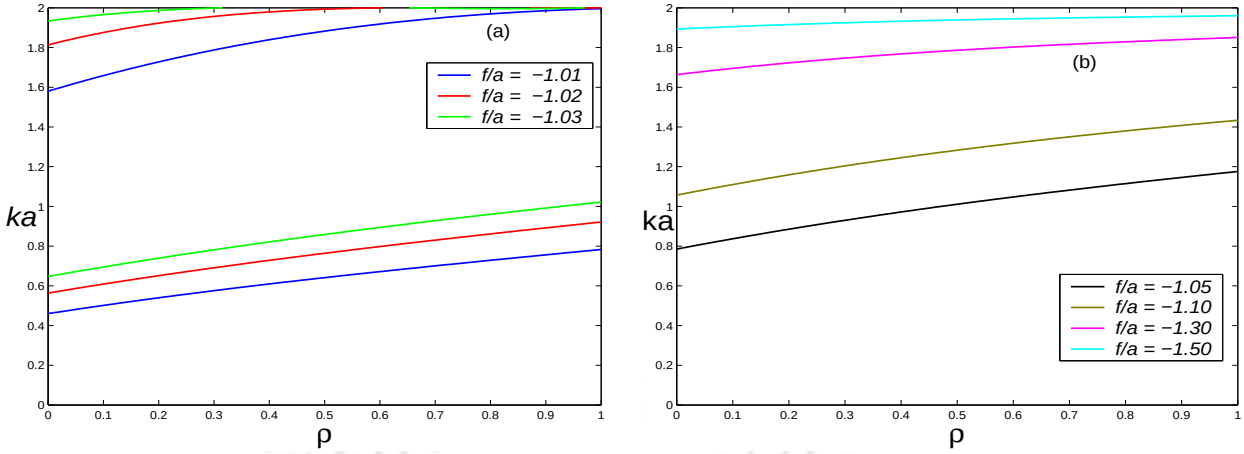

Figure 2.5: Trapped mode frequencies plotted against ρ for a cylinder in the lower fluid layer for different submergence depths f/a; $la = 2$, $d/a = 3$ and $h/a = 6$.

ratio increases.

2.3.2 Cylinder submerged in the upper layer

We now consider the problem with the cylinder positioned in the upper fluid layer. The multipoles singular at $z = f(> 0)$ are required to be modified. This can be done in the same manner as was done previously for the case of cylinder in the lower layer ($f < 0$). The suitable symmetric multipoles are

$$\phi_n^I = K_n(lr)\cos n\theta + \int_0^\infty \cosh nu \cos(lx\sinh u)\Big[A_U(v)e^{vz} + B_U(v)e^{-vz}\Big]du, \quad (2.24)$$

$$\phi_n^{II} = \int_0^\infty \cosh nu \cos(lx\sinh u)C_U(v)\cosh v(z+h)du, \quad (2.25)$$

with

$$A_U(v) = e^{-2vd}\frac{(-1)^n e^{vf}\Big(v - K\sigma - (v+K)e^{-2vh}\Big) + e^{-vf}\Big(v - K - (v+K\sigma)e^{-2vh}\Big)}{G(v)},$$

$$B_U(v) = \frac{\Big((-1)^{n+1}e^{v(f-2d)} - e^{-vf}\Big)\Big((v+K\sigma)e^{-2vh} + K - v\Big)}{G(v)},$$

$$C_U(v) = \frac{2K(1-\sigma)B_U(v)}{(v+K\sigma)e^{-vh} + (K-v)e^{vh}},$$

where $G(v)$ is same as in Eq. (2.19). The polar expansion of the multipoles, following the previous procedure, is

$$\phi_n^I = K_n(lr)\cos n\theta + \sum_{m=0}^{\infty} B_{mn}I_m(lr)\cos m\theta, \quad (2.26)$$

where

$$B_{mn} = \epsilon_n \int_0^\infty \cosh mu \cosh nu\Big[(-1)^n A_U(v)e^{vf} + B_U(v)e^{-vf}\Big]du. \quad (2.27)$$

Once again, the integrand has no singularities on the real axis. By applying the body boundary condition (2.15), we obtain a similar kind of system of equations like (2.23) for β_m:

$$\beta_n + \frac{I_n'(la)}{K_n'(la)} \sum_{m=0}^{\infty} \beta_m B_{mn} = 0, \qquad n = 0, 1, 2, \ldots \tag{2.28}$$

Here also, as in the previous case, by varying the frequencies ka and fixing the other parameters, we conveniently locate the zeros of the truncated determinant. It is already known that those frequencies correspond to the trapped modes. The results presented below are obtained correct up to three decimal places where a 32×32 system has been used after truncating the system arising from (2.28).

Numerical results

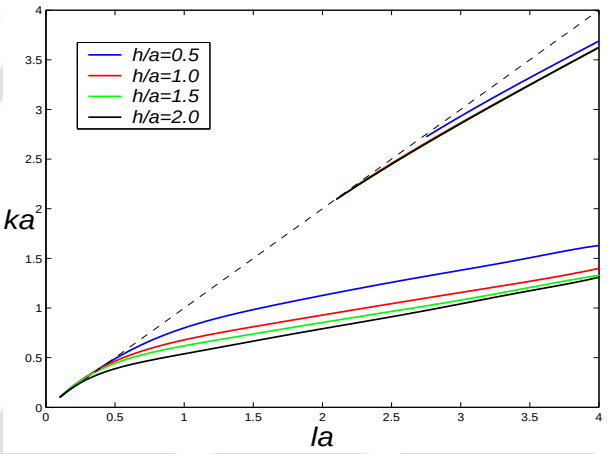

Figure 2.6: Trapped mode frequencies plotted against la for a cylinder in the upper fluid layer for different depths h/a of the lower layer; $\rho = 0.95$, $f/a = 1.01$ and $d/a = 3$.

Figures 2.6–2.9 show the plots of the non-dimensional trapped mode frequencies for a circular cylinder of radius a immersed in the upper layer of the two-layer fluid. In all cases, the depth d/a of the upper layer is taken as 3.0. For Figs. 2.6 and 2.7, the submergence depth f/a is taken as 1.01 which means that the cylinder is very close to the interface and the depth h/a of the lower layer is taken as 6.0 for Figs. 2.8 and 2.9.

Figure 2.6 shows the dispersion curves for four different depths of the lower layer: $h/a = 0.5$, 1.0, 1.5 and 2.0. For each set of parameter values, there are two curves corresponding to two modes which are displayed in the graphs. We clearly observe that the frequency of the trapped modes decreases when the depth of the lower layer increases, the first mode being affected more than the second mode.

Figure 2.7 shows the plot of trapped mode frequencies against ρ when $la = 2$. Corresponding to different depths of the lower layer: $h/a = 0.5$, 1.0, 1.5 and 2.0, we observe two modes for density ratios $\rho \geq 0.5$. For the limiting case $\rho \to 0$, trapped mode frequency ceases to exist. The limit $\rho \to 0$ corresponds to $\rho^{II} \to \infty$. Consequently the dispersion relation reduces to $u = 0$ which is the dispersion relation for a finite depth homogenous fluid bounded above by a rigid lid. We know that trapped modes do not exist in this case. By letting the density ratio tend to zero, we are being able to recover the same.

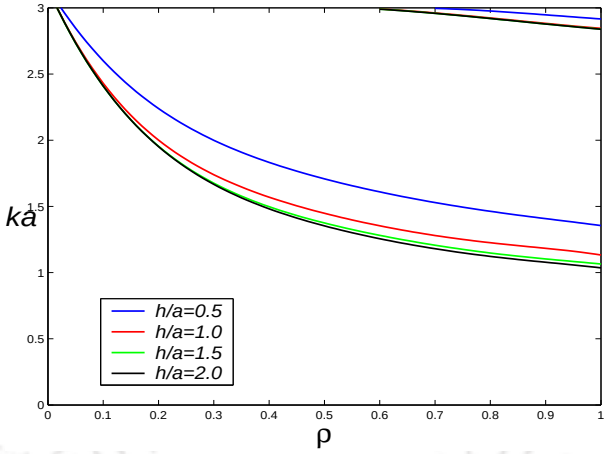

Figure 2.7: Trapped mode frequencies plotted against ρ for a cylinder in the upper fluid layer for different depths h/a of the lower layer ; $la = 3$, $f/a = 1.01$ and $d/a = 3$.

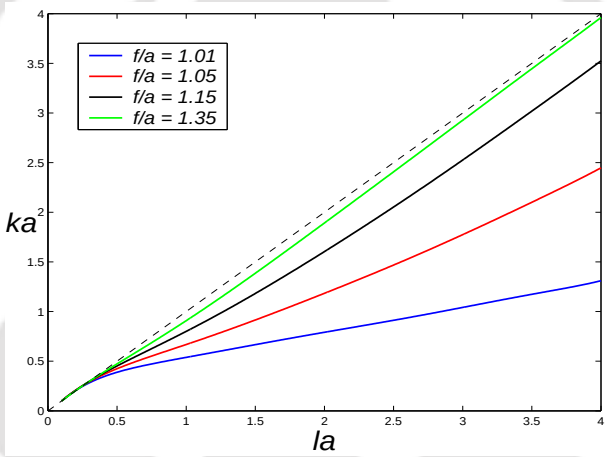

Figure 2.8: Trapped mode frequencies plotted against la for a cylinder in the upper fluid layer for different submergence depths f/a; $\rho = 0.95$, $d/a = 3$ and $h/a = 6$.

Figure 2.8 shows the dispersion curves for the case in which $\rho = 0.95$. There are four different curves corresponding to different submergence depths of the cylinder in the upper layer: $f/a = 1.01$, 1.05, 1.15 and 1.35. As the cylinder approaches the interface, the curves fold out from the interface. Similar effects were observed when the cylinder was placed in the lower layer.

In Fig. 2.9, the different curves correspond to the different submergence depths of the cylinder: $f/a = 1.01$, 1.03, 1.05 and 1.10 for $la = 2$. Different modes can be found by fixing the depth of both layers and also the density ratio ρ, and then by varying the submergence depth. For the limiting case $\rho \to 1$, the wavenumber ka tends to some fixed but different limit corresponding to different submergence depths. If we move the cylinder away from the interface towards the upper surface, these trapped mode frequencies increase and the trapped mode ceases to exist as the cylinder comes closer to the rigid lid. By varying the submergence depth and fixing all the parameters, it is observed that the trapped mode ka increases up to $la = 2$ as ρ decreases. There exist no trapped modes for density ratio approximately less than

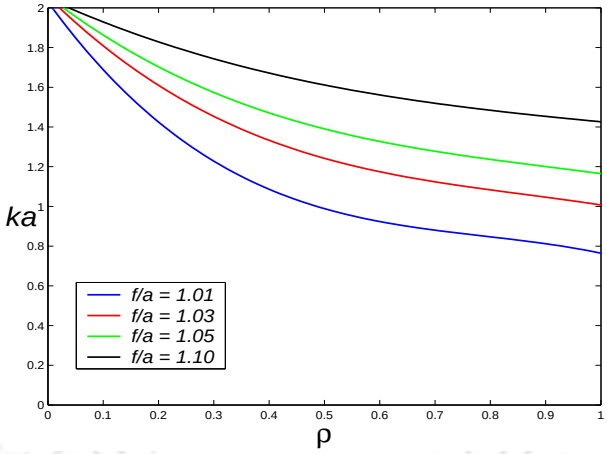

Figure 2.9: Trapped mode frequencies plotted against ρ for a cylinder in the upper fluid layer for different submergence depths f/a ; $la = 2$, $d/a = 3$ and $h/a = 6$.

0.01 as observed from the figure. Hence as $\rho \to 0$, it is possible to recover the problem in which a homogenous fluid is bounded above by a rigid lid.

Intuitively it is very likely to come to one's mind that single-layer fluid results may be obtained if the density ratio $\rho \to 1$. More precisely, one might expect that there will be no trapped modes when the cylinder is submerged in either layer of a two-layer fluid bounded above by a rigid lid for the limiting case $\rho \to 1$ since in this case the upper and lower fluids have almost the same density. But from Figs. 2.3 and 2.7, where trapped mode frequencies are plotted against density ratio, we observe that for each set of parameter values there are two curves corresponding to two modes. In the limit $\rho \to 1$, the second mode ceases to exist but the first mode tends to some value which gives a trapped mode. To explain what takes place, we next consider the boundary value problem, given by Eqs. (2.5)–(2.8), with the limit $\rho \to 1$.

Limit as $\rho \to 1$

In the limit $\rho \to 1$, we find that $K/k \to 0$ from the dispersion relation (2.12) and so if $l(> k)$ is fixed, then K must tend to zero. For a clear insight we consider the boundary conditions in the limit as $\rho \to 1$ and $K \to 0$ simultaneously.

We introduce small parameters ϵ and δ such that

$$K = \epsilon, \qquad \rho = 1 - \delta, \qquad K' = \frac{K}{1-\rho} = \frac{\epsilon}{\delta} = O(1). \tag{2.29}$$

In this limit, the continuity of the vertical velocity at the interface remains in the same form but that of pressure changes to

$$K'{\phi^{I}}^{I} - {\phi_z}^{II} = K'{\phi}^{I} \qquad \text{on} \qquad z = 0. \tag{2.30}$$

Oblique waves propagating in the fluid have the same form given by Eqs. (2.9)–(2.11). The dispersion relation will have only one solution k which must satisfy

$$k(1 - e^{-2kd})(1 - e^{-2kh}) = 2K'(1 - e^{-2k(d+h)}). \tag{2.31}$$

In order that trapped modes exist, we require $l > k$ so that the motion decays as $|x| \to \infty$. Thus for a fixed l, we obtain a boundary value problem in terms of a new spectral parameter K'. We compute the trapped mode frequencies by using multipole expansion method. The results match with those values observed from Figs. 2.3, 2.7 and 2.9 for which the density ratio approaches 1. Hence for a fixed l, the trapped mode problem in the limit $\rho \to 1$ is related to the limits of the trapped mode curves in these figures. But if we fix K and let $\rho \to 1$, then $k \to \infty$ and hence $l \to \infty$. Thus it is not possible to recover the single-layer fluid results in the limit $\rho \to 1$.

It is to be noted that the existence of trapped modes throughout the present work is based on numerical evidence only, i.e., we numerically locate the values of those frequencies for which the truncated determinant vanishes. However, we feel that it may be possible to derive a similar proof for a two-layer fluid on the similar line as was done for a single-layer fluid by Ursell (1951).

2.4 Conclusions

In the present chapter, based on multipole expansion method, we investigate the existence of trapped modes above a horizontal circular cylinder placed in either layer of a two-layer fluid bounded above by a rigid lid. The trapped mode frequencies are evaluated by locating the zeros of a suitably truncated determinant of the infinite system of homogenous linear equations. We find that the motion of the trapped mode is confined to the interface only. When the cylinder is placed in one of the layers, trapped mode frequency decreases with an increase in the depth of the other layer. Different modes are found by fixing the depth of both layers and density ratio, and varying the submergence depth. For a given set of parameter values and with an increase in density ratio, trapped mode frequency increases when the cylinder is placed in the lower layer but decreases when the cylinder is placed in the upper layer. When the wavenumber of the oblique incident wave is greater than or equal to two times its radius, two trapped mode frequencies exist near the interface if the cylinder is submerged in the lower layer whereas two modes will exist only for the density ratio greater than or equal to 0.5 when the cylinder is submerged in the upper layer. When the upper layer is bounded above by a free surface, we observe that, by varying the density ratio, the modes of the free surface get transferred to the modes of the interface as was observed in Linton and Cadby (2003) but such results are not observed when the free surface is approximated by a rigid lid. When the density ratio tends to zero, the problems in a two-layer fluid can be compared with those in a single-layer fluid. In this limit, the trapped mode problem reduces to a finite depth single-layer fluid problem bounded above by a free surface or a rigid lid, depending on whether the cylinder is placed in the lower or the upper layer, respectively. We also examine why the single-layer results cannot be recovered when the density ratio tends to 1.

Hence it can be concluded that if the free surface in a two-layer fluid gets approximated by a rigid lid, then also trapped modes exist and occur at frequencies below a cut-off value. Strong numerical evidence supports our investigation. For a given set of parameter values and with an increase in submergence depth, these trapped mode frequencies increase but disappear after a certain value of submergence depth. Therefore, for a fixed geometrical configuration,

it is possible to formulate a scattering problem due to the interaction of an obliquely incident wave with the cylinder above that specific submergence depth only, which corresponds to a particular density ratio, and with the frequency more than the cut-off value. Unique reflection and transmission coefficients can also be determined in this case. In other words, the evidence of existence of trapped mode for our problem will allow the related scattering problem to be solved under restrictions as mentioned above. It is hoped that our investigation, not carried out by anyone earlier as far as we know, will pave the way for many more investigations to follow in this area.

Chapter 3

Flexural gravity waves trapped in a two-layer fluid of finite depth

3.1 Introduction

The objective of the present work is to investigate whether a submerged horizontal circular cylinder in a two-layer inviscid, incompressible and immiscible fluid of finite depth bounded above by a thin ice-cover and below by an impermeable horizontal bottom supports trapped mode. In this case, two trapped waves are developed: one with the higher wavenumber at the interface and another with the lower wavenumber at the ice-cover. The wavenumbers of these waves are large compared to the wavenumbers of the corresponding gravity waves. Furthermore, in these problems, a fifth-order boundary condition is satisfied at the upper surface which makes the problem more complex. In order to examine the existence of trapped modes, multipole expansion method of Ursell (1951), along with the properties of infinite system of homogenous linear equations, is used. For a fixed geometrical configuration, we numerically estimate the values of those frequencies for which the trapped modes exist. The trapped mode wavenumbers are plotted against the density ratio for different depths of the upper layer and the lower layer, the submergence depths and different sets of ice-parameters. The dispersion curves for different geometrical configurations with a fixed set of the other parameters are also discussed.

3.2 Mathematical formulation of the problem

Under the usual assumptions of linear water wave theory, we consider the problem in three dimensional Cartesian coordinate system with the xy-plane in the horizontal direction and the z-axis in the vertically upward direction. A two-layer fluid of finite depth is considered in which the upper layer is covered by a thin uniform ice-sheet modeled as a thin elastic plate, while the lower layer is bounded below by a rigid infinite horizontal bottom. The upper fluid layer of constant density ρ_I occupies the region $-\infty < x < \infty$, $-\infty < y < \infty$, $0 < z < d$ with $z = d$ as the mean position of the thin ice-cover. The lower fluid of constant density ρ_{II} occupies the region $-\infty < x < \infty$, $-\infty < y < \infty$, $-h < z < 0$ with $z = 0$ as the mean position of the interface and $z = -h$ as the bottom surface. The effect due to surface tension at the interface between the two fluids is neglected. With the fluid assumed to be inviscid and

incompressible, and the motion irrotational, the fluid motion is described by the two velocity potentials $\Phi^j(x,y,z,t)$, $j = I, II$. Let $\eta(x,y,t)$ and $\zeta(x,y,t)$ be the small displacements at the upper surface and the interface, respectively. Each of the velocity potentials $\Phi^j(x,y,z,t)$ satisfies the Laplace's equation

$$\frac{\partial^2\Phi^j}{\partial x^2} + \frac{\partial^2\Phi^j}{\partial y^2} + \frac{\partial^2\Phi^j}{\partial z^2} = 0 \qquad \text{in the appropiate fluid region.} \tag{3.1}$$

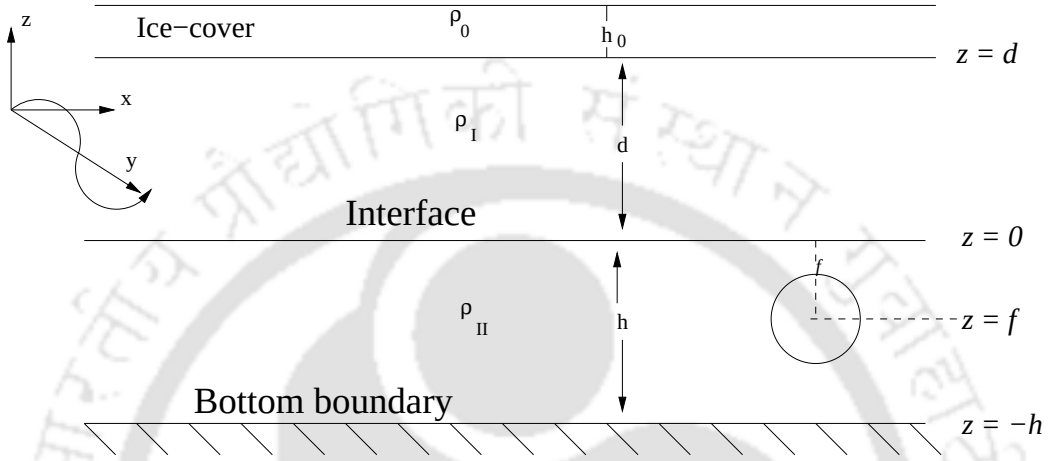

Figure 3.1: Cross-sectional view for a two-layer fluid covered by an ice-cover in the presence of a cylinder.

The linearized kinematic conditions at the mean free surface and the mean interface, respectively, are given by

$$\frac{\partial\eta}{\partial t} = \frac{\partial\Phi^I}{\partial z} \qquad \text{on} \qquad z = d, \tag{3.2}$$

$$\frac{\partial\zeta}{\partial t} = \frac{\partial\Phi^I}{\partial z} = \frac{\partial\Phi^{II}}{\partial z} \qquad \text{on} \qquad z = 0. \tag{3.3}$$

According to the linearized theory of water waves, the hydrodynamic pressure p_j in the corresponding fluid region is given by

$$p_j = -\rho_j g\Big(z + \frac{1}{g}\frac{\partial\Phi^j}{\partial t}\Big). \tag{3.4}$$

Assuming no cavitation between the ice-cover and the ocean surface, the linearized kinematic and dynamic conditions, given by Eqs. (3.2) and (3.4), hold at the equilibrium upper surface. The hydrodynamic pressure p_I is the pressure at the upper surface due to the atmosphere, the static pressure of the ice-cover and the dynamic pressure due to the inertia, the stiffness of the ice-cover etc. It is assumed that the ice-cover acts as a thin, linearly elastic plate of uniform mass density ρ_0 and thickness h_0. Consideration of linearity is justified because of the small curvature involved as the ice-cover bends to the passing waves; that of elasticity is justified because of the oscillatory nature of the problem which does not allow an elastic process to act in any significant way. With these assumptions, the displacement η from equilibrium position is related to the differential pressure P_0 by the equation (derived in Appendix A)

$$P_0 = \mathfrak{D}\nabla^4_{x,y}\eta + m\left(\frac{\partial^2\eta}{\partial t^2} + g\right), \tag{3.5}$$

where $\mathfrak{D} = E{h_0}^3/\{12(1-\nu^2)\}$ and $m = \rho_0 h_0$ the mass per unit surface area of the ice-cover, and $\nabla^4_{x,y} = (\partial^4/\partial x^4) + 2(\partial^2/\partial x^2)(\partial^2/\partial y^2) + (\partial^4/\partial y^4)$ the biharmonic operator in the plane of the ice-cover.

When the upper surface pressure $p_I(x,y)$ in the linearized dynamic condition (3.4) is equated to the sum of P_0 and the constant atmospheric pressure, we find that the velocity potential Φ^I must satisfy

$$\Big(D\nabla^4_{x,y} + 1 + \frac{\varepsilon}{g}\frac{\partial^2}{\partial t^2}\Big)\frac{\partial \Phi^I}{\partial z} + \frac{1}{g}\frac{\partial^2 \Phi^I}{\partial t^2} = 0 \qquad \text{on} \qquad z = d, \tag{3.6}$$

where Eq. (3.2) is used to eliminate η; $D = \mathfrak{D}/(\rho_I g)$, $\varepsilon = \rho_0 h_0/\rho_I$.

It is further assumed that all the motions are time harmonic along the body in the y-direction. Under these assumptions of linear water wave theory, the velocity potentials in the upper and lower layers can, respectively, be defined for oblique waves in the form

$$\Phi^I(x,y,z,t) = \mathrm{Re}[\phi^I(x,z)e^{ily}e^{-i\omega t}],$$
$$\Phi^{II}(x,y,z,t) = \mathrm{Re}[\phi^{II}(x,z)e^{ily}e^{-i\omega t}],$$

where $\phi^I(x,z)$ and $\phi^{II}(x,z)$ are the complex-valued potentials and Re denotes the real part. In this case, each $\phi^j(x,z)$, $j = I, II$, satisfies the modified Helmholtz equation $(\nabla^2_{x,z} - l^2)\phi^j = 0$. The linearized boundary condition at the upper surface is given by

$$\Big[D\Big(\frac{\partial^4}{\partial x^4} - 2l^2\frac{\partial^2}{\partial x^2} + l^4\Big) + 1 - \varepsilon K\Big]\frac{\partial \phi^I}{\partial z} - K\phi^I = 0 \qquad \text{on} \qquad z = d. \tag{3.7}$$

Denoting the ratio $\rho_I/\rho_{II}(<1)$ of the densities of the two fluids by ρ and using Eqs. (3.3) and (3.4), the interface matching conditions due to the continuity of velocity and pressure are, respectively, given by

$$\frac{\partial \phi^I}{\partial z} = \frac{\partial \phi^{II}}{\partial z} \qquad \text{on} \qquad z = 0, \tag{3.8}$$

$$\rho\Big(\frac{\partial \phi^I}{\partial z} - K\phi^I\Big) = \frac{\partial \phi^{II}}{\partial z} - K\phi^{II} \qquad \text{on} \qquad z = 0. \tag{3.9}$$

The impermeable bottom boundary condition is given by

$$\frac{\partial \phi^{II}}{\partial z} = 0 \qquad \text{on} \qquad z = -h. \tag{3.10}$$

Within this framework, progressive waves or incident waves take the form (up to an arbitrary multiplicative constant)

$$\phi^I = \exp(\pm ix\sqrt{u^2 - l^2})\Big(F_+(u)e^{u(z-d)} + F_-(u)e^{-u(z-d)}\Big), \tag{3.11}$$

$$\phi^{II} = \exp(\pm ix\sqrt{u^2 - l^2})\cosh u(z+h)F(u), \tag{3.12}$$

where

$$F(u) = \frac{F_+(u)e^{-ud} - F_-(u)e^{ud}}{\sinh uh}, \tag{3.13}$$

$$F_\pm(u) = \Big(Du^4 + 1 - \varepsilon K\Big)u \pm K, \tag{3.14}$$

and u satisfies the dispersion relation

$$(u+K\sigma)F_+(u)e^{-2u(d+h)}+(u-K\sigma)F_-(u)-(u+K)F_-(u)e^{-2uh}-(u-K)F_+(u)e^{-2ud}=0. \quad (3.15)$$

The above equation has exactly two positive real roots u_1 and u_2 ($u_1 < u_2$, say). The detail analysis of the roots for dispersion relation is given in the Appendix of Bhattacharjee and Sahoo (2008). If $D = \varepsilon = 0$, then this relation produces two wavenumbers for a two-layer fluid of finite depth bounded above by a free surface. If $\rho = 0$, then either $u(Du^4 + 1 - \varepsilon K) = K \coth ud$ or $u = K \coth uh$, i.e., if the density ratio equals zero, then the problem reduces to a single-layer finite depth problem bounded above by a thin ice-cover or by a free surface.

For the existence of trapped modes, it is required that

$$\phi^{I}, \phi^{II}, |\nabla\phi^{I}|, |\nabla\phi^{II}| \to 0 \quad \text{as} \quad |x| \to \infty \quad (3.16)$$

and hence l is restricted to be in the range $l > u_2 > u_1$ which ensures that no wave propagation to infinity takes place at the interface or near the ice-cover.

3.3 Solutions by multipoles

A horizontal circular cylinder of radius a having its axis along $z = f$, $a < |f|$, and its generator running parallel to the y-axis is placed in a two-layer fluid. If $f > 0$, the cylinder is in the upper fluid, whereas for $f < 0$ the cylinder is in the lower fluid. It is assumed that the resulting motion is two-dimensional; this assumption is justified because the cylinder is long compared to the wavelengths (Ursell (1949)). It is to be noted that the insertion of the cylinder in no way affects the elasticity of the ice-cover. Taking the origin of the rectangular Cartesian coordinates at the mean position of the axis of the cylinder, polar coordinates (r, θ) are defined as

$$x = r\sin\theta \text{ and } z = f - r\cos\theta.$$

Incident potential ϕ_{inc} satisfies the modified Helmholtz equation in both layers, boundary conditions (3.7)–(3.10) and the trapped modes condition (3.16). Now if the cylinder is placed in either of the layers, there exists an associated diffracted potential ϕ_{diff} in that layer. The total potential $\phi = \phi_{inc} + \phi_{diff}$ satisfies the modified Helmholtz equation and Eqs. (3.7)–(3.10). In addition, the total velocity potential also satisfies the body boundary condition in either of the layers:

$$\frac{\partial\phi_{diff}}{\partial r} = -\frac{\partial\phi_{inc}}{\partial r} \qquad \text{on} \qquad r = a. \quad (3.17)$$

Following the method of Ursell (1951), multipoles, which are singular at $(0, f)$ and symmetric about $x = 0$, are constructed. For this purpose, v is written as $v = l\cosh(u)$ for notational convenience. Solutions to $(\nabla^2 - l^2)\phi(r, \theta) = 0$, which are singular at $r = 0$, are $K_n(lr)\cos(n\theta)$. The total potential is then taken as a linear combination of all the possible multipoles. Subsequent application of the body boundary condition (3.17) to the problem results in an infinite system of homogenous linear equations.

3.3.1 Cylinder submerged in the upper layer

Since the singularity is in the upper fluid, it follows that

$$\phi_n^I \sim K_n(lr)\cos(n\theta) \qquad \text{as} \qquad r=\sqrt{x^2+(z-f)^2}\to 0;\ n=1,2,3,\ldots \tag{3.18}$$

We try the following as solutions: (Linton and Cadby (2002))

$$\phi_n^I = K_n(lr)\cos n\theta + \int_0^\infty \cosh nu\cos(lx\sinh u)\Big[A_{_U}(v)e^{vz}+B_{_U}(v)e^{-vz}\Big]du, \tag{3.19}$$

$$\phi_n^{II} = \int_0^\infty \cosh nu\cos(lx\sinh u)C_{_U}(v)\cosh v(z+h)du, \tag{3.20}$$

and use the following integral representation (Ursell (1951)):

$$K_n(lr)\cos n\theta = \begin{cases} \displaystyle\int_0^\infty \cosh nu\cos(lx\sinh u)e^{v(z-f)}du & \text{for} \quad z<f, \\ \displaystyle(-1)^n\int_0^\infty \cosh nu\cos(lx\sinh u)e^{v(f-z)}du & \text{for} \quad z>f. \end{cases}$$

It is evident that ϕ_n^I and ϕ_n^{II}, as given above, satisfy the modified Helmholtz equation and ϕ_n^{II} satisfies the condition (3.10). Conditions (3.7), (3.8) and (3.9) are satisfied if

$$\begin{aligned} A_{_U}(v) &= \frac{F_+(v)e^{-2vd}}{F_-(v)}\Big(B_{_U}(v)+(-1)^n e^{vf}\Big), \\ B_{_U}(v) &= \frac{\Big((-1)^{n+1}F_+(v)e^{v(f-2d)}-F_-(v)e^{-vf}\Big)}{G(v)}\Big((v+K\sigma)e^{-2vh}-v+K\Big), \\ C_{_U}(v) &= \frac{2K(1-\sigma)B_{_U}(v)}{(v+K\sigma)e^{-vh}+(K-v)e^{vh}}, \end{aligned}$$

where

$$G(v)=(v+K\sigma)F_+(v)e^{-2v(d+h)}+(v-K\sigma)F_-(v)-(v+K)F_-(v)e^{-2vh}-(v-K)F_+(v)e^{-2vd}. \tag{3.21}$$

Now, $G(v)$ has two simple zeros at $v=u_1$ and $v=u_2$ on the real axis of v. This introduces simple poles for the integrals in ϕ_n^I, ϕ_n^{II} and the path of integration is indented to pass beneath the poles. But by using the trapped mode condition (3.16), we have $l>u_2>u_1$ and since already $v>l$, so there will be no singularities of the integrand on the real axis.

The total velocity potential can now be written as

$$\phi=\sum_{n=0}^\infty \alpha_n\phi_n^I, \tag{3.22}$$

with

$$\phi_n^I = K_n(lr)\cos n\theta+\sum_{m=0}^\infty A_{mn}I_m(lr)\cos m\theta, \tag{3.23}$$

and

$$A_{mn}=\epsilon_n\int_0^\infty \cosh mu\cosh nu\Big[(-1)^nA_{_U}(v)e^{vf}+B_{_U}(v)e^{-vf}\Big]du, \tag{3.24}$$

with $\epsilon_0=1,\epsilon_n=2,n\geq 1$.

Applying the body boundary condition (3.17), we obtain an infinite system of homogenous linear equations in the unknowns α_n:

$$\alpha_n + \frac{I_n'(la)}{K_n'(la)} \sum_{m=0}^{\infty} \alpha_m A_{mn} = 0, \qquad n = 0, 1, 2, \ldots \tag{3.25}$$

where $'$ denotes differentiation with respect to r.

For computing the trapped mode frequency the algorithm that is used is described in brief. For a given set of values of geometrical configurations, along with the density ratio, the problem of finding the trapped mode frequencies is completely specified by the two non-dimensional parameters Ka and la. For a fixed value of la, the parameter Ka increases from 0 and stops when the corresponding higher wavenumber reaches the cut-off value la. Within this variation we locate the intervals of Ka for which the value of the truncated determinant changes its sign. Then for each of these intervals, we locate the roots of the truncated determinant correct upto three decimal places by employing the Bisection method. By using the dispersion relation, we get the values of wavenumbers corresponding to these specific trapped frequencies. This algorithm is followed repeatedly for each cut-off value la. Different graphs are then plotted by assembling all the trapped mode frequencies against la. The largest computational expense occurs while computing the integrals in (3.24) the values of which are used in evaluating the determinant of the matrix in Eq. (3.25).

3.3.2 Cylinder submerged in the lower layer

Now we take up the problem with the cylinder placed in the lower layer. The multipoles singular at $z = f(< 0)$ are required to be modified. This can be done in the same manner as was done previously for the case of the cylinder located in the upper layer ($f > 0$). The suitable symmetric multipoles are

$$\phi_n^I = \int_0^\infty \cosh nu \cos(lx \sinh u) \Big[A_{_L}(v) e^{vz} + B_{_L}(v) e^{-vz} \Big] du, \tag{3.26}$$

$$\phi_n^{II} = K_n(lr) \cos n\theta + \int_0^\infty \cosh nu \cos(lx \sinh u) \Big[C_{_L}(v) e^{vz} + D_{_L}(v) e^{-vz} \Big] du, \tag{3.27}$$

where the integrals are Cauchy Principal Value integrals with

$$\begin{aligned}
A_{_L}(v) &= \frac{F_+(v)}{F_-(v)} B_{_L}(v) e^{-2vd}, \\
B_{_L}(v) &= \frac{K(1+\sigma) F_-(v)}{G(v)} \Big((-1)^{n+1} e^{vf} - e^{-v(f+2h)} \Big), \\
C_{_L}(v) &= \frac{B_{_L}(v)}{K(1+\sigma) F_-(v)} [(v + K\sigma) F_+(v) e^{-2vd} - (v+K) F_-(v)], \\
D_{_L}(v) &= \Big(C_{_L}(v) + e^{-vf} \Big) e^{-2vh},
\end{aligned}$$

where $F_\pm(v)$ and $G(v)$ are given by Eqs. (3.14) and (3.21) respectively. Here also, due to the trapped mode condition, there exist no singularities on the real axis. The polar expansion of the multipoles, following the previous procedure, is

$$\phi_n^{II} = K_n(lr) \cos n\theta + \sum_{m=0}^{\infty} B_{mn} I_m(lr) \cos m\theta, \tag{3.28}$$

where

$$B_{mn} = \epsilon_n \int_0^\infty \cosh mu \cosh nu \Big[(-1)^n C_{_L}(v) e^{vf} + D_{_L}(v) e^{-vf}\Big] du. \tag{3.29}$$

By applying the body boundary condition (3.17), the same kind of system of equations like (3.25) is obtained for β_n:

$$\beta_n + \frac{I_n'(la)}{K_n'(la)} \sum_{m=0}^{\infty} \beta_m B_{mn} = 0, \qquad n = 0, 1, 2, ... \tag{3.30}$$

Here also, as in the previous case, by varying the frequencies Ka and fixing the other parameters, the zeros of the truncated determinant are conveniently located. It is already known that those frequencies correspond to the trapped modes.

3.4 Numerical Results

When the cylinder is placed in either layer of a two-layer fluid, in order to find the unknown coefficients α_n and β_n in Eqs. (3.25) and (3.30), respectively, it is required to truncate the corresponding systems at some N. A 32×32 system is sufficient for solving each of the systems of equations (3.25) and (3.30). That these systems of equations can be truncated after 32 terms is clearly evident from the following table. The results presented in this section are obtained correct up to three decimal places.

N	$\rho = 0$		$\rho = 0.2$		$\rho = 0.8$		$\rho = 0.999$	
	Lower	Upper	Lower	Upper	Lower	Upper	Lower	Upper
10	0.756191	1.826038	0.795734	1.907688	0.912679	–	0.950136	–
15	0.740752	1.728682	0.779404	1.831339	0.894504	1.992753	0.931457	–
20	0.737126	1.696345	0.775629	1.804692	0.890233	1.986071	0.926874	1.999904
25	0.736195	1.686813	0.774684	1.796891	0.889284	1.983929	0.926169	1.999656
30	0.736009	1.684284	0.774549	1.794807	0.889047	1.983362	0.925992	1.999570
32	0.736009	1.683946	0.774414	1.794538	0.889205	1.983285	0.925992	1.999558
35	0.736009	1.683609	0.774414	1.794269	0.888414	1.983260	0.925992	1.999550
40	0.736009	1.683440	0.774414	1.794202	0.888414	1.983175	0.925992	1.999550

Table 3.1: Values of wavenumber $u_2 a$ for different values of N with the cylinder placed in the lower layer; $la = 2$, $f/a = -1.01$, $h/a = 6$, $d/a = 1$, $D/a^4 = 0.001$ and $\varepsilon/a = 0.001$

From Table 3.1, it is observed that even with a small-dimensional matrix system, it is possible to compute the lower mode correct up to three decimal places but for the second mode, there arises a requirement to consider larger values of N so as to get the desired accuracy of three decimal places. Therefore, consideration of $N = 32$ is sufficient for our numerical computation throughout.

3.4.1 Dispersion curves

Figures 3.2–3.4 show the dispersion curves when a horizontal circular cylinder of radius a is submerged in either layer of a two-layer fluid bounded above by a thin ice-cover. For all the cases, the non-dimensionalized ice parameters are kept fixed at $D/a^4 = 0.001$ and $\varepsilon/a = 0.001$, and the density ratio is taken as 0.95. Submergence depth f/a of the cylinder is considered

as -1.01 for Figs. 3.2 and 3.4, which implies that the cylinder is very close to the interface. Trapped modes require $l > u_2$ so that $l = u_2$ (the thin dashed line) is an upper bound for all the figures.

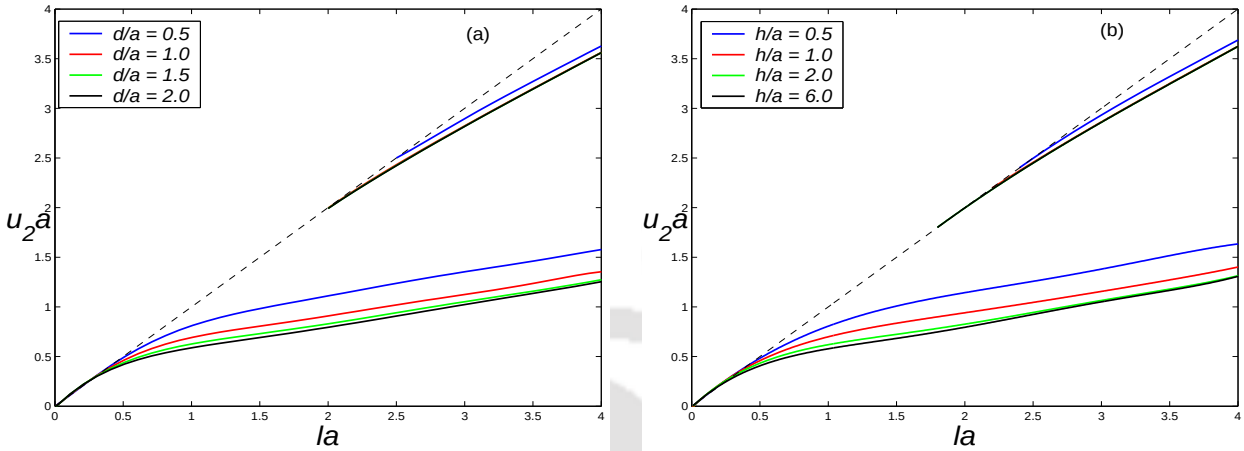

Figure 3.2: Dispersion curves for a cylinder of radius a (a) in the lower layer for different depths d/a of the upper layer; $\rho = 0.95$, $f/a = -1.01$, $h/a = 6$, $D/a^4 = 0.001$ and $\varepsilon/a = 0.001$ (b) in the upper layer for different depths h/a of the lower layer; $\rho = 0.95$, $f/a = 1.01$, $d/a = 3$, $D/a^4 = 0.001$ and $\varepsilon/a = 0.001$.

For the case when the cylinder is placed in the lower layer, Fig. 3.2(a) shows the dispersion curves for the wavenumber u_2a for different depths of the upper layer: $d/a = 0.5$, 1.0, 1.5 and 2.0. Figure 3.2(b) shows the dispersion curves for different depths of the lower layer when the cylinder is submerged in the upper layer: $h/a = 0.5$, 1.0, 2.0 and 6.0. The dispersion curves for both cases are found to follow the same trend. Corresponding to each value of the depth of the other layer, there are two curves showing the first and second modes. With an increase in the depth of the other layer, the trapped mode wavenumber decreases – the first mode being affected more than the second mode. In Fig. 3.3, different curves correspond to the different submergence depths of the cylinder. As the cylinder approaches the interface, i.e., $|f/a| \to 1$, the curve folds out from the upper bound. When we plot dispersion curves for the different depths of the layer in which the cylinder is placed, it is observed that there exist two modes but there is no variation in those modes with respect to the change of the depths, as can be seen from Fig. 3.4.

3.4.2 Cylinder submerged in the upper layer

Figure 3.5 shows the plot of trapped mode wavenumbers against the density ratio when the cylinder is placed in the upper layer. For both wavenumbers, different pairs of curves, each pair consisting of a thick line and a dashed line, correspond to the four different submergence depths of the cylinder: $f/a = 1.05$, 1.06, 1.07 and 1.10. A third mode exists corresponding only to $f/a = 1.10$ for very small density ratios, as is clearly evident from the figure. It is further observed that corresponding to each value of the submergence depth, there are at least two curves for each of the wavenumbers u_1a and u_2a. For the wavenumber u_1a, the first modes remain constant while the second modes, the higher curves, decrease and appear to cross the

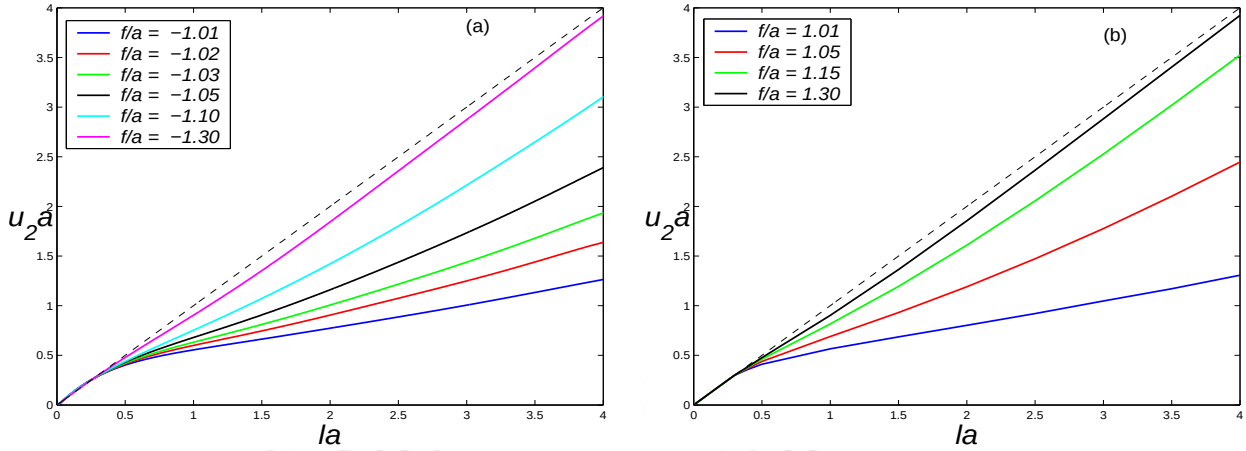

Figure 3.3: Dispersion curves for a cylinder of radius a (a) in the lower layer for different submergence depths f/a; $\rho = 0.95$, $d/a = 3$, $h/a = 6$, $D/a^4 = 0.001$ and $\varepsilon/a = 0.001$ (b) in the upper layer for different submergence depths f/a; $\rho = 0.95$, $h/a = 6$, $d/a = 3$, $D/a^4 = 0.001$ and $\varepsilon/a = 0.001$.

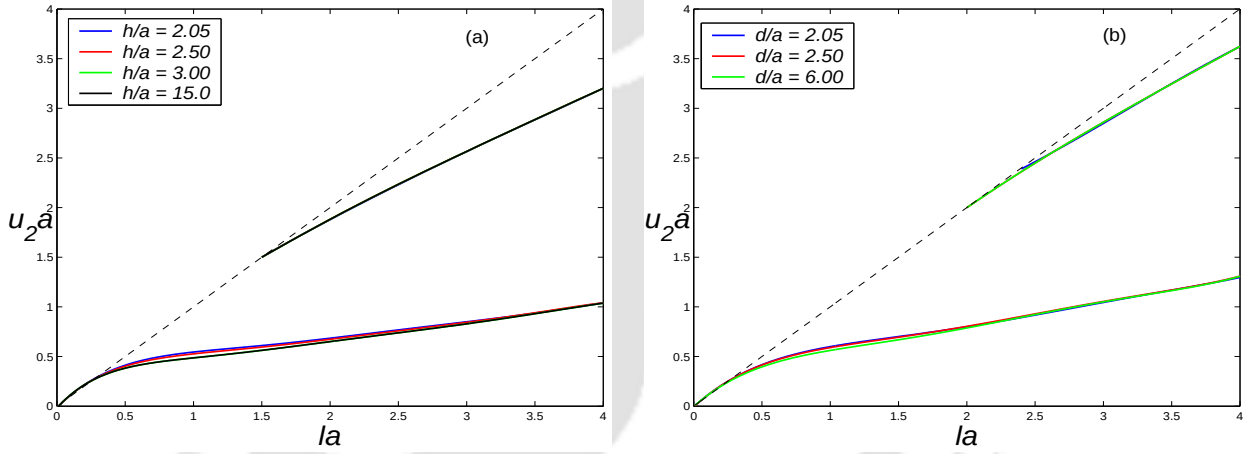

Figure 3.4: Dispersion curves for a cylinder of radius a (a) in the lower layer for different depths h/a of the lower layer; $\rho = 0.95$, $d/a = 3$, $f/a = -1.01$, $D/a^4 = 0.001$ and $\varepsilon/a = 0.001$ (b) in the upper layer for different depths d/a of the upper layer; $\rho = 0.95$, $h/a = 6$, $f/a = 1.01$, $D/a^4 = 0.001$ and $\varepsilon/a = 0.001$.

first modes at some points. However, we observe near crossing of the modes at these points. If the density ratio ρ increases further, the second modes remain constant and terminate at a certain value of ρ for different submergence depths whereas the first modes decrease to zero. For the wavenumber u_2a, the first modes increase and the second modes decrease with an increase in density ratio and they come very close to each other at near crossing points (Fig. 3.6). As ρ increases further, the modes interchange their properties, i.e., the second modes increase and terminate at $la = 2$ corresponding to a fixed value of ρ for all submergence depths while the first mode decreases to some fixed value for each submergence depth.

Figure 3.7 shows the trapped mode wavenumbers where the different curves correspond to four different depths of the upper fluid layer: $d/a = 2.05$, 2.15, 2.25 and 2.50. This figure corresponds to the case when the cylinder is submerged nearer the interface and it is observed

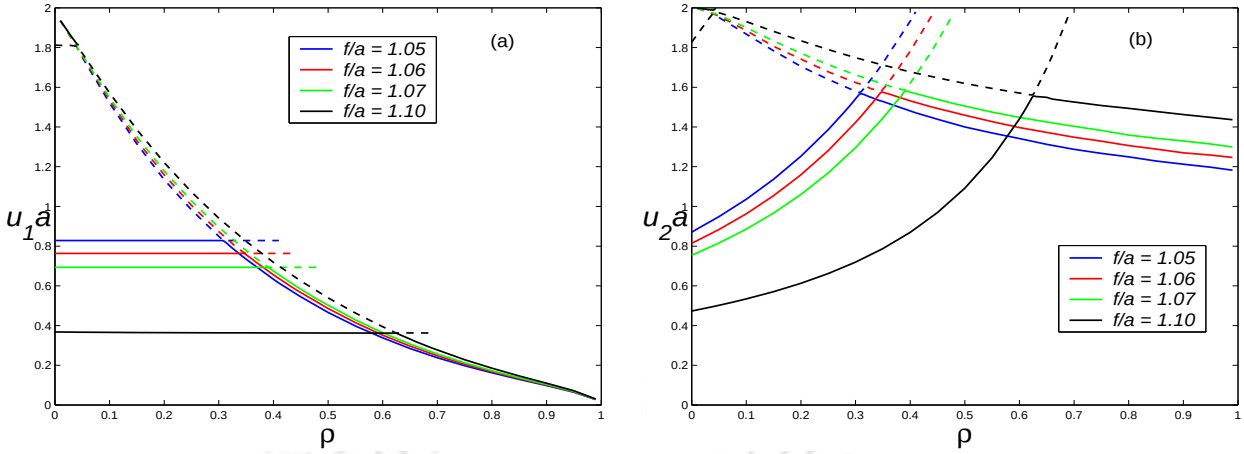

Figure 3.5: Trapped mode wavenumbers plotted against ρ for a cylinder of radius a in the upper fluid layer for different submergence depths f/a; $la = 2$, $d/a = 2.1$, $h/a = 6$, $D/a^4 = 0.001$ and $\varepsilon/a = 0.001$.

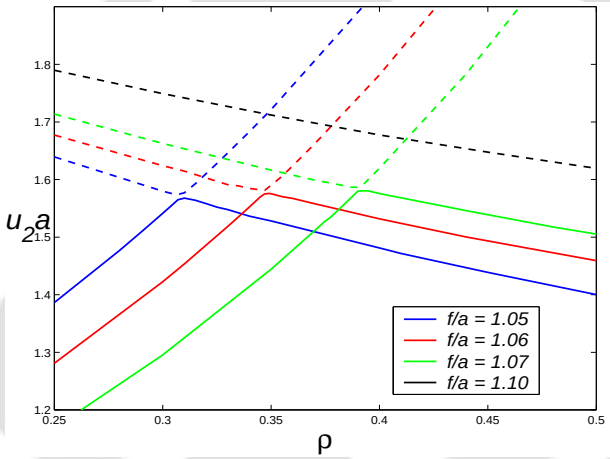

Figure 3.6: Trapped mode wavenumbers plotted against ρ for a cylinder of radius a in the upper fluid layer for different submergence depths f/a, close-up of near crossing; $la = 2$, $d/a = 2.1$, $h/a = 6$, $D/a^4 = 0.001$ and $\varepsilon/a = 0.001$.

that two trapped modes exist for depths approximately upto 2.5 and hence near crossing points also exist. With an increase in the depth of the upper layer, these near crossing points shift upwards to $la = 2$ and when the depth increases further, only the first mode always exists and it becomes independent of the depth of the upper layer.

Figure 3.8 shows the plot of trapped mode wavenumbers for different depths of the lower layer: $h/a = 0.5$, 1.0, 2.0 and 6.0. The depth d/a of the upper layer is considered as 3.0 and hence based on the discussion of Fig. 3.7, there exists only one mode. The trapped mode wavenumber u_1a increases with an increase in the depth of the lower layer for small density ratios. Then as ρ increases further towards 1, these modes cross each other at some points, and for the density ratios ≥ 0.95, the wavenumber u_1a decreases with an increase in the depth of the lower layer (Fig. 3.9). As the depth of the lower layer increases, the trapped mode wavenumber u_2a decreases. As $\rho \to 1$, the wavenumber $u_1a \to 0$ and each wavenumber u_2a tends to some finite value for each depth of the lower layer.

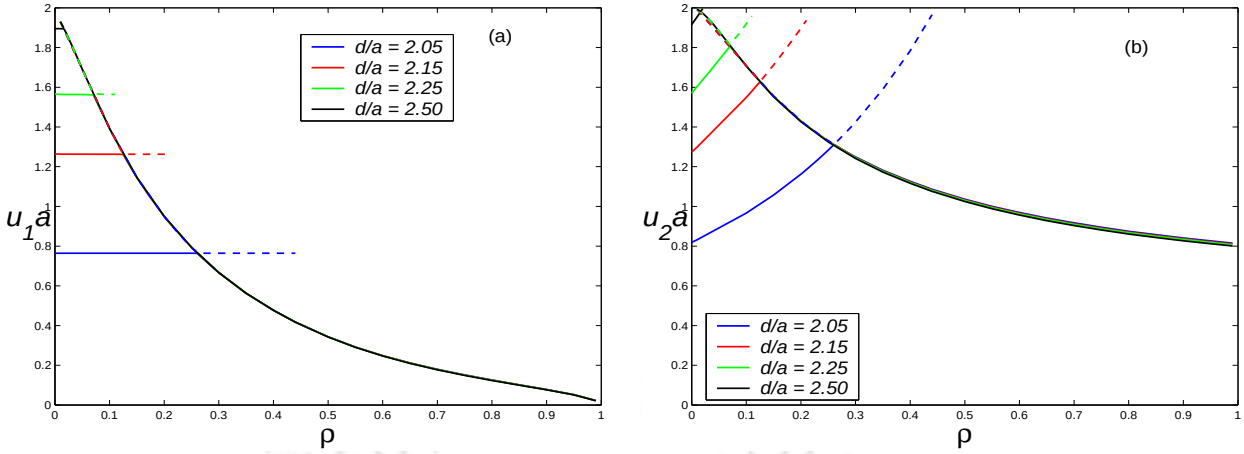

Figure 3.7: Trapped mode wavenumbers plotted against ρ for a cylinder of radius a in the upper fluid layer for different depths d/a of the upper layer; $la = 2$, $f/a = 1.01$, $h/a = 6$, $D/a^4 = 0.001$ and $\varepsilon/a = 0.001$.

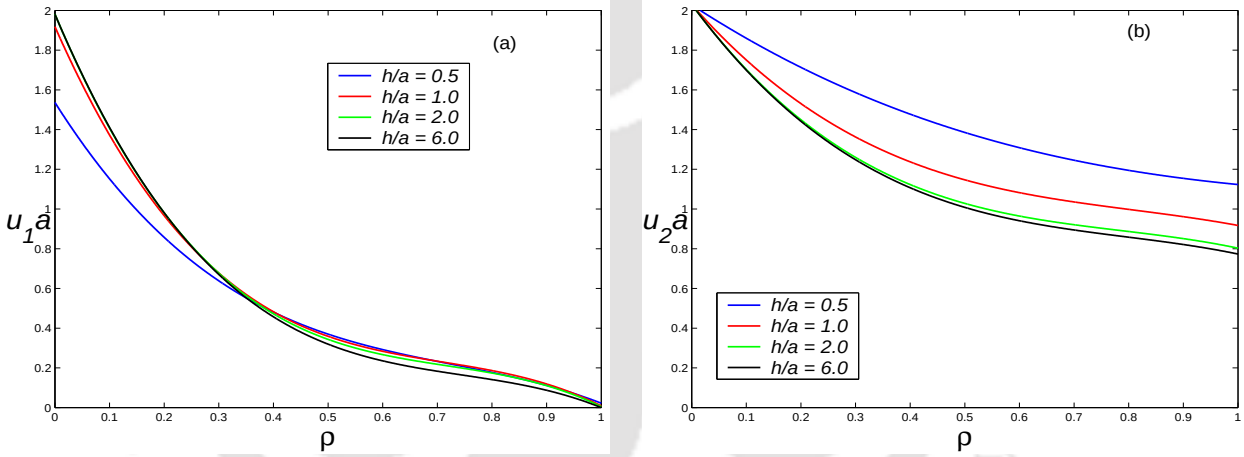

Figure 3.8: Trapped mode wavenumbers plotted against ρ for a cylinder of radius a in the upper fluid layer for different depths h/a of the lower layer h/a; $la = 2$, $f/a = 1.01$, $d/a = 3$, $D/a^4 = 0.001$ and $\varepsilon/a = 0.001$.

The different pairs of curves, each pair consisting of a thick line and a dashed line in Figs. 3.10(a) and 3.10(b), correspond to different sets of ice parameters $(D/a^4 = 0.001; \varepsilon/a = 0.001)$, $(D/a^4 = 0.01; \varepsilon/a = 0.01)$, $(D/a^4 = 0.1; \varepsilon/a = 0.01)$ and $(D/a^4 = 1.0; \varepsilon/a = 0.01)$. For the first two sets, there exist two modes and hence near crossing points also exist. For the last two sets of ice-parameters, there exists only one mode. For $d/a = 2.1$, the existence of near crossing points, when the upper layer is bounded above by a thin ice-cover, has already been observed. If the value of ice-parameter D/a^4 is increased, then the second mode for both wavenumbers ceases to exist. In other words, with an increase in flexural rigidity, the ice-cover behaves more like a rigid lid and consequently there exists only one mode corresponding to both wavenumbers which is very similar to the modes found in the rigid lid problem discussed in Chapter 2.

When the cylinder is placed in the upper layer, the limit $\rho \to 0$ corresponds to $\rho_{II} \to \infty$. Consequently the dispersion relation reduces to $u(Du^4+1-\varepsilon K) = K \coth ud$ and the multipoles

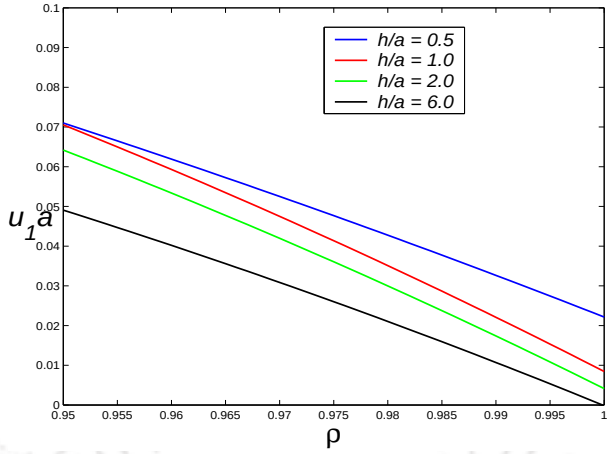

Figure 3.9: Trapped mode wavenumbers plotted against ρ for a cylinder of radius a in the upper fluid layer for different depths h/a of the lower layer, close-up; $la = 2$, $f/a = 1.01$, $d/a = 3$, $D/a^4 = 0.001$ and $\varepsilon/a = 0.001$.

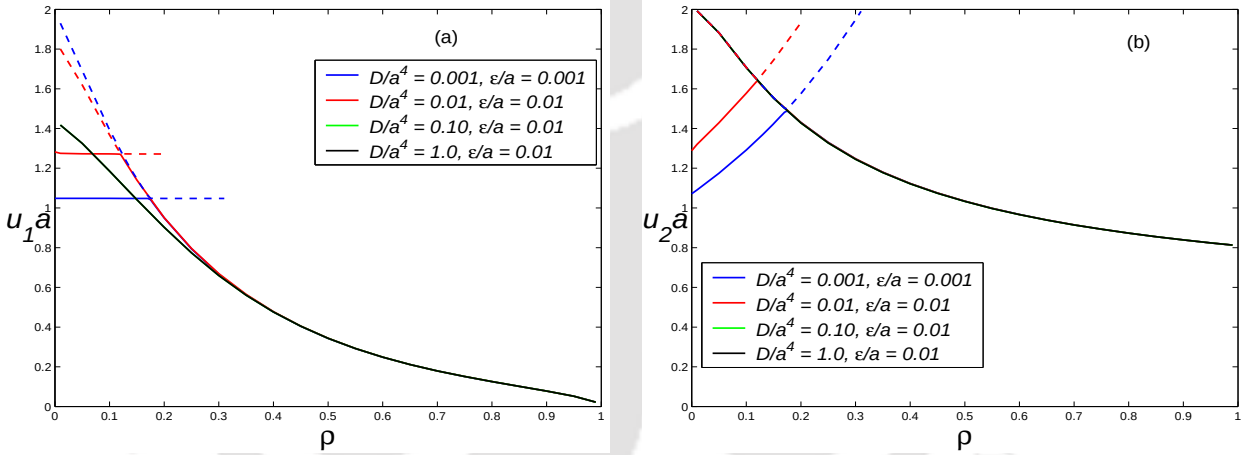

Figure 3.10: Trapped mode wavenumbers plotted against ρ for a cylinder of radius a in the upper fluid layer for different ice-parameters; $la = 2$, $f/a = 1.01$, $d/a = 2.1$ and $h/a = 6$.

become those for a finite depth homogenous fluid bounded above by a thin ice-cover. This equation has exactly one positive real root $u = k$ (say). For trapped modes it is required that $l > k$. To the best of our knowledge, these modes have not been computed earlier by anyone else. In Figs. 3.11(a) and 3.11(b), the trapped mode wavenumber ka is plotted against la for fixed values of ice-parameters $D/a^4 = 0.001$ and $\varepsilon/a = 0.001$. In Fig. 3.11(a), the wavenumber is plotted for different submergence depths of the cylinder: $f/a = 1.09$, 1.05, 1.03 and 1.01, where the depth d/a of the upper layer is 2.1. In Fig. 3.11(b), the wavenumber is plotted for different depths d/a with f/a also varying accordingly so that $(d - f)/a = 1.01$, i.e, the cylinder is submerged nearer to the thin ice-cover.

Additional numerical computations confirm that as the cylinder moves towards the ice-cover, i.e., $(d - f)/a \to 1$, the trapped mode wavenumber ka decreases and as it comes further closer, a second mode appears. When the cylinder is very close to the ice-cover, i.e., say $f/a = 1.09$, there exist two modes for $1.9 \leq la \leq 2.1$. But from the work of Linton and Cadby (2003), it is observed that when the cylinder is placed near the free surface, a second mode

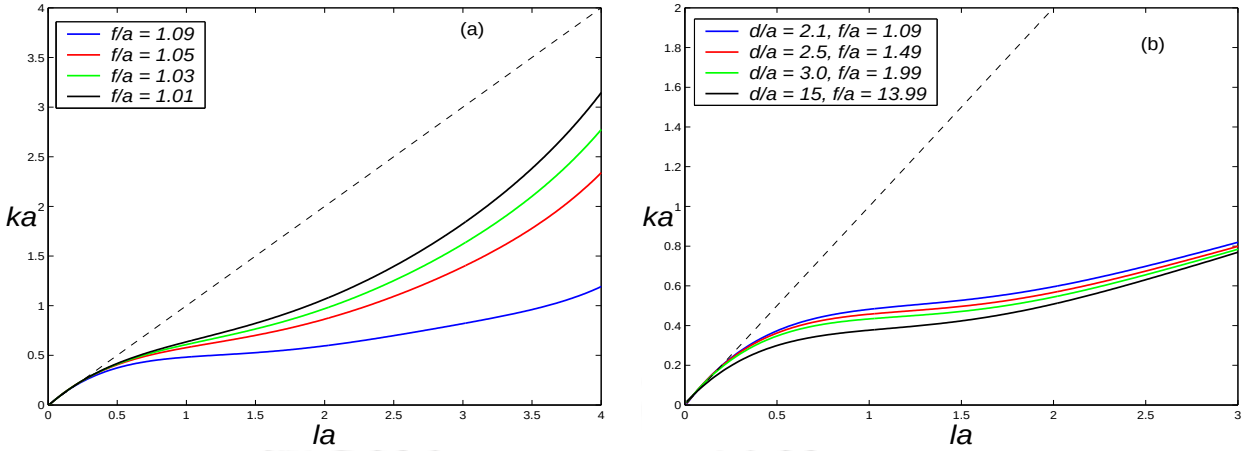

Figure 3.11: Trapped mode wavenumbers in a single-layer fluid; $D/a^4 = 0.001$; $\varepsilon/a = 0.001$ and $h/a = 6$ (a) for different submergence depths f/a; $d/a = 2.1$ (b) for different depths of the layer d/a; $(d - f)/a = 1.01$.

exists only for those values of la which are approximately greater than or equal to 0.8. When the upper surface of the cylinder just touches the ice cover, i.e, $f/a = 1.1$, then a second mode exists for $0.8 \leq la \leq 3.2$. The trapped mode wavenumber ka decreases by a small amount with an increase in depth. These results bear similarities to those corresponding to the first mode in Linton and Cadby (2003).

3.4.3 Cylinder submerged in the lower layer

Figures 3.12 and 3.13 show the trapped mode wavenumbers against the density ratio when the cylinder is placed in the lower layer. In both cases, the depth h/a of the lower layer is taken as 6.0 and the values of ice-parameters as $D/a^4 = 0.001$ and $\epsilon/a = 0.001$. In Fig. 3.12 the submergence depth f/a is taken as -1.01 which means that the cylinder is very close to the interface, and for Fig. 3.13, the height d/a of the upper layer is taken as 3.0.

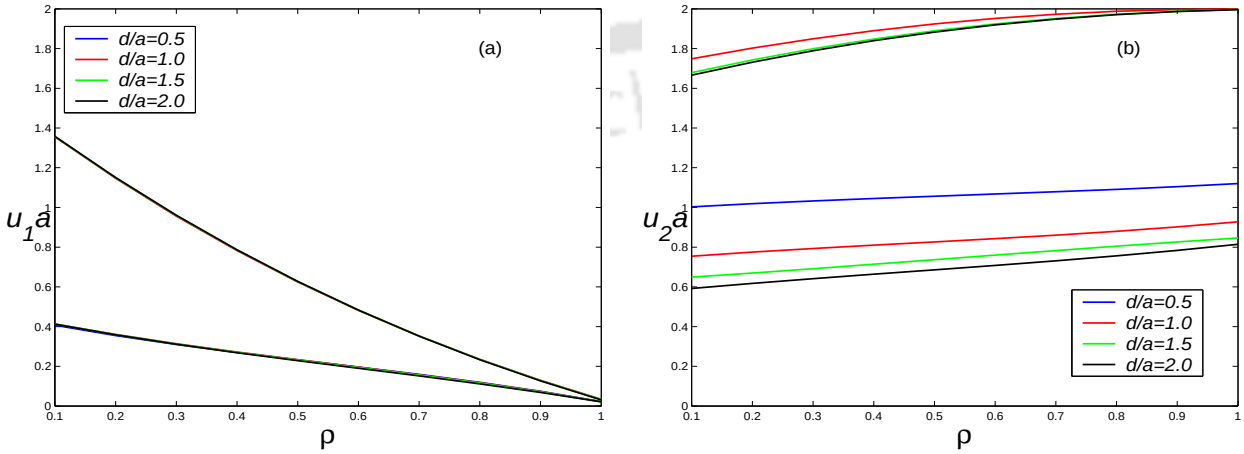

Figure 3.12: Trapped mode wavenumbers plotted against ρ for a cylinder of radius a in the lower fluid layer for different depths d/a of the upper layer; $la = 2$, $h/a = 6$, $f/a = -1.01$, $D/a^4 = 0.001$ and $\varepsilon/a = 0.001$.

Figure 3.12 shows the trapped mode wavenumbers against ρ when $la = 2$. Corresponding to the different depths of the upper layer: $d/a = 0.5$, 1.0, 1.5 and 2.0, there are two curves which correspond to the two modes for each of the wavenumbers u_1a and u_2a. For the wavenumber u_1a, these two modes tend to zero as $\rho \to 1$ for any depth of the upper layer. With a change in the depth of the upper layer, there is no variation of the two modes for the wavenumber u_1a but these two modes decrease with an increase in the depth of the upper layer for the wavenumber u_2a. For the wavenumber u_2a, as $\rho \to 1$, the first mode increases marginally to a fixed value corresponding to each depth of the upper layer and the second mode tends to $la = 2$.

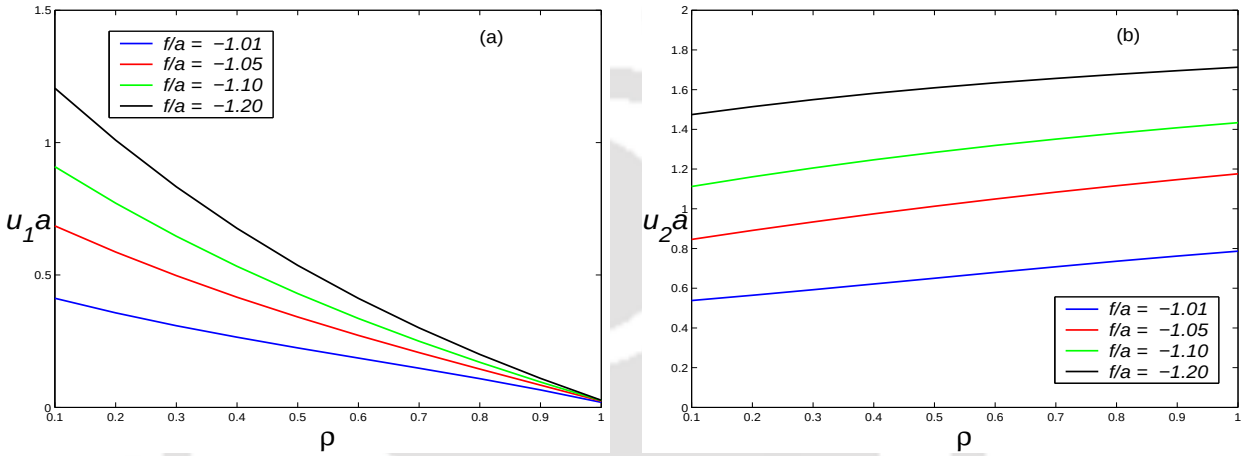

Figure 3.13: Trapped mode wavenumbers plotted against ρ for a cylinder of radius a in the lower fluid layer for different submergence depths f/a; $la = 2$, $h/a = 6$, $d/a = 3$, $D/a^4 = 0.001$ and $\varepsilon/a = 0.001$.

In Fig. 3.13, the different curves correspond to the different submergence depths of the cylinder: $f/a = -1.01$, -1.05, -1.10 and -1.20 for $la = 2$. As the submergence depth increases, i.e., the cylinder moves away from the interface, the second mode ceases to exist but the first mode always exists with the same properties as discussed above. As the submergence depth increases, both the wavenumbers u_1a and u_2a increase. For the wavenumber u_1a and for a small density ratio, the gap between two consecutive curves is more and as ρ increases towards the value 1, all the curves merge and tend to zero but for the wavenumber u_2a, the gap between two consecutive curves remains almost the same as the density ratio increases towards 1. The single-layer finite depth results for the depth h/a and the cylinder submergence depth f/a are recovered when $\rho = 0$ (with the interface now playing the role of the free surface) which are discussed in Linton and Cadby (2003).

Ursell (1951) established the existence of a trapped surface wave mode in the vicinity of a long and totally submerged horizontal circular cylinder of small radius in deep water. Throughout our numerical computation, we non-dimensionalize all the parameters with respect to the radius a of the cylinder. Therefore, our present work reveals that a single trapped mode appears to exist for all values of $a < |f|$ and not just when the radius of the cylinder is small.

Limit as $\rho \to 1$

Like in the rigid lid problem considered in Chapter 2, it is very likely to come to one's mind

that the single-layer fluid results may be obtained if the density ratio $\rho \to 1$. But from all the figures where trapped mode wavenumbers are plotted against the density ratio, we observe something intriguingly different. It is observed that corresponding to each set of parameter values, there are two curves corresponding to two modes for the wavenumber $u_2 a$. In the limit $\rho \to 1$, the second mode ceases to exist but the first mode tends to some value which represents a trapped mode. For the wavenumber $u_1 a$, both modes tend to zero as $\rho \to 1$. For the density ratios having values closer to 1, we have already seen that $u_2 > u_1 > K$. So, if $u_1 a \to 0$, we must have $Ka \to 0$ as $\rho \to 1$. Thus, for a cylinder in either fluid layer, though the first mode tends to some value for the wavenumber $u_2 a$, it certainly does not correspond to the one for a single-layer fluid because $Ka \to 0$. Hence, from our numerical investigations, we can conclude that it is not possible to recover the single-layer fluid results in the limit $\rho \to 1$. To explain this occurrence we consider the boundary conditions in the limit as $\rho \to 1$ and $K \to 0$ simultaneously.

Small parameters ϵ and δ are introduced such that (same as Eq. (2.28))

$$K = \epsilon, \qquad \rho = 1 - \delta, \qquad K' = \frac{K}{1-\rho} = \frac{\epsilon}{\delta} = O(1). \tag{3.31}$$

In this limit, the upper surface condition becomes

$$\frac{\partial \phi^{I}}{\partial z} = 0 \qquad \text{on} \qquad z = d. \tag{3.32}$$

The continuity condition of the vertical velocity at the interface and the bottom boundary condition remain the same but that of pressure at the interface changes and becomes

$$K' \phi^{II} - \frac{\partial \phi^{II}}{\partial z} = K' \phi^{I} \qquad \text{on} \qquad z = 0. \tag{3.33}$$

In the absence of any structure, oblique waves propagating in the fluid take the form

$$\phi^{I} = \exp(\pm ix\sqrt{k^2 - l^2})\left(e^{k(z-d)} + e^{-k(z-d)}\right), \tag{3.34}$$

$$\phi^{II} = \exp(\pm ix\sqrt{k^2 - l^2}) \cosh k(z+h) F(k), \tag{3.35}$$

with

$$F(k) = \frac{e^{-kd} - e^{kd}}{\sinh kh}, \tag{3.36}$$

where k is the only root of the dispersion relation

$$k(1 - e^{-2kd})(1 - e^{-2kh}) = 2K'(1 - e^{-2k(d+h)}). \tag{3.37}$$

In order that the trapped modes exist, it is required that $l > k$ so that the motion decays as $|x| \to \infty$. Thus for a fixed l, a boundary value problem is obtained in terms of a new spectral parameter K'. The trapped mode frequencies are computed by using the multipole expansion method. These results match with those observed from the figures in sections 3.4.2 and 3.4.3 when the density ratio approaches 1. Hence for a fixed l, the trapped mode problem in the limit $\rho \to 1$ is related to the limits of the trapped mode curves in these figures. But if we fix K and let $\rho \to 1$, then $u \to \infty$ from dispersion relation (3.15) and since $l > u$ for trapped modes, hence $l \to \infty$. Thus it is not possible to recover the single-layer fluid results in the limit $\rho \to 1$.

3.5 Conclusions

In the present chapter, the flexural gravity trapped modes are investigated in a two-layer fluid of finite depth. The dispersion relation is analyzed for various water depths and also for different submergence depths of a cylinder placed in either of the layers. For a fixed set of parameters, when the cylinder is submerged nearer the interface, there always exist two modes for the wavenumbers u_1a and u_2a. We also examine the variation of the trapped mode wavenumbers against the density ratio for different depths of the layers, for different submergence depths and also for different values of the ice-parameters. For a cylinder placed in the upper layer, the trapped motion is confined only to the vicinity of the ice-cover and the interface. We find that a trapped mode at the ice-cover gets transferred to the interface and vice-versa at the near crossing points. For each submergence depth, these near crossing points are also observed in the free surface problem but the positions of these points get shifted downwards due to the presence of the ice-cover. For the free surface problem, with the same depth of the upper layer, the existence of a third mode is observed from the submergence depth 1.07 onwards but for the ice-cover problem, a third mode exists only for the submergence depth 1.10. In other words, for the ice-cover problem, when the surface of the cylinder just touches the ice-cover, there exists a third mode but for the free surface problem, a third mode exists when the cylinder is nearer to the free surface. When an ice-cover replaces a free surface, the wavenumbers u_1a and u_2a of the trapped modes increase. It is also observed that with an increase in flexural rigidity, the ice-cover behaves more like a rigid lid and for that there exists only one mode for both the wavenumbers which is very similar to the modes found in the rigid lid problem in Chapter 2. Hence it can be concluded that when the cylinder is placed in the upper layer, the trapped mode wavenumbers always exist but they do so below a certain cut-off value of the frequency only.

For the case when the cylinder is placed in the lower layer, the motion is confined to the vicinity of the interface only. As the cylinder gets shifted downwards, higher trapped mode wavenumbers disappear. If the cylinder is shifted further towards the bottom, lower trapped modes also cease to exist. Hence for a fixed geometrical configuration and a specific arrangement of a set of other parameters, there is a fixed submergence depth above which no trapped mode exists and it is possible to formulate a scattering problem due to the interaction of an obliquely incident wave with the cylinder. But below that submergence depth, there exist trapped modes which are associated with some cut-off values. In this case also, periodic motions are, above that cut-off value, uniquely defined by the prescribed boundary conditions along with a radiation condition at infinity. When the density ratio tends to zero, the problems in a two-layer fluid can be compared with those in a single-layer fluid. In this limit the trapped mode problem reduces to a finite depth single-layer fluid problem bounded above by a free surface or a thin ice-cover, depending on whether the cylinder is placed in the lower or the upper layer, respectively. That the single-layer results cannot be recovered when the density ratio tends to 1 is also discussed.

The evidence of the existence of trapped modes for our present problem will allow the corresponding scattering problem to be solved under restrictions as mentioned above. The consideration of finite depth for both the fluids with ice-cover makes the problem physically

more acceptable. However, the observations will hold even if the lower layer is of infinite depth. The present study is expected to facilitate the analysis of various physical problems in ocean engineering besides other branches of mathematical physics, where higher-order boundary conditions arise in a natural way.

Chapter 4

Elastic bottom effect on trapped waves in a two-layer fluid

4.1 Introduction

The understanding of the free vibration characteristics of the fluid-structure interaction plays a significant role in various branches of engineering, for example, very large floating oil storage tanks, ships and submarines can avoid or be subjected to reduced localized vibrations. The objective of our present work is to replace the usual rigid and flat bottom for a two-layer fluid flow by an elastic bottom and then to examine its effect on trapped modes. To the best of our knowledge, no investigation of trapped mode for such type of sea-bed has taken place till date. Due to the elastic bed topography, the linearized bottom boundary condition at the bed becomes a fifth order one unlike a simple homogenous Neumann condition satisfied in the case of a rigid bed. The effects of the depth of the layers, the submergence depth and the elastic plate parameters on trapped modes are examined. The special case of trapped modes supported by a horizontal circular cylinder in a homogenous fluid with an elastic bottom is also presented.

4.2 Mathematical formulation of the problem

We consider here a two-layer fluid flowing over an elastic bottom. We also assume that the thickness of the elastic bottom, considered as a thin elastic plate obeying Euler-Bernoulli beam equation, is small compared to the wavelength of the incident wave. The problem is formulated in three-dimensional Cartesian coordinate system with the xy-plane in the horizontal direction and the z-axis in the vertically upward positive direction (Fig. 4.1). The upper fluid layer of constant density $\rho_{_I}$ occupies the region $-\infty < x < \infty$, $-\infty < y < \infty$, $0 < z < d$ with $z = d$ as the mean position of the free surface. The lower fluid of constant density $\rho_{_{II}}$ occupies the region $-\infty < x < \infty$, $-\infty < y < \infty$, $-h < z < 0$ with $z = 0$ as the mean position of the interface and $z = -h$ as the mean position of the elastic plate. Let $\chi(x, y, t)$ be the deflection of the elastic plate which has the form $\chi(x, y, t) = \mathrm{Re}[\bar{\chi}(x)e^{ily}e^{-i\omega t}]$. We further assume that the fluid is inviscid, incompressible and immiscible, the motion is irrotational and simple harmonic in time with radian frequency ω. The effect due to the surface tension at the free surface and interface is neglected.

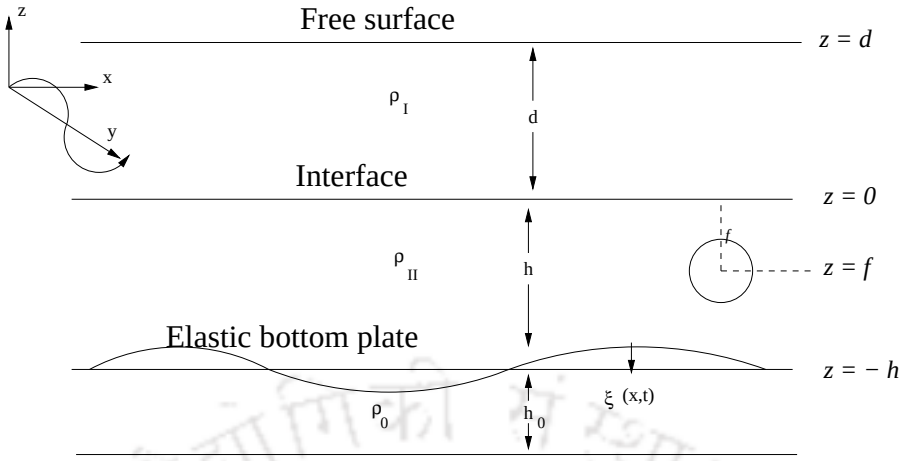

Figure 4.1: Schematic diagram for elastic bottom plate in finite water depth two-layer fluid.

We consider $\Phi^{I}(x,y,z,t)$ and $\Phi^{II}(x,y,z,t)$ to be the time-dependent velocity potentials corresponding to the upper and lower fluid layers respectively. Then for oblique waves, they can be written in the form

$$\Phi^{j}(x,y,z,t) = \mathrm{Re}[\phi^{j}(x,z)e^{ily}e^{-i\omega t}], \qquad j = I, II.$$

The governing equation for the boundary value problems involving these spatial potentials $\phi^{I}(x,z)$ and $\phi^{II}(x,z)$ is the modified Helmholtz equation

$$\left(\nabla^2_{x,z} - l^2\right)\phi^{j} = 0 \qquad \text{in the respective fluid regions.} \tag{4.1}$$

The linearized free surface boundary condition at the mean free surface $z = d$ is given by

$$\frac{\partial \phi^{I}}{\partial z} - K\phi^{I} = 0 \qquad \text{on} \qquad z = d. \tag{4.2}$$

The ratio of the densities, $\rho_{I}/\rho_{II}(< 1)$, is denoted by ρ. The linearized boundary condition at the mean interface $z = 0$ is given by

$$\frac{\partial \phi^{I}}{\partial z} = \frac{\partial \phi^{II}}{\partial z} \qquad \text{on} \qquad z = 0, \tag{4.3}$$

$$\rho\left(\frac{\partial \phi^{I}}{\partial z} - K\phi^{I}\right) = \frac{\partial \phi^{II}}{\partial z} - K\phi^{II} \qquad \text{on} \qquad z = 0. \tag{4.4}$$

Boundary conditions (4.3) and (4.4), respectively, represent the continuity of the normal velocity and pressure at the interface between the two layers. The linearized bottom boundary condition is

$$\left[D\left(\frac{\partial^2}{\partial x^2} - l^2\right)^2 + 1 - \varepsilon K\right]\frac{\partial \phi^{II}}{\partial z} - K\phi^{II} = 0 \qquad \text{on} \qquad z = -h. \tag{4.5}$$

All the quantities considered here are same as those for the ice-cover problem in Chapter 3. The bottom boundary condition (4.5) is same as the ice-cover condition (3.7) used in Chapter 3 though it is used in different contexts in both the problems.

Within this framework, progressive waves or incident waves take the form (up to an arbitrary multiplicative constant)

$$\phi^{I} = \exp(\pm ix\sqrt{u^2-l^2})[(u+K)e^{u(z-d)}+(u-K)e^{-u(z-d)}], \tag{4.6}$$
$$\phi^{II} = \exp(\pm ix\sqrt{u^2-l^2})[F_+(u)e^{u(z+h)}+F_-(u)e^{-u(z+h)}]g(u), \tag{4.7}$$

where

$$F_\pm(u) = (Du^4+1-\varepsilon K)u \pm K, \tag{4.8}$$
$$g(u) = \frac{(u+K)e^{-ud}-(u-K)e^{ud}}{F_+(u)e^{uh}-F_-(u)e^{-uh}}, \tag{4.9}$$

with u satisfying the dispersion relation

$$(u^2-K^2)F_-(u)e^{-2uh}-(u-K\sigma)(u-K)F_+(u)+(u^2-K^2)F_+(u)e^{-2ud} \tag{4.10}$$
$$-(u+K)(u+K\sigma)F_-(u)e^{-2u(d+h)}=0,$$

where $u=0$ is a root of this equation.

For a fixed geometrical configuration and fixed values of the density ratio, Eq. (4.10) has exactly two positive real roots u_1 and u_2 ($u_1<u_2$, say) corresponding to a value of K.

For the existence of trapped modes, the following are required to be valid:

$$\phi^{I},\phi^{II},|\nabla\phi^{I}|,|\nabla\phi^{II}|\to 0 \quad \text{as} \quad |x|\to\infty \tag{4.11}$$

and hence l is restricted to be in the range $l>u_2>u_1>K>0$ which ensures that no wave propagation to infinity takes place on both the free surface and the interface.

4.3 Solutions by multipoles

In the previous section, we presented the expression of velocity potentials for the progressive or incident wave. Now, we introduce an obstacle into the fluid in the form of a horizontal circular cylinder to examine the trapped waves by the obstacle. The radius of the cylinder is taken as a; its axis along $z=f$, $|f|>a$; its generator parallel to the y-axis and it is totally submerged in either of the layers. It is to be noted that the elasticity of the bed does not get affected by the pressure exerted by the cylinder. Because of the presence of the cylinder, in addition to the incident potential, now a diffracted potential also enters into the picture and hence the total velocity potential satisfies all the boundary conditions (4.2)–(4.5) along with the governing equation (4.1). The total complex velocity potential ϕ also satisfies the body boundary condition in either of the layers:

$$\frac{\partial\phi}{\partial r}=0 \qquad \text{on} \qquad r=a. \tag{4.12}$$

Considering the origin of the rectangular Cartesian coordinates at the mean position of the axis of the cylinder, polar coordinates (r,θ) are defined as

$$x=r\sin\theta \text{ and } z=f-r\cos\theta.$$

4.3.1 Cylinder submerged in the lower layer

At first we consider the cylinder to be placed in the lower layer and hence $f < 0$. Now, following the method of Kassem (1982), multipoles which are singular at $(0, f)$ and symmetric about $x = 0$, are constructed. The total potential is then taken as a linear combination of all the possible multipoles. Subsequent application of the body boundary condition (4.12) results in an infinite system of homogenous linear equations.

Symmetric multipoles about the line $x = 0$, $\phi_n^{II}\,(n \geq 0)$, are defined by

$$\phi_n^{I} = \int_0^\infty \cosh nu \cos(lx \sinh u)\Big[A_L(v)e^{vz} + B_L(v)e^{-vz}\Big]du, \tag{4.13}$$

$$\phi_n^{II} = K_n(lr)\cos n\theta + \int_0^\infty \cosh nu \cos(lx \sinh u)\Big[C_L(v)e^{vz} + D_L(v)e^{-vz}\Big]du, \tag{4.14}$$

where $v = l\cosh u$.

With the help of the boundary conditions, the coefficients $A_L(v)$, $B_L(v)$, $C_L(v)$ and $D_L(v)$ appearing in Eqns. (4.13) and (4.14) are obtained as

$$\begin{aligned}
A_L(v) &= \frac{v+K}{v-K}e^{-2vd}B_L(v),\\
B_L(v) &= \frac{K(1+\sigma)(v-K)}{G(v)}\Big[(-1)^n F_+(v)e^{vf} + F_-(v)e^{-v(f+2h)}\Big],\\
C_L(v) &= \frac{v+K}{v-K}\frac{B_L(v)}{K(1+\sigma)}\Big[(v+K\sigma)e^{-2vd} - (v-K)\Big],\\
D_L(v) &= \frac{F_+(v)}{F_-(v)}\Big[C_L(v) + e^{-vf}\Big]e^{-2vh},
\end{aligned}$$

where

$$\begin{aligned}
G(v) &= (v^2-K^2)F_-(v)e^{-2vh} - (v-K\sigma)(v-K)F_+(v)\\
&+ (v^2-K^2)F_+(v)e^{-2vd} - (v+K)(v+K\sigma)F_-(v)e^{-2v(d+h)}.
\end{aligned} \tag{4.15}$$

It is to be noted that $G(v) = 0$ is the dispersion relation in the variable v which is same as Eq. (4.10) and consequently $v = u_1$ and $v = u_2$ are simple zeros of $G(v)$. Therefore, all the integrals in Eqs. (4.13) and (4.14) have simple poles at $v = u_1$, $v = u_2$ and $v = 0$. But by using the trapped mode condition (4.11) and noting that $v > l$, we get $v > l > u_2 > u_1 > K > 0$ which implies that there will be no singularities of the integrand on the real axis.

The total velocity potential ϕ can now be written as

$$\phi = \sum_{n=0}^{\infty} \alpha_n \phi_n^{II}, \tag{4.16}$$

with

$$\phi_n^{II} = K_n(lr)\cos n\theta + \sum_{m=0}^{\infty} A_{mn} I_m(lr)\cos m\theta, \tag{4.17}$$

where

$$A_{mn} = (-1)^m \epsilon_n \int_0^\infty \cosh mu \cosh nu\Big[(-1)^n C_L(v)e^{vf} + D_L(v)e^{-vf}\Big]\,du. \tag{4.18}$$

Applying the body boundary condition (4.12), we obtain an infinite system of linear equations in the unknowns α_n:

$$\alpha_n + \frac{I_n'(la)}{K_n'(la)} \sum_{m=0}^{\infty} \alpha_m A_{mn} = 0, \qquad n = 0, 1, 2, \ldots \tag{4.19}$$

where $'$ denotes differentiation with respect to r.

This is the system whose non-trivial solutions will determine the trapped wave due to the presence of a horizontal circular cylinder as mentioned above. For a fixed geometrical configuration and fixed density ratio, this system of equations is completely dependent on the two non-dimensional parameters Ka and la. For a fixed value of la, the non-trivial solutions of the unknown coefficients will exist if the value of the determinant vanishes for a certain value of Ka. This value of Ka will then correspond to a trapped mode frequency. Trapped wavenumbers u_1a and u_2a can also be determined corresponding to those values of Ka by using dispersion relation (4.10). The results presented below are obtained correct up to three decimal places.

Numerical Results

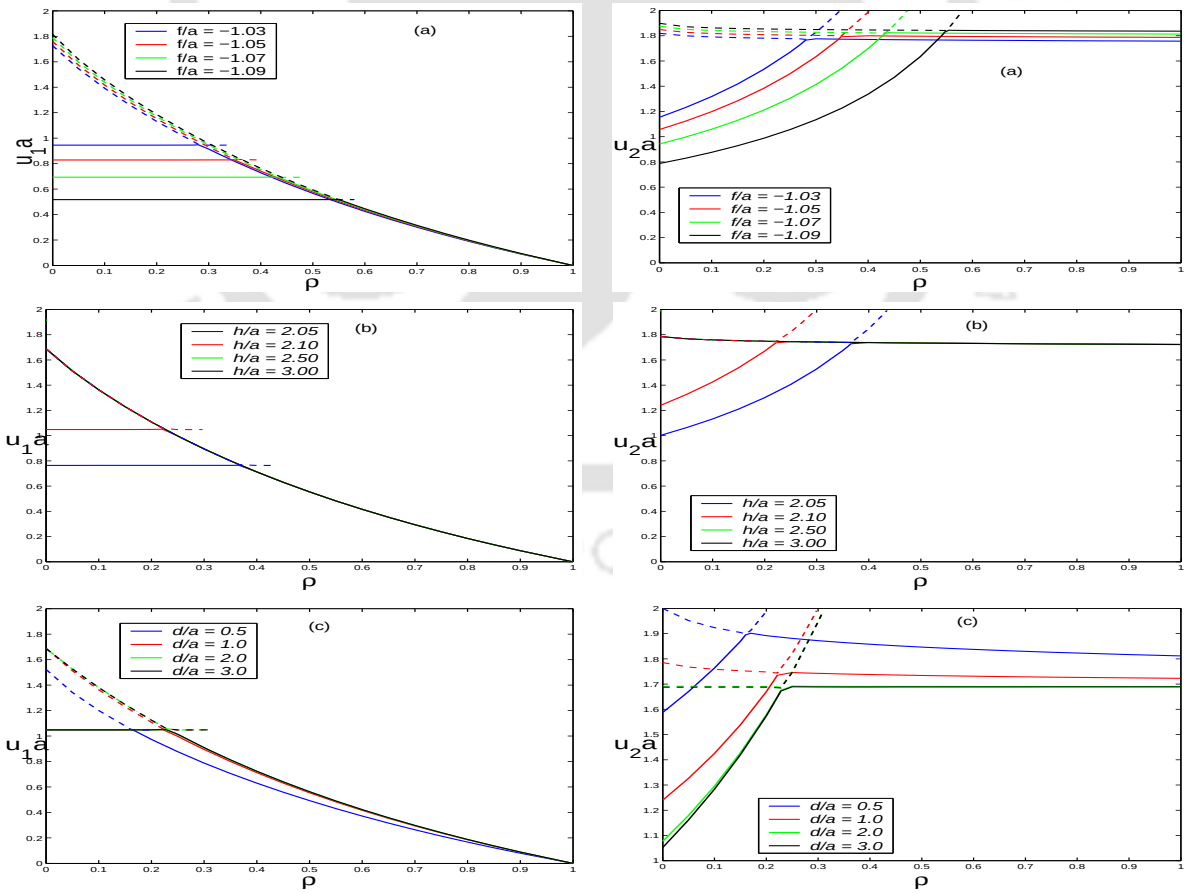

Figure 4.2: Trapped mode wavenumbers versus ρ for a cylinder of radius a in the lower fluid layer for different (a) submergence depths f/a, (b) depths h/a of the lower layer, (c) depths d/a of the upper layer; $la = 2$, $D/a^4 = 0.001$ and $\varepsilon/a = 0.001$.

Graphical results presented in Fig. 4.2 illustrate the effects of density ratio on trapped mode wavenumbers for the cylinder placed in the lower layer. The pair of graphs in Fig. 4.2(a) gives the plot for different values of the submergence depth f/a when $h/a = 2.1$ and $d/a = 1.0$, the one in Fig. 4.2(b) for different depths h/a of the lower layer with $f/a = -1.01$ and $d/a = 1.0$. For different depths d/a of the upper layer, the plots shown in the pair of graphs in Fig. 4.2(c) correspond to $f/a = -1.01$ and $h/a = 2.1$. Corresponding to each value of the submergence depth, two trapped modes exist for both wavenumbers u_1a and u_2a as is observed from Fig. 4.2(a). With an increase in ρ, the first and second modes come closer to each other at near crossing points. Then, the second modes disappear and the first modes tend to some finite value as $\rho \to 1$. For the wavenumber u_1a, this value is zero and thus also for Ka since $Ka < u_1a$. Linton and Cadby (2003) reported the existence of near crossing points for the case of the cylinder placed in the upper layer. But now in addition, we also observe these points even when the cylinder is placed in the lower layer which is bounded by an elastic bottom. Fig. 4.2(b) demonstrates that with an increase in the depth of the lower layer, only one trapped mode exists which tends to the same value as $\rho \to 1$ irrespective of the values of the depth of the lower layer. Considering the lower layer to be of infinite depth with $d/a = 2.1$, $f/a = -1.01$ and $la = 2$, Linton and Cadby (2003) showed the existence of two trapped modes. If we consider a finite depth lower layer over an elastic bottom, two modes exist for a small width of the lower layer and then as the distance of the plate from the cylinder increases, only one mode exists. Existence of two trapped modes does not depend on the variation of the depth d/a of the upper layer but values of those modes vary with an increase in d/a as can be seen in Fig. 4.2(c).

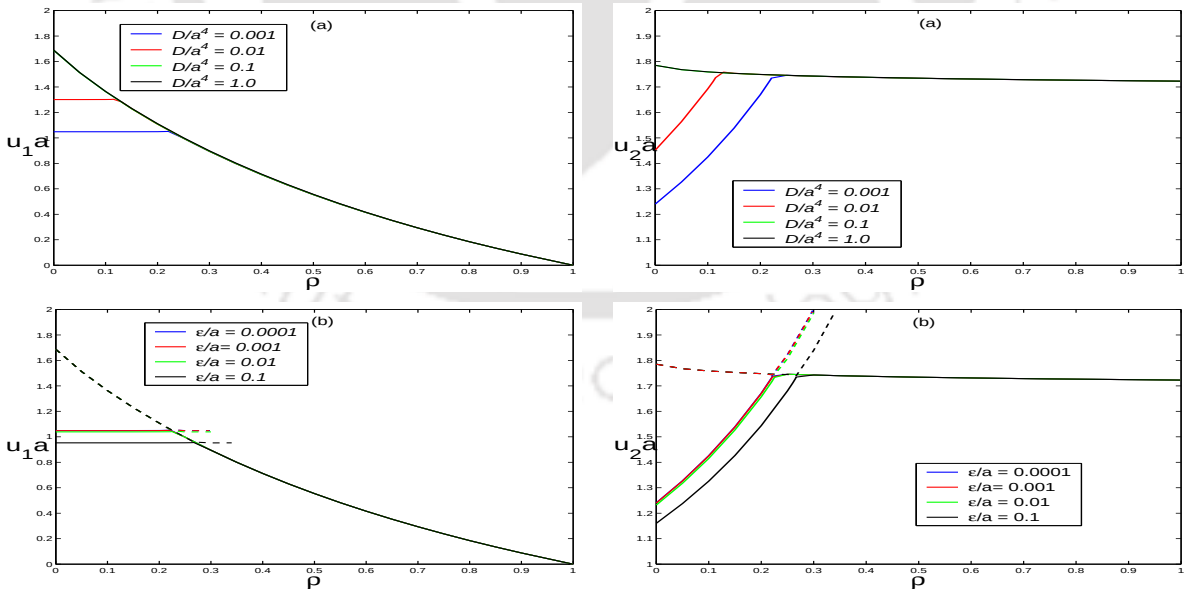

Figure 4.3: Trapped mode wavenumbers versus ρ for a cylinder of radius a in the lower fluid layer for different values of D/a^4 and ε/a; $la = 2$, $h/a = 2.1$, $d/a = 1$ and $f/a = -1.01$.

In Figs. 4.3(a) and 4.3(b), trapped mode wavenumbers are plotted for different values of elastic plate parameters, i.e., for different values of D/a^4 and ε/a. Flexural rigidity D/a^4 also affects trapped modes as is observed from Fig. 4.3(a). An increase in flexural rigidity

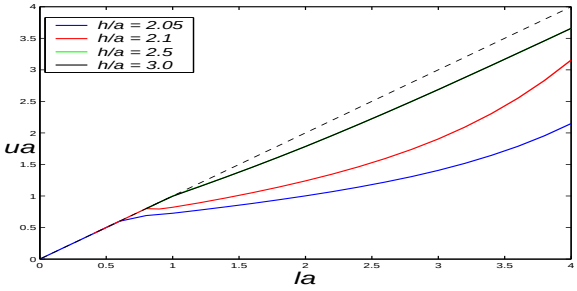

Figure 4.4: Dispersion curves for a cylinder of radius a placed in the lower layer for different depths h/a of the lower layer; $D/a^4 = 0.001$, $\varepsilon/a = 0.001$, $\rho = 0$, $h/a = 3.0$ and $d/a = 1.0$.

suppresses the existence of the second mode. But ε/a does not have any appreciable effect on the modes except for the case $\varepsilon/a = 0.1$ as presented in Fig. 4.3(b). Because of the presence of the elastic plate, the values of the wavenumbers $u_1 a$ and $u_2 a$ increase.

When we take $\rho = 0$, the present case of the cylinder in the lower layer gets converted to that in a homogenous fluid over an elastic bottom. Investigation of trapped modes for a single-layer fluid over an elastic bottom has also not been reported till date. We show the dispersion curves for the case with the cylinder nearer to the free surface (here the interface plays the role of the free surface). The existence of trapped mode requires $l > k$ so that $l = k$ (thin dashed line) gives an upper bound for the curves in Fig. 4.4. As the depth of the lower layer decreases, the curve folds out from the upper bound. For a homogenous fluid also, the presence of the elastic plate results in only one mode as compared to the existence of two modes for the case with a rigid and flat bottom.

4.3.2 Cylinder submerged in the upper layer

Now the problem is considered with the cylinder placed in the upper layer. We are required to modify the multipoles singular at $z = f(> 0)$. This can be done in the same manner as was done previously for the case of the cylinder located in the lower layer ($f < 0$). The suitable symmetric multipoles now are

$$\phi_n^I = \int_0^\infty \cosh nu \cos(lx \sinh u) \Big[A_U(v)e^{vz} + B_U(v)e^{-vz}\Big] du, \tag{4.20}$$

$$\phi_n^{II} = K_n(lr)\cos n\theta + \int_0^\infty \cosh nu \cos(lx \sinh u) \Big[C_U(v)e^{vz} + D_U(v)e^{-vz}\Big] du, \tag{4.21}$$

where the integrals are Cauchy Principal Value integrals with

$$A_U(v) = \frac{v+K}{v-K} e^{-2vd}[B_U(v) + (-1)^n e^{vf}],$$

$$B_U(v) = \frac{(v+K\sigma)F_-(v)e^{-2vh} - (v-K)F_+(v)}{G(v)} \Big[(v-K)e^{-vf} + (-1)^n (v+K)e^{v(f-2d)}\Big],$$

$$C_U(v) = \frac{K(\sigma-1)B_U(v)F_+(v)}{(v+K\sigma)F_-(v)e^{-2vh} - (v-K)F_+(v)},$$

$$D_U(v) = \frac{F_-(v)}{F_+(v)} e^{-2vh} C_U(v),$$

where $G(v)$ is same as in Eq. (4.15). Here also, due to the trapped mode condition, there will be no singularities on the real axis. The polar expansion of the multipoles, following the

previous procedure, is

$$\phi_n^I = K_n(lr)\cos n\theta + \sum_{m=0}^{\infty} B_{mn} I_m(lr)\cos m\theta, \tag{4.22}$$

where

$$B_{mn} = \epsilon_n \int_0^{\infty} \cosh mu \cosh nu \Big[(-1)^n A_L(v)e^{vf} + B_L(v)e^{-vf}\Big]\, du. \tag{4.23}$$

By applying the body boundary condition (4.12), a similar kind of system of equations like (4.19) is obtained for β_n as follows:

$$\beta_n + \frac{I_n'(la)}{K_n'(la)} \sum_{m=0}^{\infty} \beta_m B_{mn} = 0, \qquad n = 0, 1, 2, ... \tag{4.24}$$

Here also, as in the previous case, a frequency will correspond to a trapped mode if the determinant of the system vanishes corresponding to that value. For the sake of numerical computation of the trapped mode frequency, we truncate each of the systems (4.19) and (4.24) to a 32×32 system. Then, for a fixed value of la, the parameter Ka is varied in such a way that the roots of the dispersion equation never cross la. With this variation of Ka, we locate the zeros of the truncated determinant.

Numerical Results

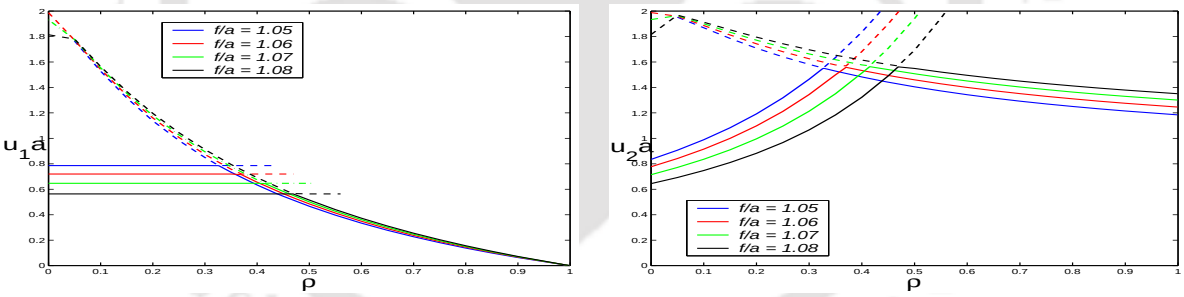

Figure 4.5: Trapped mode wavenumbers versus ρ for a cylinder of radius a in the upper fluid layer for different submergence depths f/a; $D/a^4 = 0.001$, $\varepsilon/a = 0.001$, $la = 2$, $h/a = 3.0$ and $d/a = 2.1$.

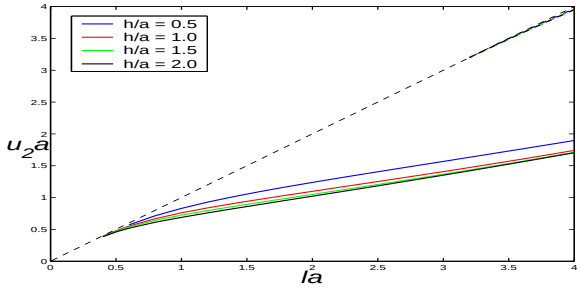

Figure 4.6: Dispersion curves for a cylinder of radius a placed in the upper layer for different depths h/a of the lower layer; $D/a^4 = 0.001$, $\varepsilon/a = 0.001$, $\rho = 0.5$, $f/a = 1.01$ and $d/a = 3.0$.

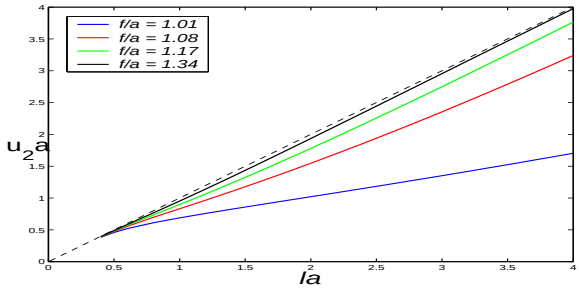

Figure 4.7: Dispersion curves for a cylinder of radius a placed in the upper layer for different submergence depths f/a; $D/a^4 = 0.001$, $\varepsilon/a = 0.001$, $\rho = 0.5$, $h/a = 3.0$ and $d/a = 3.0$.

Figure 4.5 displays the trapped modes for different submergence depths. This result agrees well with the trapped mode wavenumber of Fig. 5 in Linton and Cadby (2003) with an infinite depth lower layer. Figure 4.6 shows the dispersion curves for the case with the cylinder placed nearer to the interface for different depths of the lower layer. The upper bound $u_2 = l$ is included and shown by a thin dashed line. Corresponding to each value of h/a, there are two curves showing the first and the second modes. We notice that as the depth of the lower layer increases, both trapped modes decrease but the first mode gets more affected. By fixing d/a, h/a and ρ, and varying the submergence depth, we can find different numbers of modes. As f/a approaches the value -1, we observe a fanning out of the curves as higher modes appear, in an identical manner as was observed in the results of Linton and Cadby (2003). Since the cylinder is placed in the upper layer at a reasonable distance away from the elastic bottom, there is no significant effect of the bottom on trapped mode wavenumbers and hence the results bear similarity with the ones in the work of Linton and Cadby (2003).

4.4 Conclusions

A two-layer incompressible fluid flowing over an elastic bottom is considered. The thickness of the elastic plate is assumed to be small as compared to the wavelengths. Based on the small amplitude wave theory and by using multipole expansion method, we examine the effect of the elastic bottom on trapped modes. We also demonstrate the effects of the other parameters such as depths of the upper and lower layers and submergence depth of the cylinder on trapped modes.

For the case of the cylinder placed in the lower layer, the trapped modes get significantly affected in the presence of the elastic bed at the bottom which suppresses the existence of the second mode which is clearly a different inference compared to the case of infinite depth lower layer. Both trapped mode wavenumbers increase due to the consideration of the elasticity of the sea-bed as against when a flat and rigid bed is considered. For the case of the cylinder placed in the upper layer, the elasticity of the bottom does not produce considerable effect and hence the corresponding results bear similarity with the hydrodynamic set up of a two-layer fluid of infinite depth.

By placing the cylinder in the lower layer and considering the density ratio $\rho = 0$, we show that the problem of trapped modes in a finite depth single-layer fluid flowing over an

elastic bottom can be recovered. All these modes discussed in this work occur at frequencies below a cut-off value. Their occurrence indicates that large amplitude motions of the fluid and structure(s) are possible when the system is forced at a frequency close to that of the trapped mode. The solutions to problems related to trapped water wave in a two-layer fluid, with both layers of finite depth, over an elastic bottom topography have not been investigated by anyone earlier. It is hoped that the results obtained here can be used quantitatively for this kind of problems.

Chapter 5

Trapped modes in a three-layer fluid

5.1 Introduction

Though Chakrabarti et al. (2005) showed the existence of trapped modes in a three-layer fluid, they did not provide any numerical justification as is available for a two-layer case. This motivates us to consider the same set-up and to investigate the existence of trapped modes in a three-layer fluid by providing numerical evidence. In this chapter, a three-layer fluid is considered in which each layer has a distinct constant density. The upper and the middle layers are considered to be of finite depth while the lower layer is of infinite depth. The set-up that we consider here is basically a simple representation of a smooth pycnocline between two layers. A pycnocline is a layer in an ocean or any other body of water in which water density increases rapidly with depth. The set-up will be more realistic if the middle layer is linearly stratified instead of having constant density. The objective of the present work is to investigate the existence of trapped modes and the effect of the width of the middle layer when a submerged horizontal circular cylinder is placed in either the lower or the upper layer of the three-layer fluid. The solution is based on the multipole expansion method adopted by Kassem (1982) in which the singular solutions of the modified Helmholtz equation are modified to include all the prescribed boundary conditions.

The generalized problem considered here contains two parameters ρ and ρ^*, representing the ratios of the densities of the adjacent layers of the three-layer fluid under consideration. For the hydrodynamic set-up considered here, three different trapped waves are developed: one at the free surface corresponding to the lowest wavenumber and the other two at the internal interfaces corresponding to the other two wavenumbers. Two-layer fluid results are recovered by taking either ρ or ρ^* to be zero. The effects of the width of the middle layer and the submergence depth on the dispersion curves and the trapped modes are discussed.

5.2 Mathematical formulation of the problem

Under the usual assumptions of linear water wave theory, the proposed problem is considered in three-dimensional Cartesian coordinate system with the xy-plane in the horizontal direction and the z-axis in the vertically upward direction. We consider a three-layer inviscid, incompressible and immiscible fluid in which the lower layer is of infinite depth. The topmost layer W^I contains fresh water of density ρ_I and has depth $(h-d)$ with $z=h$ as the mean position

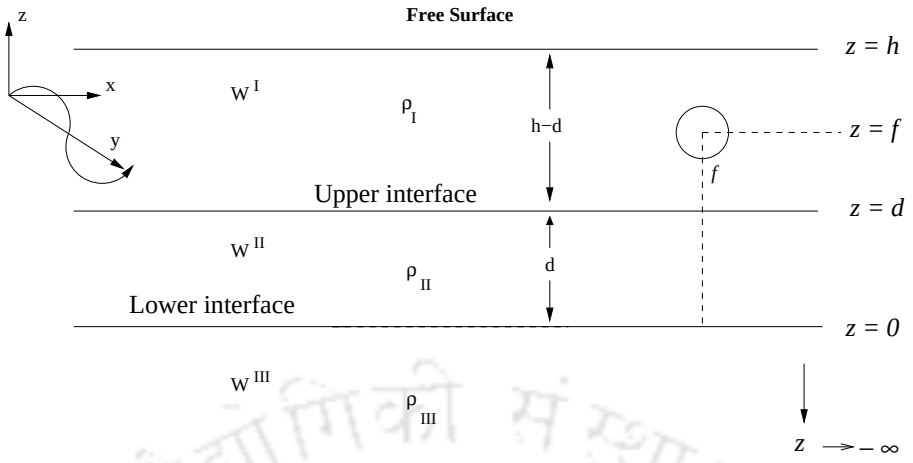

Figure 5.1: Cross-sectional view of a three-layer fluid of infinite depth.

of the free surface. The middle layer W^{II} consists of salt water of constant density ρ_{II} and has depth $d > 0$ with $z = d$ as the mean position of the interface between the middle and top layers. The bottom (lowermost) layer W^{III} contains muddy water of constant density ρ_{III} and is of infinite depth with $z = 0$ as the mean position of the interface between the bottom and the middle layers (Fig. 5.1). The effect due to surface tension at the free surface and both the interfaces is neglected.

Let $\Phi^{I}(x, y, z, t)$, $\Phi^{II}(x, y, z, t)$ and $\Phi^{III}(x, y, z, t)$ be the time-dependent velocity potentials corresponding to the irrotational motion of the fresh, salty and muddy water respectively. Then for oblique waves, they can be written in the form

$$\Phi^{I}(x, y, z, t) = \mathrm{Re}[\phi^{I}(x, z)e^{ily}e^{-i\omega t}],$$
$$\Phi^{II}(x, y, z, t) = \mathrm{Re}[\phi^{II}(x, z)e^{ily}e^{-i\omega t}],$$
$$\Phi^{III}(x, y, z, t) = \mathrm{Re}[\phi^{III}(x, z)e^{ily}e^{-i\omega t}],$$

where $\phi^{I}(x, z)$, $\phi^{II}(x, z)$ and $\phi^{III}(x, z)$, respectively, are complex-valued potential functions for the fresh, salty and muddy water. The governing equation for the boundary value problems involving spatial potentials $\phi^{I}(x, z)$, $\phi^{II}(x, z)$ and $\phi^{III}(x, z)$ in three layers is the modified Helmholtz equation

$$\left(\nabla^2_{x,z} - l^2\right)\phi^{I} = 0 \quad \text{in} \quad -\infty < x < \infty,\ d < z < h, \tag{5.1}$$
$$\left(\nabla^2_{x,z} - l^2\right)\phi^{II} = 0 \quad \text{in} \quad -\infty < x < \infty,\ 0 < z < d, \tag{5.2}$$
$$\left(\nabla^2_{x,z} - l^2\right)\phi^{III} = 0 \quad \text{in} \quad -\infty < x < \infty,\ -\infty < z < 0. \tag{5.3}$$

Denoting the ratio $\rho_{I}/\rho_{II}(< 1)$ of the densities of the fresh and salty water by ρ and that $\rho_{II}/\rho_{III}(< 1)$ of the densities of the salty and muddy water by ρ^*, the linearized boundary and

matching conditions at the free surface and both interfaces are

$$\frac{\partial \phi^I}{\partial z} - K\phi^I = 0 \qquad \text{on} \qquad z = h, \tag{5.4}$$

$$\frac{\partial \phi^I}{\partial z} = \frac{\partial \phi^{II}}{\partial z} \qquad \text{on} \qquad z = d, \tag{5.5}$$

$$\rho\Big(\frac{\partial \phi^I}{\partial z} - K\phi^I\Big) = \frac{\partial \phi^{II}}{\partial z} - K\phi^{II} \qquad \text{on} \qquad z = d, \tag{5.6}$$

$$\frac{\partial \phi^{II}}{\partial z} = \frac{\partial \phi^{III}}{\partial z} \qquad \text{on} \qquad z = 0, \tag{5.7}$$

$$\rho^*\Big(\frac{\partial \phi^{II}}{\partial z} - K\phi^{II}\Big) = \frac{\partial \phi^{III}}{\partial z} - K\phi^{III} \qquad \text{on} \qquad z = 0. \tag{5.8}$$

Equation (5.4) is the combined linearized dynamic and kinematic boundary condition on the free surface. Boundary conditions (5.5) and (5.6), respectively, represent the continuity of normal velocity and pressure at the upper interface $z = d$. Similarly, boundary conditions (5.7) and (5.8) arise due to the same reason at the lower interface $z = 0$.

Since the lower layer is of infinite depth, therefore the following limiting values hold:

$$\phi^{III}, |\nabla \phi^{III}| \to 0 \quad \text{as} \quad z \to -\infty. \tag{5.9}$$

Within this framework, progressive waves or incident waves take the form (up to an arbitrary multiplicative constant)

$$\phi^I = \exp(\pm ix\sqrt{u^2 - l^2})[A_1 e^{uz} + e^{-uz}], \tag{5.10}$$

$$\phi^{II} = \exp(\pm ix\sqrt{u^2 - l^2})[A_2 e^{uz} + B_2 e^{-uz}], \tag{5.11}$$

$$\phi^{III} = \exp(\pm ix\sqrt{u^2 - l^2}) A_3 e^{uz}, \tag{5.12}$$

where

$$A_1 = \frac{u + K}{u - K} e^{-2uh}, \tag{5.13}$$

$$A_2 = \frac{u + K}{u - K} \frac{1}{K(1 + \sigma)} \Big[(u + K\sigma)e^{-2uh} - (u - K)e^{-2ud}\Big], \tag{5.14}$$

$$B_2 = \frac{\Big[(u + K)e^{-2u(h-d)} - (u - K\sigma)\Big]}{K(1 + \sigma)}, \tag{5.15}$$

$$A_3 = A_2 - B_2, \tag{5.16}$$

and either $u = K$ or u satisfies the dispersion relation

$$(u+K)(u+K\sigma)e^{-2uh} - (u^2 - K^2)e^{-2ud} - (u+K)(u-K\sigma^*)e^{-2u(h-d)} + (u-K\sigma)(u-K\sigma^*) = 0, \tag{5.17}$$

with $\sigma = (1 + \rho)/(1 - \rho)$ and $\sigma^* = (1 + \rho^*)/(1 - \rho^*)$.

For a fixed geometrical configuration and fixed values of both density ratios, Eq. (5.17) has exactly two positive real roots u_1 and u_2 ($u_1 < u_2$, say) corresponding to a value of K. If $\rho = 0$, then either $u - K\sigma - (u + K)e^{-2ud} = 0$ or $u - K - (u + K)e^{-2u(h-d)} = 0$, i.e., if the density ratio ρ equals zero, then the problem reduces to a two-layer free surface problem of

infinite extent with d as the depth of upper layer in the former case or to a single-layer free surface problem with $(h-d)$ as finite depth in the latter case. If $\rho^* = 0$,

$$(u+K)(u+K\sigma)e^{-2uh}-(u^2-K^2)e^{-2ud}-(u+K)(u-K)e^{-2u(h-d)}+(u-K\sigma)(u-K)=0, \quad (5.18)$$

i.e., if the density ratio ρ^* equals zero, then the problem reduces to the two-layer free surface problem of finite depth with d as the depth of the lower layer and $h-d$ as the depth of the upper layer.

For the existence of trapped modes, the following are required to be valid:

$$\phi^I, \phi^{II}, \phi^{III}, |\nabla\phi^I|, |\nabla\phi^{II}|, |\nabla\phi^{III}| \to 0 \quad \text{as} \quad |x| \to \infty \quad (5.19)$$

and hence l is restricted to be in the range $l > u_2 > u_1 > K$, which ensures that no wave propagation to infinity takes place at both the interfaces or near the free surface.

5.3 Solutions by multipoles

A horizontal circular cylinder of radius a having its axis along $z = f$, $|f| > a$, and its generator running parallel to the y-axis is placed in either the top layer or the lower layer of a three-layer fluid. For the cylinder to be totally submerged in the lower layer, we need $f < 0$. For the same cylinder to be totally submerged in the upper layer we require $f > 0$ alongwith $(d/a+1) < f/a < (h/a-1)$ so that it does not touch the free surface as well as the interface between the upper and middle layers. Considering the origin of the rectangular Cartesian coordinates at the mean position of the axis of the cylinder, polar coordinates (r,θ) are defined as

$$x = r\sin\theta \text{ and } z = f - r\cos\theta.$$

5.3.1 Cylinder submerged in the lower layer

Symmetric multipoles about the line $x = 0$, ϕ_n^{III} $(n \geq 0)$, are defined by, as detailed in Linton and Cadby (2002),

$$\phi_n^I = (-1)^n \int_0^\infty \cosh nu \cos(lx\sinh u)\Big[A_L(v)e^{vz} + B_L(v)e^{-vz}\Big]du, \quad (5.20)$$

$$\phi_n^{II} = (-1)^n \int_0^\infty \cosh nu \cos(lx\sinh u)\Big[C_L(v)e^{vz} + D_L(v)e^{-vz}\Big]du, \quad (5.21)$$

$$\phi_n^{III} = K_n(lr)\cos n\theta + (-1)^n \int_0^\infty \cosh nu \cos(lx\sinh u)E_L(v)e^{vz}du. \quad (5.22)$$

With the help of the boundary conditions at the interfaces and the free surface, the coefficients $A_L(v)$, $B_L(v)$, $C_L(v)$, $D_L(v)$ and $E_L(v)$ appearing in Eqs. (5.20)–(5.22) are obtained

as

$$\begin{aligned}
A_L(v) &= \frac{v+K}{v-K}e^{-2vh}\frac{K^2(1+\sigma)(1+\sigma^*)e^{vf}}{G(v)},\\
B_L(v) &= \frac{K^2(1+\sigma)(1+\sigma^*)e^{vf}}{G(v)},\\
C_L(v) &= \frac{v+K}{v-K}\frac{K(1+\sigma^*)e^{vf}}{G(v)}\Big[(v+K\sigma)e^{-2vh}-(v-K)e^{-2vd}\Big],\\
D_L(v) &= \Big[(v+K)e^{-2v(h-d)}-(v-K\sigma)\Big]\frac{K(1+\sigma^*)e^{vf}}{G(v)},\\
E_L(v) &= \frac{v+K}{v-K}\frac{e^{vf}}{G(v)}M(v),
\end{aligned}$$

where

$$\begin{aligned}
M(v) &= (v+K\sigma^*)(v+K\sigma)e^{-2vh}-(v+K\sigma^*)(v-K)e^{-2vd}\\
&- (v^2-K^2)e^{-2v(h-d)}+(v-K)(v-K\sigma), \qquad (5.23)\\
G(v) &= (v+K)(v+K\sigma)e^{-2vh}-(v^2-K^2)e^{-2vd}\\
&- (v+K)(v-K\sigma^*)e^{-2v(h-d)}+(v-K\sigma)(v-K\sigma^*). \qquad (5.24)
\end{aligned}$$

It is to be noted that $G(v)=0$ is the dispersion relation in the variable v which is same as in Eq. (5.17) and consequently $v=u_1$ and $v=u_2$ are simple zeros of $G(v)$. Therefore, all the integrals in Eqs. (5.20)–(5.22) above have simple poles at $v=u_1$, $v=u_2$ and $v=K$. But by using the trapped mode condition (5.19) and noting that $v>l$, we get $v>l>u_2>u_1>K$ which implies that there will be no singularities of the integrand on the real axis.

The total velocity potential ϕ can now be written as

$$\phi=\sum_{n=0}^{\infty}\alpha_n\phi_n^{III}, \qquad (5.25)$$

with

$$\phi_n^{III}=K_n(lr)\cos n\theta+\sum_{m=0}^{\infty}A_{mn}I_m(lr)\cos m\theta, \qquad (5.26)$$

where

$$A_{mn}=(-1)^{m+n}\epsilon_n\int_0^{\infty}\cosh mu\cosh nu\; e^{vf}E_L(v)du. \qquad (5.27)$$

Applying the body boundary condition $\partial\phi/\partial r=0$ on $r=a$, we obtain an infinite system of homogenous linear equations in the unknowns α_n:

$$\alpha_n+\frac{I_n'(la)}{K_n'(la)}\sum_{m=0}^{\infty}\alpha_m A_{mn}=0, \qquad n=0,1,2,\ldots \qquad (5.28)$$

where $'$ denotes differentiation with respect to r.

For a fixed geometrical configuration and fixed density ratios, the problem of finding the trapped mode frequencies is completely specified by the two non-dimensional parameters Ka and la. For a fixed value of la, the parameter Ka is varied in such a way that the roots of the dispersion equation never cross la. With this variation of Ka, we locate the zeros of the

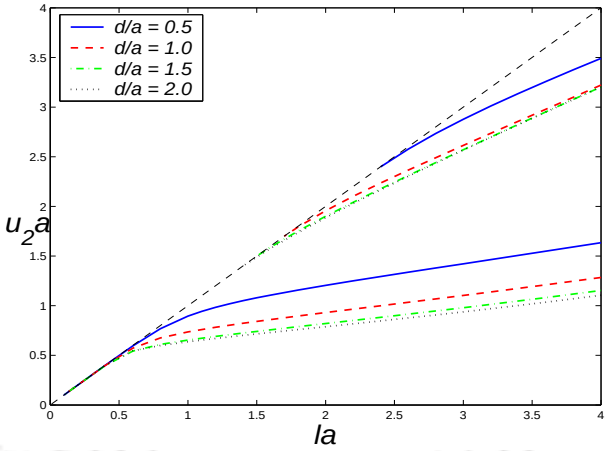

Figure 5.2: Dispersion curves for a cylinder of radius a placed in the lower layer for different depths d/a of the middle layer; $f/a = -1.01$, $h/a = 3$, $\rho = 0.4$, $\rho^* = 0.5$.

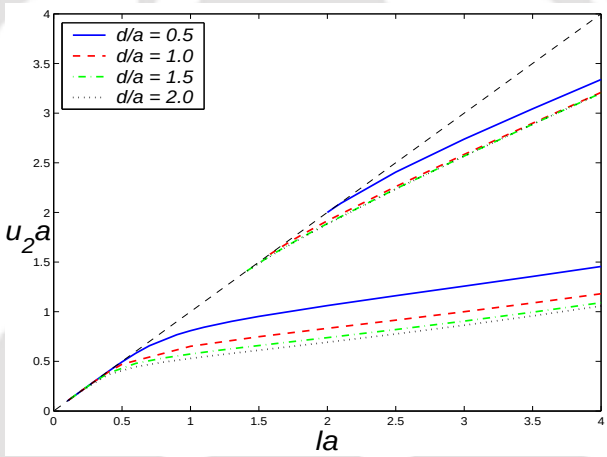

Figure 5.3: Dispersion curves for a cylinder of radius a placed in the lower layer for different depths d/a of the middle layer; $f/a = -1.01$, $h/a = 3$, $\rho = 0$, $\rho^* = 0.5$.

truncated determinant. Then corresponding to those specific values of Ka, we can determine two wavenumbers u_1a and u_2a by using the dispersion relation (5.17). For the numerical evaluation of the zeros of the determinant, we truncate the system to a 32×32 system and the result presented below are obtained correctly up to three decimal places.

Results and discussion

Figures 5.2–5.7 show the results obtained for trapped modes above a horizontal circular cylinder placed in the lower layer of a three-layer fluid. In all the figures when trapped modes are plotted for different depths d/a of the middle layer, the submergence depth f/a of the cylinder is taken as -1.01 which indicates that the cylinder is very close to the interface between the lower and the middle layers.

Figure 5.2 shows the trapped mode wavenumber u_2a for density ratios $\rho = 0.4$, $\rho^* = 0.5$ which clearly implies that the fluid consists of three layers as against two layers in Fig. 5.3. The different curves correspond to the four different depths of the middle layer: $d/a =$

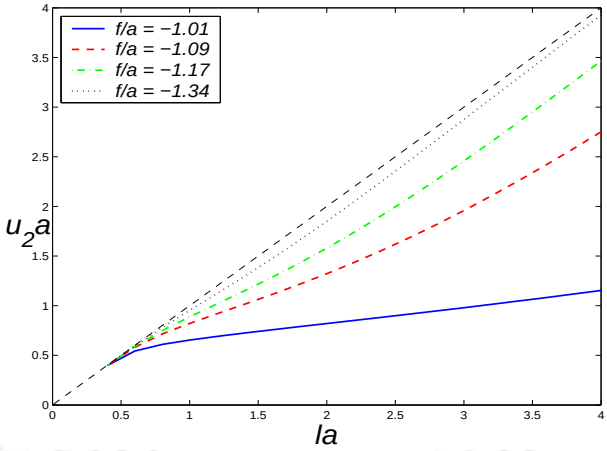

Figure 5.4: Dispersion curves for a cylinder of radius a placed in the lower layer for different submergence depths f/a; $d/a = 1.5$, $h/a = 3$, $\rho = 0.4$, $\rho^* = 0.5$.

$0.5, 1.0, 1.5, 2.0$, and to each value d/a, there corresponds two curves. The existence of trapped modes requires $l > u_2$ so that $l = u_2$ (thin dashed line) gives an upper bound for these curves. Interestingly these curves are similar to those obtained for a two-layer fluid in Linton and Cadby (2003) even though a three-layer fluid is considered in the present case. This clearly indicates that the presence of the upper layer has no effect on the dispersion curves. It is observed that with an increase in the width of the pycnocline, these trapped mode frequencies decrease. It is also observed that the wavenumber decreases as la decreases and converges in the lower range of la. The dispersion curves for the infinite depth two-layer fluid bounded above by a free surface is recovered when $\rho = 0$ (with the upper interface now playing the role of a free surface). These curves in Fig. 5.3 are similar to those in Fig. 1 in Linton and Cadby (2003). By fixing d/a and varying the submergence depth f/a in Fig. 5.4, first mode is observed and by increasing the submergence depth, these modes are seen to have the tendency to attain the upper bound. As f/a approaches the value -1, we observe a 'fanning out' of the curves giving rise to a second mode, just like in the two-layer case.

In Fig. 5.5, trapped mode wavenumbers are plotted against the density ratio ρ^* with ρ taken to be zero. With an increase in ρ^*, Ka decreases to zero in the same pattern as was shown in Linton and Cadby (2003). For the first mode, as the depth of the middle layer increases, the wavenumber u_1a increases while the wavenumber u_2a decreases, and then they interchange their properties at the near crossing points. Further, as $\rho^* \to 1$, u_2a tends to some finite limit corresponding to each value of d/a and $u_1a \to 0$. For the second mode also, the same features are observed as can be seen in Fig. 5.5(c). For those values of d/a where near crossing points do not exist, infinite depth two-layer fluid results can be recovered by the wavenumber u_2a for both the first and second modes. If near crossing points exist for some values of d/a, then u_1a corresponds to the two-layer fluid results before the near crossing points and beyond that, u_2a corresponds to the results for the same.

In Fig. 5.6, $\rho = 0.4$ is considered and in this case two modes are observed only for values of $\rho^* > 0.3$. When $\rho = 0$ (Fig. 5.5), it was observed that the first mode increased steadily to some fixed value as $\rho^* \to 1$ but in this case it is observed that though both modes corresponding

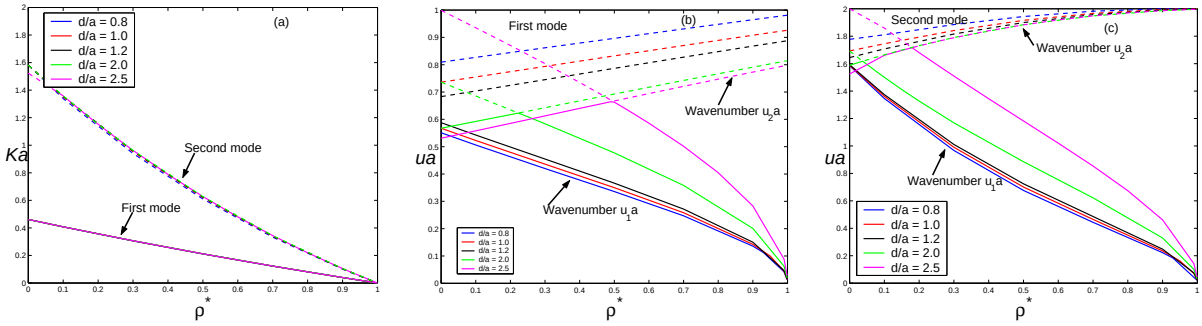

Figure 5.5: Trapped mode wavenumbers plotted against ρ^* for a cylinder of radius a in the lower fluid layer for different depths d/a of the middle layer; $f/a = -1.01$, $h/a = 3$, $\rho = 0$, $la = 2$.

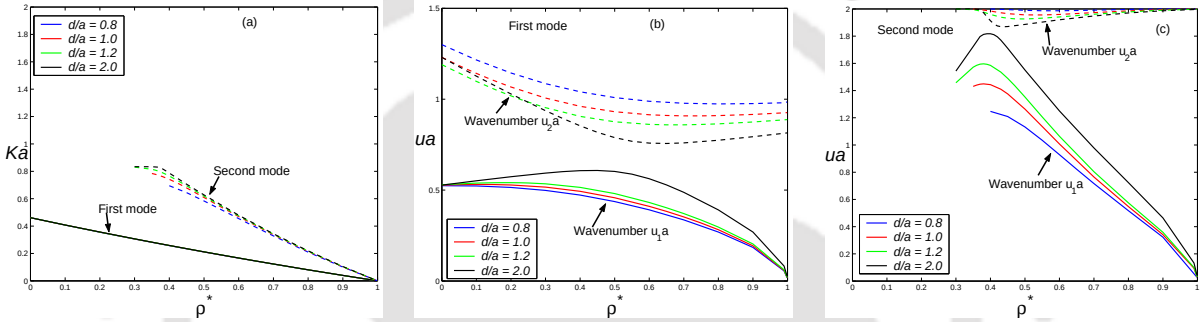

Figure 5.6: Trapped mode wavenumbers plotted against ρ^* for a cylinder of radius a in the lower fluid layer for different depths d/a of the middle layer; $f/a = -1.01$, $h/a = 3$, $\rho = 0.4$, $la = 2$.

to the wavenumbers u_1a and u_2a tend to some fixed values as $\rho^* \to 1$, they do not follow a fixed pattern as was observed in Fig. 5.5. It is seen that as $\rho^* \to 1$, the wavenumber u_1a for both the first and the second modes tend to 0; the wavenumber u_2a tends to some finite limit for the first mode, and for the second mode it tends to $la = 2$. Thus, the rate of decay of the exponential term decreases as ρ^* comes closer to unity and in the limit there exists no trapped mode. Figure 5.7 shows that as the submergence depth f/a increases, the first modes cease to exist for decreasing values of ρ^*.

5.3.2 Cylinder submerged in the upper layer

For the case when the cylinder is placed in the upper layer, the velocity potential can be expanded exactly in the same manner as was done for the case of the cylinder placed in the lower layer. Now the multipoles can be written as

$$\phi_n^I = K_n(lr)\cos n\theta + \sum_{m=0}^{\infty} B_{mn} I_m(lr)\cos m\theta, \tag{5.29}$$

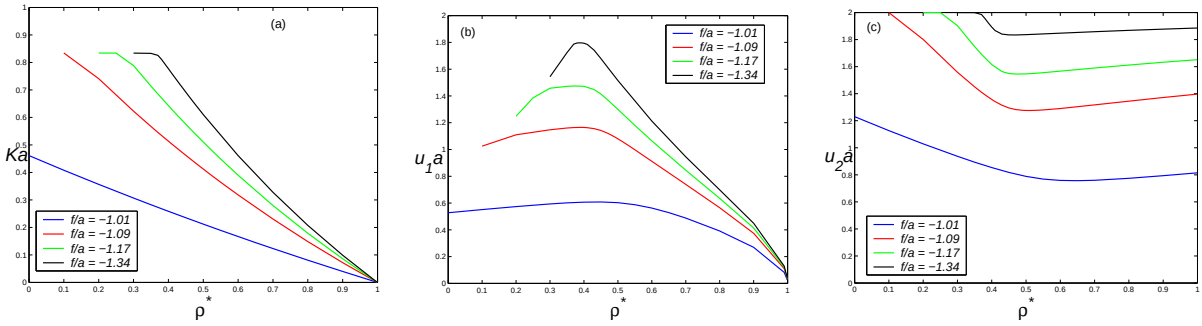

Figure 5.7: Trapped mode wavenumbers plotted against ρ^* for a cylinder of radius a in the lower fluid layer for different submergence depths f/a; $d/a = 2.0$, $h/a = 3$, $\rho = 0.4$, $la = 2$.

where

$$B_{mn} = \epsilon_n \int_0^\infty \cosh mu \cosh nu \Big[(-1)^n A_U(v) e^{vf} + B_U(v) e^{-vf}\Big] du, \tag{5.30}$$

$$A_U(v) = \frac{v+K}{v-K}\Big[B_U(v) + (-1)^n e^{vf}\Big] e^{-2vh}, \tag{5.31}$$

$$B_U(v) = \frac{\Big((v-K\sigma^*)e^{2vd} - (v+K\sigma)\Big)\Big((-1)^n(v+K)e^{v(f-2h)+(v-K)e^{-vf}}\Big)}{G(v)}, \tag{5.32}$$

where $G(v)$ is same as in Eq. (5.24). Here also, due to the trapped mode condition, there will be no singularities on the real axis.

By applying the body boundary condition, we obtain the same kind of system of equations for β_n identical to (5.28):

$$\beta_n + \frac{I_n'(la)}{K_n'(la)} \sum_{m=0}^{\infty} \beta_m B_{mn} = 0, \qquad n = 0, 1, 2, \ldots \tag{5.33}$$

Here also, as in the previous case, by varying the frequencies Ka and fixing the other parameters, the zeros of the truncated determinant are conveniently located. It is already known that those frequencies correspond to the trapped modes. The results presented next are obtained correct up to three decimal places where a 32×32 system is used after truncating the system arising from (5.33). However, it is noticed that the first modes can be located even by considering a system of lesser order, say a 10×10 system.

Results and discussion

Figure 5.8 shows the dispersion curves when the cylinder is placed in the upper layer for the following fixed values: $h/a = 0.4$, $\rho = 0.4$, $\rho^* = 0.5$. There are three curves corresponding to three different depths of the middle layer with $(f-d)/a = 1.01$. That is, the cylinder is nearer to the interface between the upper and the middle layers. The upper bound for trapped modes $u_2 = l$ is included and shown by the thin dashed line. As the depth of the middle layer increases, trapped mode wavenumber decreases. With the same set of parameters, dispersion curves are plotted against the submergence depth as shown in Fig. 5.9. It is observed that the curves fold out from the upper bound as $(f-d)/a \to 1$, i.e., when the cylinder approaches the first interface. Similar effects are observed when the cylinder approaches the second interface from the lower layer.

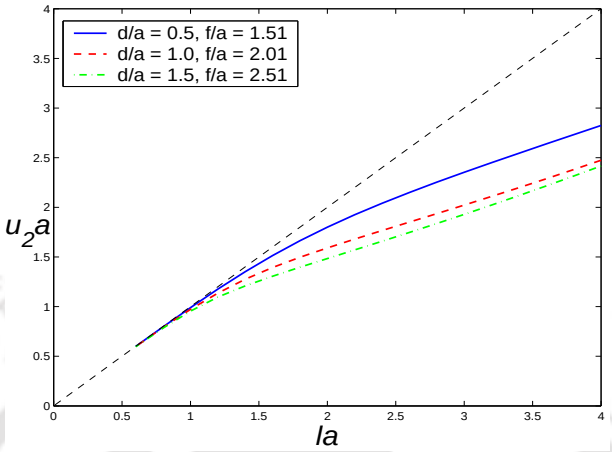

Figure 5.8: Dispersion curves for a cylinder of radius a placed in the upper layer; $(f-d)/a = 1.01$, $h/a = 4.0$, $\rho = 0.4$, $\rho^* = 0.5$.

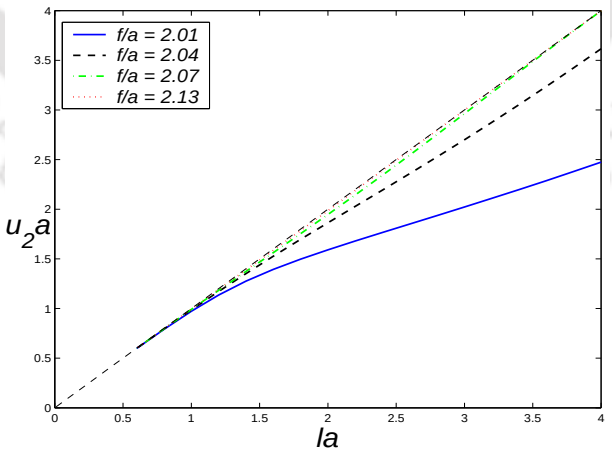

Figure 5.9: Dispersion curves for a cylinder of radius a placed in the upper layer for different submergence depths f/a; $d/a = 1.0$, $h/a = 4$, $\rho = 0.4$, $\rho^* = 0.5$.

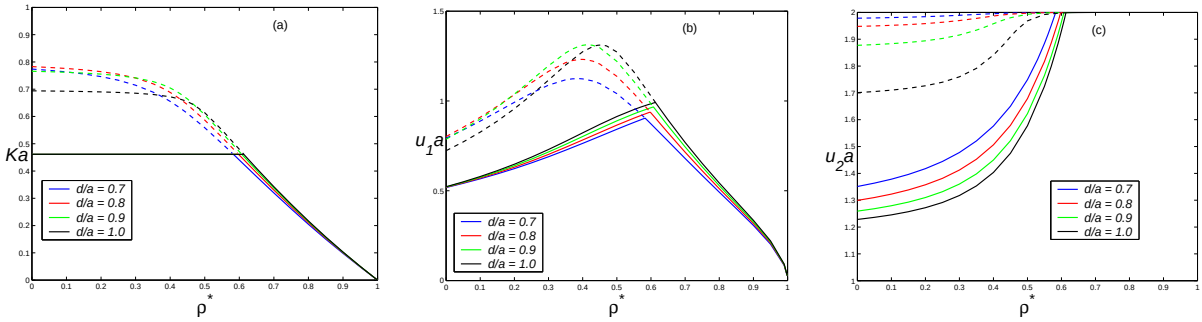

Figure 5.10: Trapped mode wavenumbers plotted against ρ^* for a cylinder of radius a in the upper fluid layer for different depths d/a of the middle layer; $f/a = 2.09$, $h/a = 3.1$, $\rho = 0.4$, $la = 2$.

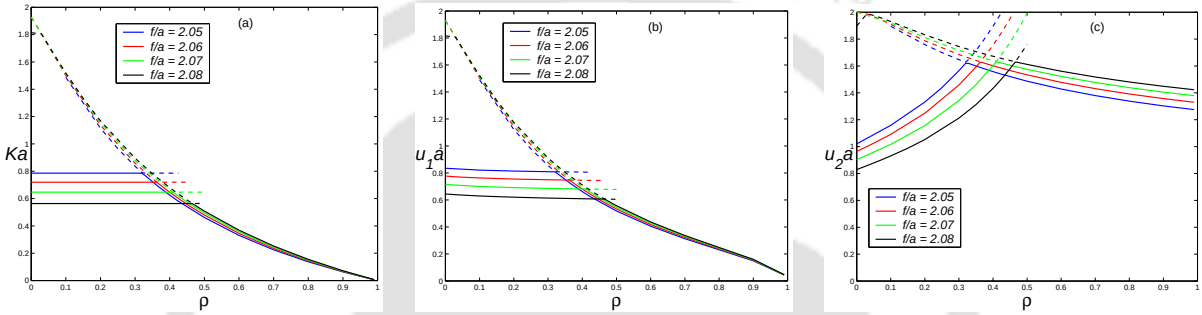

Figure 5.11: Trapped mode wavenumbers plotted against ρ for a cylinder of radius a in the upper fluid layer for different submergence depths f/a; $d/a = 1.0$, $h/a = 3.1$, $\rho^* = 0$, $la = 2$.

In all the figures where trapped mode wavenumbers are plotted against density ratios, the curves with continuous lines give the first modes and the ones with dashed lines give the second modes. In Fig. 5.10, the trapped mode wavenumbers are shown against the density ratio ρ^* when $la = 2$, $h/a = 3.1$ $f/a = 2.09$, $\rho = 0.4$. We then consider the case when the cylinder is nearer to the free surface, i.e., when $(h - f)/a = 1.01$. The results are presented for four different values of the depth of the middle layer: $d/a = 0.7, 0.8, 0.9, 1.0$. Corresponding to each value of d/a, there are two curves showing the first and the second modes. The first modes, presented by the lower ones of each pair of curves, appear to cross the second modes, the higher curves, at near crossing points. Then, with an increase in ρ^*, the first and second modes come very close to each other at some point, after which the second mode terminates with $u_2a = 2 = la$; the first mode for both the wavenumbers Ka and u_1a decreases to zero whereas it remains constant at $la = 2$ for the wavenumber u_2a. Hence, in the limit $\rho^* \to 1$, the first mode for the wavenumber u_2a also ceases to exist.

As expected, the result for the finite depth two-layer fluid with the cylinder in the upper layer is recovered when $\rho^* = 0$ in Fig. 5.11 (with the lower interface now playing the role of the rigid horizontal bottom). The depth of the upper layer is considered as 2.1 and that of the lower layer as 1.0. The results are similar to the ones in Fig. 5 in Linton and Cadby (2003).

In Fig. 5.12, we assign a non-zero value to the density ratio ρ^* by considering $\rho^* = 0.5$ and plot trapped mode wavenumbers against the density ratio ρ. In this case totally different patterns are observed for the wavenumber u_1a. When the cylinder is closer to the free surface,

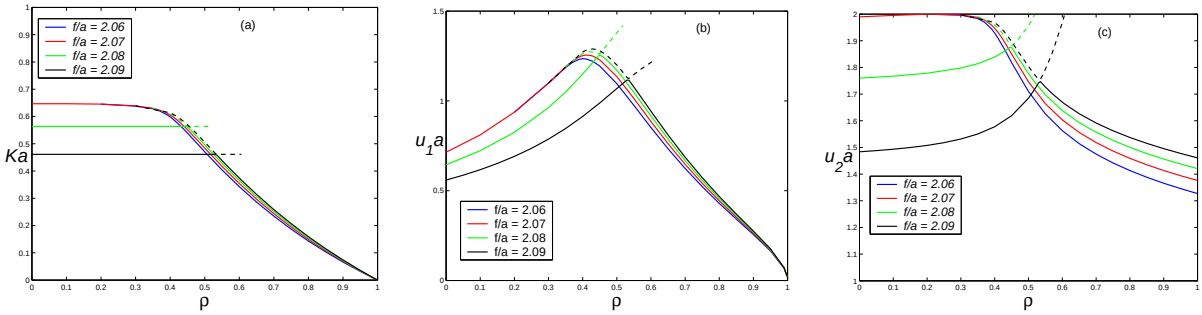

Figure 5.12: Trapped mode wavenumbers plotted against ρ for a cylinder of radius a in the upper fluid layer for different submergence depths f/a; $d/a = 1.0$, $h/a = 3.1$, $\rho^* = 0.5$, $la = 2$.

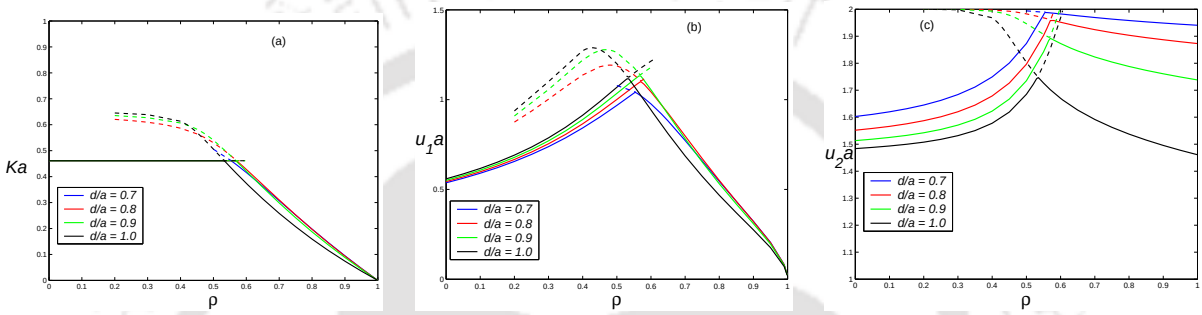

Figure 5.13: Trapped mode wavenumbers plotted against ρ for a cylinder of radius a in the upper fluid layer for different depths d/a of the middle layer; $f/a = 2.09$, $h/a = 3.1$, $\rho^* = 0.5$, $la = 2$.

i.e., say for $(h - f)/a = 1.01$, the second mode exists within a small interval of the density ratio ρ. For both the wavenumbers u_1a and u_2a, the second mode decreases while the first mode increases and they come closer to each other at near crossing points. Then the second mode terminates but the first mode tends to some finite value as $\rho \to 1$. As the submergence depth decreases, i.e., as the cylinder moves downwards from the free surface towards the first interface, the second mode ceases to exist resulting in the appearance of only one mode. For the wavenumber u_1a, the first mode initially increases and then decreases to zero as $\rho \to 1$ for all values of submergence depth.

Figure 5.13 shows the plots of trapped wavenumbers against the density ratio ρ for the fixed values of $la = 2$, $\rho_1 = 0.5$. In this case $h/a = 3.1$ and $f/a = 2.09$ are considered such that the cylinder is very much nearer to the free surface. For all the depths of the middle layer, the second trapped mode wavenumber starts from $\rho = 0.2$. Then as ρ increases, both modes come closer to each other at near crossing points. Then the second mode terminates but the first mode exists as $\rho \to 1$. For the wavenumber u_2a, as depth of the middle layer increases, the trapped mode decreases.

5.3.3 Limiting values of the density ratios

Limit as $\rho \to 1$: The dispersion relation (5.17) can be written as:

$$\frac{(u+K)(u+K\sigma)e^{-2uh} - (u^2-K^2)e^{-2ud}}{(u+K)(u-K\sigma^*)e^{-2u(h-d)} - (u-K\sigma)(u-K\sigma^*)} = 1. \tag{5.34}$$

Considering the limit $\rho \to 1$, we have $\sigma \to \infty$. Taking limit $\sigma \to \infty$ on both sides of the Eq. 5.34, we get

$$(u + K)e^{-2uh} - u + K\sigma^* = 0, \tag{5.35}$$

This gives the dispersion relation for a two-layer fluid with the lower layer of infinite depth and upper layer is of depth h. For the fixed value of Ka the wavenumber $ka = u_1 a$ can be determined from this relation. From Figs. 5.12 and 5.13 we observe that in the limit $\rho \to 1$, the trapped mode frequency Ka and wavenumber $u_1 a$ tend to 0.

The observation on trapped mode in a two-layer fluid of infinite depth made by Linton and Cadby (2003) is that for the density ratio 0.5 there exists one trapped mode (Fig. 5, Linton and Cadby (2003)). For that trapped mode, Ka has an approximate value of 0.5 and ka takes an approximate value of 1.40. Hence results on trapped mode given by Linton and Cadby (2003) is not recovered from the result in a three-layer fluid in the limit $\rho \to 1$.

Limit as $\rho^* \to 1$: The dispersion relation (5.17) can also be written as

$$\frac{(u + K)(u + K\sigma)e^{-2uh} + (u - K\sigma)(u - K\sigma^*)}{(u^2 - K^2)e^{-2ud} + (u + K)(u - K\sigma^*)e^{-2u(h-d)}} = 1, \tag{5.36}$$

Similarly, as before, taking the limit $\rho^* \to 1$ we get

$$(u + K)e^{-2u(h-d)} - u + K\sigma = 0. \tag{5.37}$$

Corresponding to a value of frequency Ka, we get wavenumber $ka = u_2 a$ from this dispersion relation. For a cylinder in either fluid layer, the wavenumber $u_2 a$ tends to some value (Figs. 5.7 and 5.10) which is a trapped mode but certainly does not correspond to one of a two-layer fluid because $Ka \to 0$ in the limit. But for a density ratio 0.4 of a two-layer fluid of infinite depth the value of Ka is not equal to zero for a cylinder placed in either of the layers (Figs. 2 and 5 of Linton and Cadby (2003)).

Double limit as $\rho \to 1$ and $\rho^* \to 1$: When we take this double limit in the dispersion relation we get $K/u \to 0$ and for a fixed value of l ($> u$) we get $K \to 0$. Same observation follows from all the figures. And hence in the double limit to 1, it is not possible to recover the single-layer results. To explain analytically what is happening we shall consider the boundary conditions in the limit as $\rho \to 1$, $\rho^* \to 1$ and $K \to 0$ simultaneously. We introduce small parameters ε, δ and δ' such that $\delta \approx \delta'$ and define

$$\begin{aligned} &K = \varepsilon, \qquad \rho = 1 - \delta, \qquad \rho^* = 1 - \delta', \\ &K' = \frac{K}{1 - \rho} \approx \frac{K}{1 - \rho^*} = O(1). \end{aligned} \tag{5.38}$$

In this limit, boundary conditions (5.4)–(5.8) become

$$\frac{\partial \phi^I}{\partial z} = 0 \qquad \text{on} \qquad z = h, \tag{5.39}$$

$$\frac{\partial \phi^I}{\partial z} = \frac{\partial \phi^{II}}{\partial z} \qquad \text{on} \qquad z = d, \tag{5.40}$$

$$K'\phi^{II} - \frac{\partial \phi^{II}}{\partial z} = K'\phi^{I} \qquad \text{on} \qquad z = d, \tag{5.41}$$

$$\frac{\partial \phi^{II}}{\partial z} = \frac{\partial \phi^{III}}{\partial z} \qquad \text{on} \qquad z = 0, \tag{5.42}$$

$$K'\phi^{III} - \frac{\partial \phi^{III}}{\partial z} = K'\phi^{II} \qquad \text{on} \qquad z = 0. \tag{5.43}$$

The dispersion relation will have two positive solutions u_1 and u_2 which must satisfy

$$\begin{aligned}&(2K'-u)(K'-u+K'u)+(K'u^2-u^2-uK')e^{-2ud} \\ &+(2K'-u)(u+uK'-K')e^{-2u(h-d)}+(K'u^2+u^2+uK')e^{-2uh}=0.\end{aligned} \tag{5.44}$$

In the absence of any bodies, oblique waves propagating in the fluid take the form

$$\phi^{I} = \exp(\pm ix\sqrt{u^2-l^2})A_1[e^{u(h-z)}+e^{-u(h-z)}], \tag{5.45}$$

$$\phi^{II} = \exp(\pm ix\sqrt{u^2-l^2})[A_2e^{uz}-B_2e^{-uz}], \tag{5.46}$$

$$\phi^{III} = \exp(\pm ix\sqrt{u^2-l^2})\frac{e^{uz}}{u}, \tag{5.47}$$

where

$$A_1 = \frac{ue^{-ud}+(2K'-u)e^{ud}}{2K'[e^{-u(h-d)}-e^{u(h-d)}]}, \tag{5.48}$$

$$A_2 = \frac{2K'-u}{2K'u}, \tag{5.49}$$

$$B_2 = \frac{1}{2K'}. \tag{5.50}$$

$$\tag{5.51}$$

Thus, in the double limit for a fixed l, we obtain a boundary-value problem in terms of the new spectral parameter K'. After finding the forms of the multipoles for this problem and computing the trapped-mode frequencies the results match those found in the limit of Figs. 5.7–5.13. Hence for a fixed l, the trapped mode problem in the double limit $\rho \to 1$ and $\rho^* \to 1$ is related to the limits of the trapped mode curves in these figures. Thus it is not possible to recover the single-layer fluid results in the double limit.

5.4 Conclusions

A three-layer incompressible fluid is considered with the lowermost layer being of infinite depth and the other two layers of finite depth. Under the usual assumptions of linear water wave theory and by using a multipole expansion method, the existence of trapped mode is shown

when a horizonal circular cylinder is placed in either the lowermost or the uppermost layer. This generalizes the results of Linton and Cadby (2003) from a two-layer case to a three-layer one. In the case of a two-layer fluid, we have seen that trapped waves correspond to two wavenumbers but we now show in the three-layer case that trapped waves correspond to three wavenumbers at the free surface and the internal interfaces. But similar to the two-layer case, it is observed here also that for each set there exists two modes and with an increase in any of the two density ratios to 1, the second mode ceases to exist but the first mode does exist in nearly all the cases. The effects of the submergence depth and the depth of the middle layer on trapped modes are also observed.

By considering the density ratio $\rho = 0$, it is shown that the corresponding results for a two-layer fluid of infinite depth can be recovered when the cylinder is placed in the lower layer. Similarly for $\rho^* = 0$, the results of a two-layer fluid of finite depth is recovered when the cylinder is placed in the upper layer. All the modes discussed above occur at frequencies below a cut-off value. Above this cut-off value, it is possible to formulate a scattering problem corresponding to the interaction of an obliquely incident wave with the cylinder, but below it no waves can propagate into the far field. When either of the density ratios or both tend to 1, then it is not possible to recover either the two-layer or the single-layer case as is evident from the present investigation - contrary to what Chakrabarti et al. (2005) concluded. That is, however small the width of the pycnocline may be, it still commands influence over the trapped modes and the three-layer case cannot be considered as equivalent to the two-layer case in the limit. Sharp and smooth pycnoclines are, respectively, simulated by two-layer and three-layer fluids. In the latter, the middle layer is linearly stratified, whereas the upper and lower layers are homogeneous. The middle layer with constant density that is considered in our problem is basically a crude representation of a smooth pycnocline.

Chapter 6

Trapped waves supported by a pair of cylinders in an ice-covered two-layer fluid

6.1 Introduction

To the best of our knowledge, no investigation of flexural trapped waves for the case of a pair of totally submerged identical circular cylinders placed in either layer of a two-layer fluid has taken place till date. Though we have already investigated various aspects of existence of flexural trapped waves in Chapter 3, it was limited to a single cylinder placed in either layer of a two-layer fluid. The objective of the present work is to locate the distance between this pair of identical cylinders for which trapped wave exists. The variation of this distance is observed by varying the values of the ice parameters, the depth of the upper layer and the submergence depth when the pair of cylinders is placed in the lower layer. The case in which the cylinders are placed in the upper layer is also considered and the distances are located for which trapped wave exists.

6.2 Mathematical formulation of the problem

The irrotational motion of a two-layer inviscid, incompressible and immiscible fluid of relatively small amplitude under the action of gravity in an ocean is considered, neglecting any effect due to surface tension at the interface of the two-layer fluid of which the upper layer is of finite depth d and is covered by a thin uniform ice sheet modeled as a thin elastic plate, and the lower layer is of infinite depth. Each fluid is of infinite horizontal extent in the x- and y-directions while the depth is along the z-direction which is considered positive vertically upwards with $z = d > 0$ as the mean position of the thin ice-cover and $z = 0$ as the mean position of the interface. Under the usual assumptions of linear water wave theory, velocity potentials in the lower and upper layers, respectively, for oblique waves can be defined in the form

$$\Phi^I(x, y, z, t) = \mathrm{Re}[\phi^I(x, z)e^{ily}e^{-i\omega t}] \qquad \text{and} \qquad \Phi^{II}(x, y, z, t) = \mathrm{Re}[\phi^{II}(x, z)e^{ily}e^{-i\omega t}],$$

where $\phi^I(x, z)$ and $\phi^{II}(x, z)$, respectively, are complex-valued potential functions for the upper layer fluid $(-\infty < x < \infty;\ -\infty < y < \infty;\ 0 < z < d)$ of density ρ_I and the lower layer fluid

$(-\infty < x < \infty;\ -\infty < y < \infty;\ -\infty < z < 0)$ of higher density ρ_{II}.

The governing equation for the boundary value problems involving these potentials ϕ^I and ϕ^{II} is the modified Helmholtz equation:

$$\Big(\nabla^2_{x,z} - l^2\Big)\phi^I = 0 \qquad \text{in the upper fluid,} \tag{6.1}$$

$$\Big(\nabla^2_{x,z} - l^2\Big)\phi^{II} = 0 \qquad \text{in the lower fluid.} \tag{6.2}$$

Denoting the ratio $\rho_I/\rho_{II}(< 1)$ of the densities of the two fluids by ρ, the linearized boundary conditions at the interface and at the ice-cover are (same as Chapter 3)

$$\frac{\partial \phi^I}{\partial z} = \frac{\partial \phi^{II}}{\partial z} \qquad \text{on} \qquad z = 0, \tag{6.3}$$

$$\rho\Big(\frac{\partial \phi^I}{\partial z} - K\phi^I\Big) = \frac{\partial \phi^{II}}{\partial z} - K\phi^{II} \qquad \text{on} \qquad z = 0, \tag{6.4}$$

$$\Big[D\Big(\frac{\partial^2}{\partial x^2} - l^2\Big)^2 + 1 - \varepsilon K\Big]\frac{\partial \phi^I}{\partial z} - K\phi^I = 0 \qquad \text{on} \qquad z = d. \tag{6.5}$$

Since the lower layer is of infinite depth, therefore the following limiting values hold:

$$\phi^{II}, |\nabla \phi^{II}| \ \to 0 \quad \text{as} \quad z \to -\infty. \tag{6.6}$$

Within this framework, progressive waves or incident waves take the form (up to an arbitrary multiplicative constant)

$$\phi^I = \exp(\pm ix\sqrt{u^2 - l^2})\Big(F_+(u)e^{u(z-d)} + F_-(u)e^{-u(z-d)}\Big), \tag{6.7}$$

$$\phi^{II} = \exp(\pm ix\sqrt{u^2 - l^2})e^{uz}\Big(F_+(u)e^{-ud} - F_-(u)e^{ud}\Big), \tag{6.8}$$

where

$$F_\pm(u) = \Big(Du^4 + 1 - \varepsilon K\Big)u \pm K, \tag{6.9}$$

and u satisfies the dispersion relation

$$(u - K\sigma)F_-(u) - (u - K)F_+(u)e^{-2ud} = 0. \tag{6.10}$$

For a fixed geometrical configuration and a fixed density ratio, this equation has exactly two positive real roots u_1 and u_2 ($u_1 < u_2$, say) corresponding to a value of K. If $D = \varepsilon = 0$, this relation gives two wavenumbers for a two-layer fluid of infinite depth bounded above by a free surface.

6.3 Solutions by multipoles

N fixed horizontal circular cylinders of infinite length are placed on $z = f$ plane with their generators running parallel to the y-axis. If $f > 0$, the cylinders are in the upper fluid, whereas the cylinders are in the lower fluid when $f < 0$. The j-th cylinder is of radius a_j and its centre is positioned at $(x_j, z) = (h_j, f)$, $j = 1, 2, ..., N$. It is convenient to define local polar coordinates (r_j, θ_j) (see Fig. 6.1) associated with cylinder j defined by

$x_j = h_j + r_j \sin\theta_j \qquad$ and $\qquad z_j = f - r_j \cos\theta_j.$

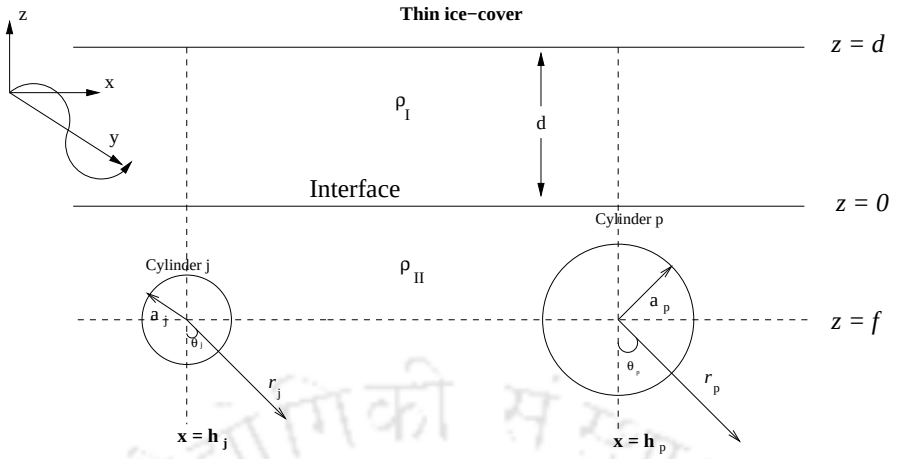

Figure 6.1: Cross-sectional view of a two-layer fluid covered by an ice-cover in the presence of two cylinders in the lower layer.

6.3.1 Cylinders submerged in the lower layer

Arbitrary single cylinder

Here we consider an arbitrary cylinder of radius a_j for $j = 1, 2, ..., N$. The symmetric and antisymmetric multipoles, $\phi^s_{nj}(n \geq 0)$ and $\phi^a_{nj}(n \geq 1)$, are, respectively, defined as based on the results of (Linton and Cadby (2003))

$$\phi^{Is}_{nj}(x_j, z_j) = (-1)^n \int_0^\infty \cosh nu \, \cos(lx_j \sinh u) \left[A_L(v)e^{vz_j} + B_L(v)e^{-vz_j}\right] du, \tag{6.11}$$

$$\phi^{IIs}_{nj}(x_j, z_j) = K_n(lr_j)\cos n\theta_j + (-1)^n \int_0^\infty \cosh nu \, \cos(lx_j \sinh u) \, e^{vz_j} \, C_L(v) \, du, \tag{6.12}$$

$$\phi^{Ia}_{nj}(x_j, z_j) = (-1)^{n+1} \int_0^\infty \sinh nu \, \sin(lx_j \sinh u) \left[A_L(v)e^{vz_j} + B_L(v)e^{-vz_j}\right] du, \tag{6.13}$$

$$\phi^{IIa}_{nj}(x_j, z_j) = K_n(lr_j)\sin n\theta_j + (-1)^{n+1} \int_0^\infty \sinh nu \, \sin(lx_j \sinh u) \, e^{vz_j} \, C_L(v) \, du, \tag{6.14}$$

where $v = l\cosh u$ and

$$\begin{aligned} A_L(v) &= \frac{F_+(v)}{F_-(v)} B_L(v) \, e^{-2vd}, \\ B_L(v) &= \frac{K(1+\sigma)F_-(v)}{G(v)} \, e^{vf}, \\ C_L(v) &= \frac{B_L(v)}{K(1+\sigma)F_-(v)}[(v+K\sigma) \, F_+(v) \, e^{-2vd} - (v+K) \, F_-(v)], \end{aligned}$$

with

$$G(v) = (v - K\sigma) \, F_-(v) - (v - K) \, F_+(v) \, e^{-2vd}. \tag{6.15}$$

The functions ϕ^s_{nj} and ϕ^a_{nj} are singular solutions to the modified Helmholtz equation which satisfy all the boundary conditions, except the one on the body boundary. Since u_1 and u_2 are the roots of the dispersion relation (6.10), the multipole potentials have simple poles at $u = \nu_1$ and $u = \nu_2$, where

$$l \cosh \nu_1 = u_1 \qquad \text{and} \qquad l \cosh \nu_2 = u_2. \tag{6.16}$$

Subsequently, all the integrals mentioned above are complex-valued.

Considering the well-known generating function of modified Bessel's function given by (B.10) in Appendix B and by putting $X = -lr_j$ and $T = \exp\Big[i(\theta_j + iu)\Big]$ in that equation, the multipoles can be expanded by considering the real and imaginary parts and the resulting expressions can be substituted into (6.12) and (6.14) to obtain (Appendix B)

$$\phi^{IIs}_{nj}(r_j, \theta_j) = K_n(lr_j)\cos n\theta_j + \sum_{m=0}^{\infty} A^s_{mn} I_m(lr_j)\cos m\theta_j, \tag{6.17}$$

$$\phi^{IIa}_{nj}(r_j, \theta_j) = K_n(lr_j)\sin n\theta_j + \sum_{m=0}^{\infty} A^a_{mn} I_m(lr_j)\sin m\theta_j, \tag{6.18}$$

where

$$A^s_{mn} = \epsilon_m(-1)^{m+n}\int_0^{\infty} \cosh mu \, \cosh nu \, e^{vf} \, C_L(v) \, du, \tag{6.19}$$

$$A^a_{mn} = 2(-1)^{m+n}\int_0^{\infty} \sinh mu \, \sinh nu \, e^{vf} \, C_L(v) \, du. \tag{6.20}$$

For computational purpose, the contour integral appearing in the above coefficients can be written as the sum of the principal value integral and the residual contribution corresponding to the simple poles ν_1 and ν_2. The principal value integrals can be calculated by using the method followed in Linton and Evans (1992b).

Multiple cylinders

We now construct a possible trapped mode potential as the sum over all the multipoles and all the cylinders: (based on the result of Evans and Porter (1997))

$$\phi^{II}(r, \theta) = \sum_{j=1}^{N}\sum_{n=0}^{\infty}\Big(A^j_n \phi^{IIs}_{nj}(r_j, \theta_j) + B^j_n \phi^{IIa}_{nj}(r_j, \theta_j)\Big), \tag{6.21}$$

for some constants A^j_n and B^j_n by looking for the possible non-trivial solutions satisfying the body boundary condition on the cylinders given by

$$\frac{\partial \phi^{II}}{\partial r_j} = 0 \qquad \text{on} \qquad r_j = a_j, \;\; j = 1, ..., N. \tag{6.22}$$

In order to impose this condition, there arises a need to shift from the local coordinates of each cylinder j to a cylinder p, say, where $p \neq j$ (Fig. 6.1). By doing so, the following important results are obtained (Appendix B):

$$K_n(lr_j)\cos n\theta_j = \sum_{m=0}^{\infty}\Big(C^{jp}_{nm}\cos m\theta_p + D^{jp}_{nm}\sin m\theta_p\Big) I_m(lr_p), \tag{6.23}$$

$$K_n(lr_j)\sin n\theta_j = \sum_{m=0}^{\infty}\Big(A^{jp}_{nm}\cos m\theta_p + B^{jp}_{nm}\sin m\theta_p\Big) I_m(lr_p), \tag{6.24}$$

and

$$(-1)^n \int_0^\infty \cosh nu \cos(lx_j \sinh u) e^{vz_j} C_L(v) du = \sum_{m=0}^{\infty} \Big(\alpha_{nm}^{jp} \cos m\theta_p + \beta_{nm}^{jp} \sin m\theta_p \Big) I_m(lr_p), \tag{6.25}$$

$$(-1)^{n+1} \int_0^\infty \sinh nu \sin(lx_j \sinh u) e^{vz_j} C_L(v) du = \sum_{m=0}^{\infty} \Big(a_{nm}^{jp} \cos m\theta_p + b_{nm}^{jp} \sin m\theta_p \Big) I_m(lr_p). \tag{6.26}$$

It follows from Eqs. (6.12), (6.14) and (6.23)–(6.26) that for $j \neq p$

$$\phi_{nj}^{2s}(r_j, \theta_j) = \sum_{m=0}^{\infty} \Big[(C_{nm}^{jp} + \alpha_{nm}^{jp}) \cos m\theta_p + (D_{nm}^{jp} + \beta_{nm}^{jp}) \sin m\theta_p \Big] I_m(lr_p), \tag{6.27}$$

$$\phi_{nj}^{2a}(r_j, \theta_j) = \sum_{m=0}^{\infty} \Big[(A_{nm}^{jp} + a_{nm}^{jp}) \cos m\theta_p + (B_{nm}^{jp} + b_{nm}^{jp}) \sin m\theta_p \Big] I_m(lr_p). \tag{6.28}$$

For the case $j = p$, the above multipoles take the form given by (6.17) and (6.18). We are now in a position to write (Evans and Porter (1997))

$$\phi^{II}(r, \theta) = \sum_{n=0}^{\infty} \Big(A_n^p \phi_{np}^{IIs} + B_n^p \phi_{np}^{IIa} \Big) + \sum_{\substack{j=1 \\ j \neq p}}^{N} \sum_{n=1}^{\infty} \Big(A_n^j \phi_{nj}^{IIs} + B_n^j \phi_{nj}^{IIa} \Big). \tag{6.29}$$

Subsequently, by imposing the condition (6.22) and using the orthogonality property of sine and cosine functions, we obtain the following:

$$A_m^p + \frac{I'_m(la_p)}{K'_m(la_p)} \sum_{n=0}^{\infty} \left[A_n^p A_{mn}^s + \sum_{\substack{j=1 \\ j \neq p}}^{N} \Big[A_n^j (C_{nm}^{jp} + \alpha_{nm}^{jp}) + B_n^j (A_{nm}^{jp} + a_{nm}^{jp}) \Big] \right] = 0, \tag{6.30a}$$

$$B_m^p + \frac{I'_m(la_p)}{K'_m(la_p)} \sum_{n=0}^{\infty} \left[B_n^p A_{mn}^a + \sum_{\substack{j=1 \\ j \neq p}}^{N} \Big[A_n^j (D_{nm}^{jp} + \beta_{nm}^{jp}) + B_n^j (B_{nm}^{jp} + b_{nm}^{jp}) \Big] \right] = 0, \tag{6.30b}$$

where $p = 1, 2, ...N; m \geq 0$. This is the system the non-trivial solutions of which will determine the trapped mode frequencies due to the presence of N cylinders arranged as stated earlier. In order to obtain non-trivial solutions of the unknown coefficients, it is required to determine those frequencies for which there exist zeros of the truncated determinant. Though the theoretical development derived above is valid for any arbitrary number of cylinders, but in order to examine the variation of trapped modes within a feasible exercise, we consider a pair of identical cylinders in the next section. The result then can be extended to any number of cylinders.

For the case of cylinders placed on $z = f$, $f > 0$, i.e., when the cylinders are placed in the upper layer, we can proceed in a similar way and again obtain an infinite system of homogenous linear equations whose non-trivial solutions correspond to the trapped modes.

6.4 Numerical results and discussion for two identical cylinders submerged in either of the layers

For the case of two identical cylinders ($a_1 = a_2 = a$) placed at $h_1 = -h_2 = \xi$, we can exploit the geometry and consider only those oscillations symmetric about $x = 0$ so that the geometry is equivalent to a horizontal cylinder placed next to a vertical wall. When the upper layer is covered by a free surface, it was shown in Linton and Cadby (2002) that the zeros of transmission for the oblique wave scattering problem occurred just below the cut-off frequency. Thereafter in Linton and Cadby (2003), the region $K < l < k$ was considered and the existence of embedded trapped modes was demonstrated. In this region, propagating waves exist with wavenumber k but not with wavenumber K. When the free surface gets replaced by a thin ice-cover, it was shown in Das and Mandal (2007) that the maximum reflection occurred for frequencies just below the cut-off frequency of the incident wave of wavenumber u_2. Hence for seeking the embedded trapped modes, the region $u_1 < l < u_2$ must be considered.

6.4.1 Cylinders submerged in the lower layer

Since we are interested in an even or a symmetric solution about $x = 0$, therefore we consider

$$\frac{\partial \phi^{II}}{\partial x} = 0 \qquad \text{on} \qquad x = 0. \tag{6.31}$$

Condition (6.31) will be satisfied if $A_n^1 = A_n^2$ and $B_n^1 = -B_n^2$. Use of this reduces the original coupled system (6.30) simply to

$$A_m^1 + \frac{I_m'(la)}{K_m'(la)} \sum_{n=0}^{\infty} (P_{nm} A_n^1 + Q_{nm} B_n^1) = 0, \tag{6.32a}$$

$$B_m^1 - \frac{I_m'(la)}{K_m'(la)} \sum_{n=0}^{\infty} (T_{nm} B_n^1 + R_{nm} A_n^1) = 0, \qquad m \geq 0, \tag{6.32b}$$

where

$$\begin{aligned} P_{nm} &= \frac{\epsilon_m}{2} \Big(K_{n-m}(2l\xi) + (-1)^m K_{n+m}(2l\xi) \Big) \cos(n+m)\frac{\pi}{2} \\ &+ \epsilon_m \, (-1)^{n+m} \int_0^{\infty} \cosh nu \, \cosh mu \, e^{vf} \, \Big(1 + \cos(2l\xi \sinh u) \Big) \, C_L(v) \, du, \end{aligned} \tag{6.33}$$

$$\begin{aligned} Q_{nm} &= \frac{\epsilon_m}{2} \Big(K_{n-m}(2l\xi) + (-1)^m K_{n+m}(2l\xi) \Big) \sin(n+m)\frac{\pi}{2} \\ &+ \epsilon_m \, (-1)^{n+m+1} \int_0^{\infty} \sinh nu \, \cosh mu \, e^{vf} \, \sin(2l\xi \sinh u) \, C_L(v) \, du, \end{aligned} \tag{6.34}$$

$$\begin{aligned} R_{nm} &= -\frac{\epsilon_m}{2} \Big(K_{n-m}(2l\xi) + (-1)^{m+1} K_{n+m}(2l\xi) \Big) \sin(n+m)\frac{\pi}{2} \\ &+ \epsilon_m \, (-1)^{n+m} \int_0^{\infty} \sinh mu \, \cosh nu \, e^{vf} \, \sin(2l\xi \sinh u) \, C_L(v) \, du, \end{aligned} \tag{6.35}$$

$$\begin{aligned} T_{nm} &= \frac{\epsilon_m}{2} \Big(K_{n-m}(2l\xi) + (-1)^{m+1} K_{n+m}(2l\xi) \Big) \cos(n+m)\frac{\pi}{2} \\ &+ \epsilon_m \, (-1)^{n+m} \int_0^{\infty} \sinh nu \, \sinh mu \, e^{vf} \, \Big(\cos(2l\xi \sinh u) - 1 \Big) \, C_L(v) \, du. \end{aligned} \tag{6.36}$$

Note that the function $C_L(v)$ now has a singularity on the real axis only at ν_2 but not at ν_1 and the path of integration is indented beneath this pole.

This system of equations can be written in matrix form as follows:

$$\mathbf{Ax} = \begin{pmatrix} \mathbf{P+I} & \mathbf{Q} \\ \mathbf{R} & \mathbf{T\text{-}I} \end{pmatrix} \begin{bmatrix} \mathbf{a} \\ \mathbf{b} \end{bmatrix} = 0, \tag{6.37}$$

where

$$\begin{aligned} \mathbf{P} &= [I'_m(la)P_{nm}/K'_m(la)], \quad \mathbf{Q} = [I'_m(la)Q_{nm}/K'_m(la)], \\ \mathbf{R} &= [I'_m(la)R_{nm}/K'_m(la)], \quad \mathbf{T} = [I'_m(la)T_{nm}/K'_m(la)], \\ \mathbf{a} &= [A^1_m], \qquad \mathbf{b} = [B^1_m], \end{aligned} \tag{6.38}$$

for $m \geq 0$ and $n \geq 0$. For non-trivial solutions, we need to find the frequencies for which the determinant of the complex matrix $\mathbf{A}$ vanishes. To find such frequencies, we truncate the matrix $\mathbf{A}$ to a $2M \times 2M$ one and calculate the determinant. This process can be repeated for symmetrical arrangements involving larger numbers of cylinders.

Numerical Results

We consider a wave with wavenumber u_2 propagating from $x = -\infty$ of the form $\exp[ib(x-\xi)]$, $b = \sqrt{u_2^2 - l^2} = u_2 \cos\alpha_{inc}$, making an angle α_{inc} to the positive x-axis and incident upon the cylinder centred at (ξ, f) assuming that the other cylinder does not affect the interaction between the wave and the cylinder under consideration. For a fixed geometrical configuration and a fixed density ratio, the problem of finding the trapped mode frequencies is completely specified by the two non-dimensional parameters Ka and ξ/a. For a fixed value of ξ/a, the parameter Ka is varied to locate the zeros of the real part of the truncated determinant. Then corresponding to those values of Ka, the absolute values of the determinant are plotted. In all the figures, the fixed values considered are: $M = 8$, $\rho = 0.50$ and $\alpha_{inc} = 0.34$. Note that α_{inc} is such that there are no propagating waves in the upper layer for all Ka. For a two-layer fluid consisting of fresh water and salt water, the value of ρ would ideally be around 0.97. The same qualitative features are observed for such a density ratio, but the effects of the interface are not very distinct. Therefore we consider $\rho = 0.5$ for our problem in order to have a clear observation.

When both the cylinders are placed in the lower layer, the values of ξ/a are considered up to 8.0 and then the variation of trapped frequencies is observed for $\xi/a \in [1, 8]$. In Figs. 6.2, 6.3 and 6.4, the depth d/a of the upper layer is taken as 2.0 and the submergence depth f/a as -1.1. In Fig. 6.2, Ka is plotted against ξ/a with the values of the ice parameters taken as zero which presents the free surface problem investigated in Linton and Cadby (2003). The curves in part (a) of this figure as well in all the subsequent figures will be treated as modes.

In Figs. 6.3 and 6.4, the flexural rigidity D/a^4 is considered as 0.001 and 0.01, respectively – a change from Fig. 6.2 and this implies that the free surface is replaced by a thin ice-cover. It is observed from Figs. 6.3 and 6.4, upon this replacement, that the first and second modes remain unchanged. With an increase in D/a^4, the frequency Ka for the third mode decreases. Within the specified range of ξ/a, the number of points for which trapped waves exist decreases with an increase in D/a^4.

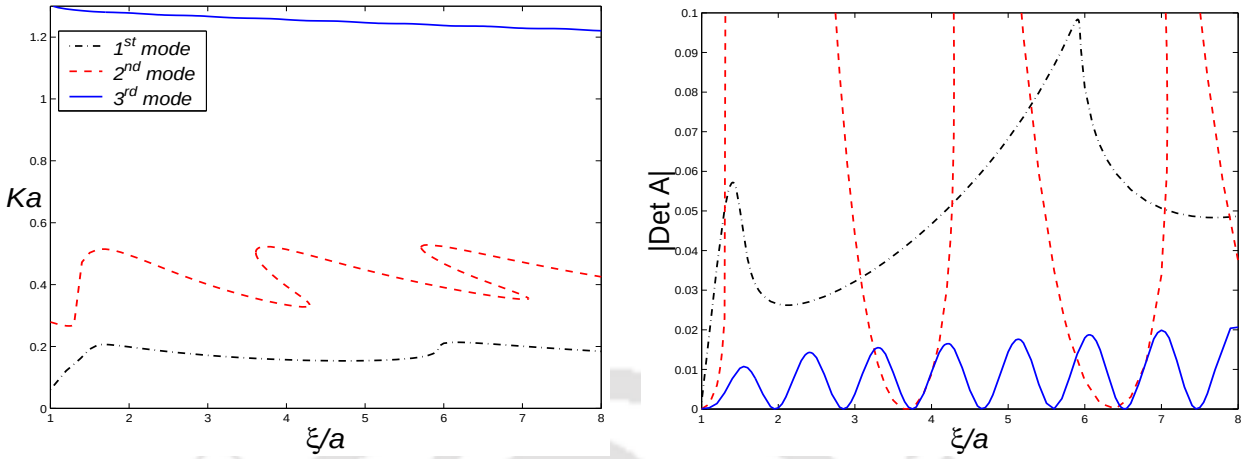

(a) (b)

Figure 6.2: (a) Values of Ka at which the real part of the determinant vanishes and (b) the absolute values of the determinant of the complex matrix for two cylinders of equal radius a submerged in the lower layer; $d/a = 2$, $f/a = -1.1$, $\rho = 0.5$, $\alpha_{inc} = 0.34$, $D/a^4 = 0$ and $\varepsilon/a = 0$.

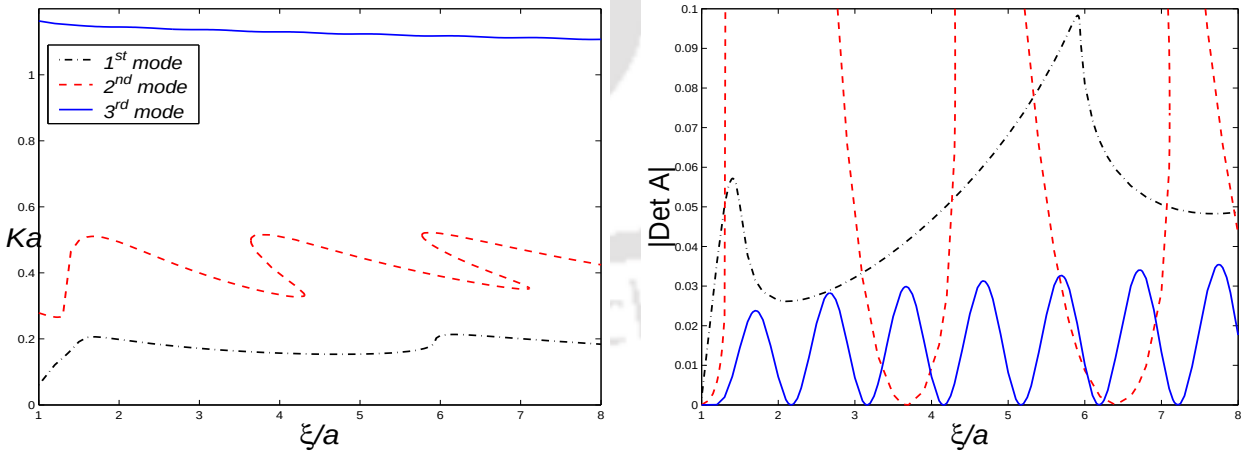

(a) (b)

Figure 6.3: (a) Values of Ka at which the real part of the determinant vanishes and (b) the absolute values of the determinant of the complex matrix for two cylinders of equal radius a submerged in the lower layer; $d/a = 2$, $f/a = -1.1$, $\rho = 0.5$, $\alpha_{inc} = 0.34$, $D/a^4 = 0.001$ and $\varepsilon/a = 0.001$.

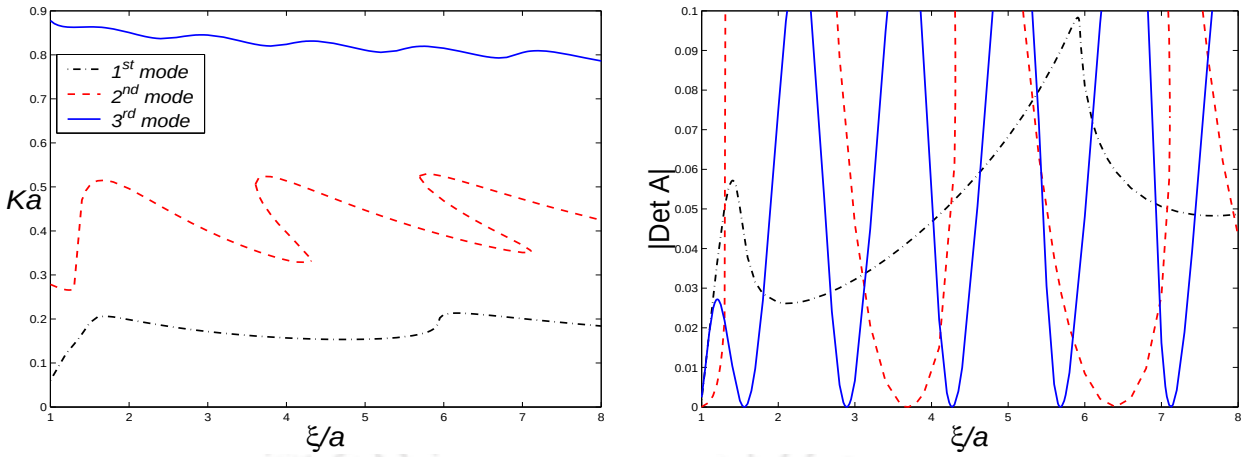

(a) (b)

Figure 6.4: (a) Values of Ka at which the real part of the determinant vanishes and (b) the absolute values of the determinant of the complex matrix for two cylinders of equal radius a submerged in the lower layer; $d/a = 2$, $f/a = -1.1$, $\rho = 0.5$, $\alpha_{inc} = 0.34$, $D/a^4 = 0.01$ and $\varepsilon/a = 0.001$.

Figures 6.5 and 6.6 show the variation of these modes for an increase in the depth d/a of the upper layer. In both the figures, the submergence depth f/a is taken as -1.1 and the values of the ice parameters as $D/a^4 = 0.001$ and $\epsilon/a = 0.001$. In this case also, there is no variation in the first mode. For the second mode, the values of ξ/a for which trapped waves exist increase with an increase in the depth of the upper layer. For the third mode, as can be seen from Fig. 6.6(a), frequency Ka decreases with an increase in the depth of the upper layer. From Fig. 6.6(b), it is observed that with a decrease in the depth of the upper layer, more points ξ/a occur for which trapped waves exist.

Three different submergence depths are considered in Figs. 6.7 and 6.8: $f/a = -1.05, -1.10, -1.15$. For both figures, the depth d/a of the upper layer is taken as 2.0 and the non-dimensionalized ice parameters are fixed at 0.001. With the variation of the submergence depth f/a, though the first mode varies but it still does not produce any point on (ξ/a)-axis for which the absolute value of the determinant vanishes. As a consequence, the first mode does not give rise to any trapped waves within the specified range of ξ/a. For the second mode, the values of ξ/a for which trapped waves exist increase as the submergence depth increases, as observed by comparing all the (b) parts of Fig. 6.7. Figure 6.8(a) shows that frequencies Ka for the third mode decreases as f/a increases. It can be seen from Fig. 6.8(b) that the values of ξ/a, for which trapped waves exist, increase with an increase in submergence depth.

6.4.2 Cylinders submerged in the upper layer

Now the problem is considered with the pair of identical circular horizontal cylinders placed in the upper fluid layer ($f > 0$) and hence the work is accomplished entirely with ϕ^I. The symmetric and antisymmetric multipoles, based on cylinder j; $j = I, II$, are given by

$$\phi^{Is}_{nj} = K_n(lr_j)\cos n\theta_j + \int_0^\infty \cosh nu \ \cos(lx_j \sinh u)\left[A^{(0)}_{Un}(v)e^{vz_j} + B^{(0)}_{Un}(v)e^{-vz_j}\right] du,$$

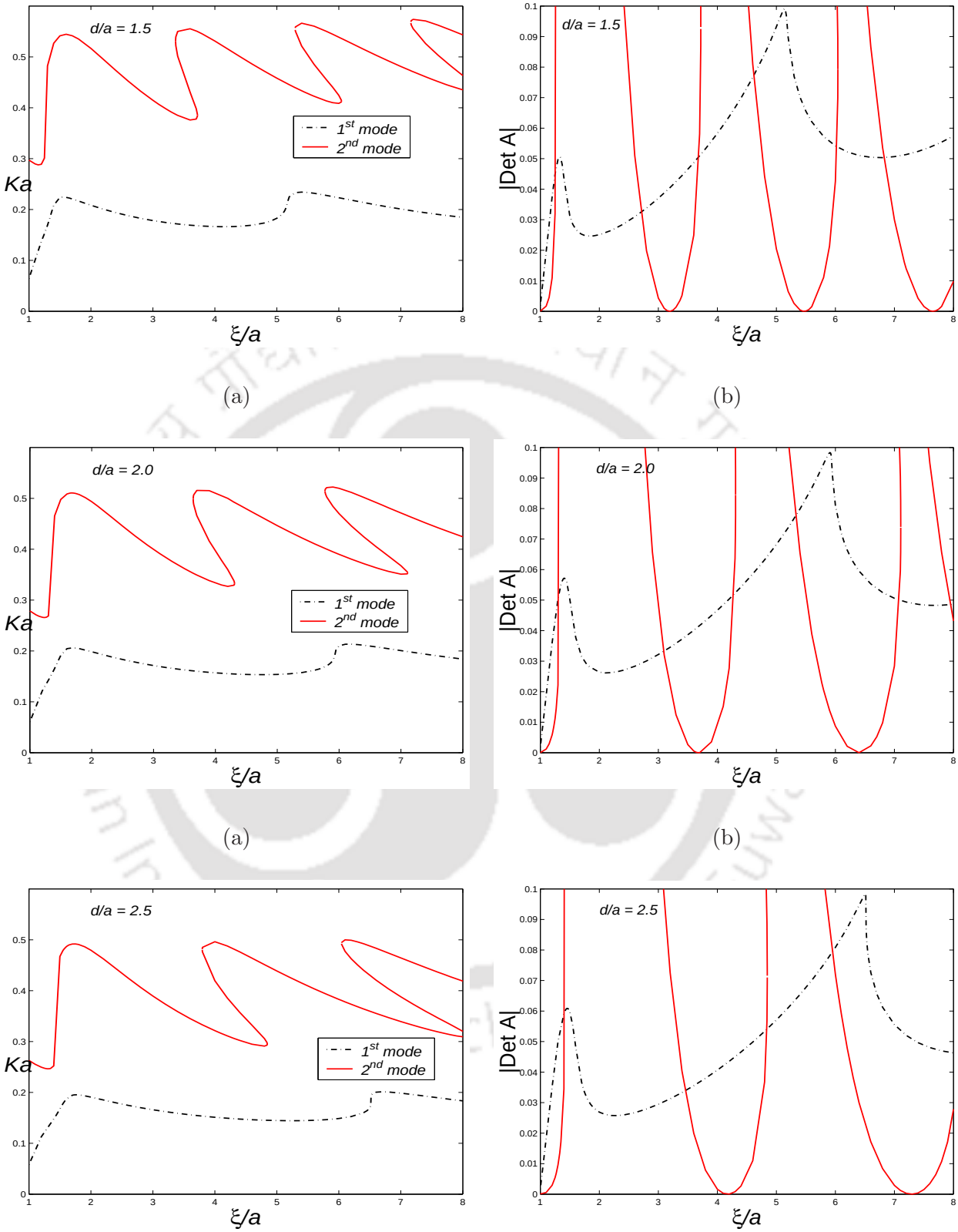

Figure 6.5: (a) Values of Ka at which the real part of the determinant vanishes and (b) the absolute values of the determinant of the complex matrix for three different values of upper layer depth d/a for two cylinders of equal radius a submerged in the lower layer; $f/a = -1.1$, $\rho = 0.5$, $\alpha_{inc} = 0.34$, $D/a^4 = 0.001$ and $\varepsilon/a = 0.001$.

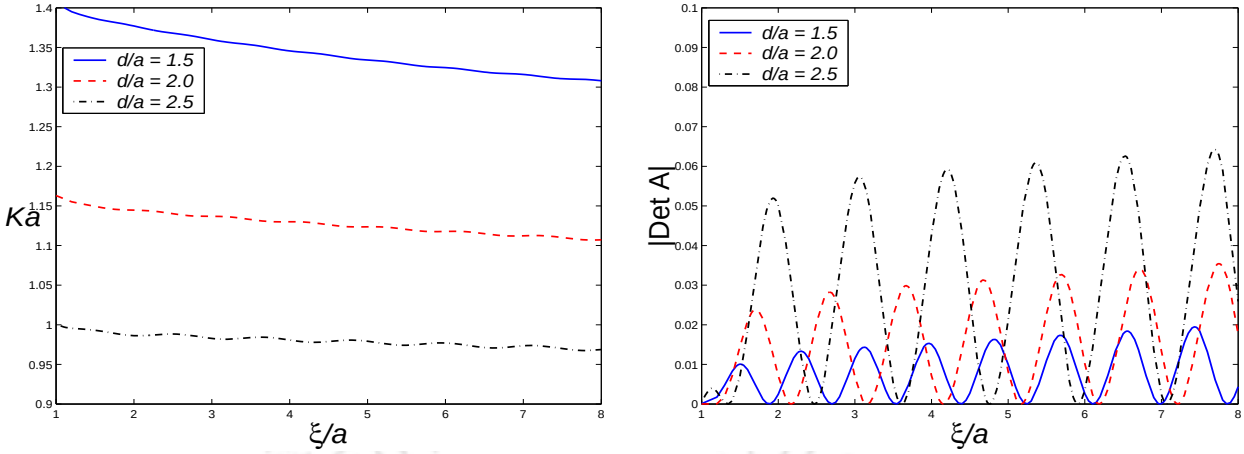

Figure 6.6: Variation of third mode for three different values of upper layer depth d/a for two cylinders of equal radius a submerged in the lower layer; $f/a = -1.1$, $\rho = 0.5$, $\alpha_{inc} = 0.34$, $D/a^4 = 0.001$ and $\varepsilon/a = 0.001$.

$$\phi_{nj}^{Ia} = K_n(lr_j)\sin n\theta_j + \int_0^\infty \sinh nu\ \sin(lx_j\sinh u)\left[A_{Un}^{(1)}(v)e^{vz_j} + B_{Un}^{(1)}(v)e^{-vz_j}\right]du,$$

where

$$A_{Un}^{(q)}(v) = \frac{F_+(v)}{F_-(v)}e^{-2vd}\Big((-1)^{n+q}e^{vf} + B_{Un}^{(q)}(v)\Big), \tag{6.39}$$

$$B_{Un}^{(q)}(v) = \frac{v-K}{G(v)}\Big(F_-(v)e^{-vf} + F_+(v)(-1)^{n+q}e^{v(f-2d)}\Big), \quad q = 0, 1. \tag{6.40}$$

Proceeding exactly as in the lower layer case, we obtain the following infinite coupled system of homogenous linear equations:

$$\alpha_m + \frac{I_m'(la)}{K_m'(la)}\sum_{n=0}^{\infty}(P_{nm}^U\alpha_n + Q_{nm}^U\beta_n) = 0, \tag{6.41a}$$

$$\beta_m - \frac{I_m'(la)}{K_m'(la)}\sum_{n=0}^{\infty}(T_{nm}^U\beta_n + R_{nm}^U\alpha_n) = 0, \quad m \geq 0, \tag{6.41b}$$

where

$$P_{nm}^U = \frac{\varepsilon_m}{2}\Big(K_{n-m}(2l\xi) + (-1)^m K_{n+m}(2l\xi)\Big)\cos(n+m)\frac{\pi}{2} + \varepsilon_m\int_0^\infty \cosh nu\ \cosh mu\ \Big(1+\cos(2l\xi\sinh u)\Big)\left[(-1)^m A_{Un}^{(0)}(v)e^{vf} + B_{Un}^{(0)}(v)e^{-vf}\right]du, \tag{6.42}$$

$$Q_{nm}^U = \frac{\varepsilon_m}{2}\Big(K_{n-m}(2l\xi) + (-1)^m K_{n+m}(2l\xi)\Big)\sin(n+m)\frac{\pi}{2} + \varepsilon_m\int_0^\infty \sinh nu\ \cosh mu\ \sin(2l\xi\sinh u)\left[(-1)^m A_{Un}^{(1)}(v)e^{vf} + B_{Un}^{(1)}(v)e^{-vf}\right]du, \tag{6.43}$$

$$R_{nm}^U = -\frac{\varepsilon_m}{2}\Big(K_{n-m}(2l\xi) + (-1)^{m+1} K_{n+m}(2l\xi)\Big)\sin(n+m)\frac{\pi}{2} + \varepsilon_m\int_0^\infty \sinh mu\ \cosh nu\ \sin(2l\xi\sinh u)\left[(-1)^m A_{Un}^{(0)}(v)e^{vf} - B_{Un}^{(0)}(v)e^{-vf}\right]du, \tag{6.44}$$

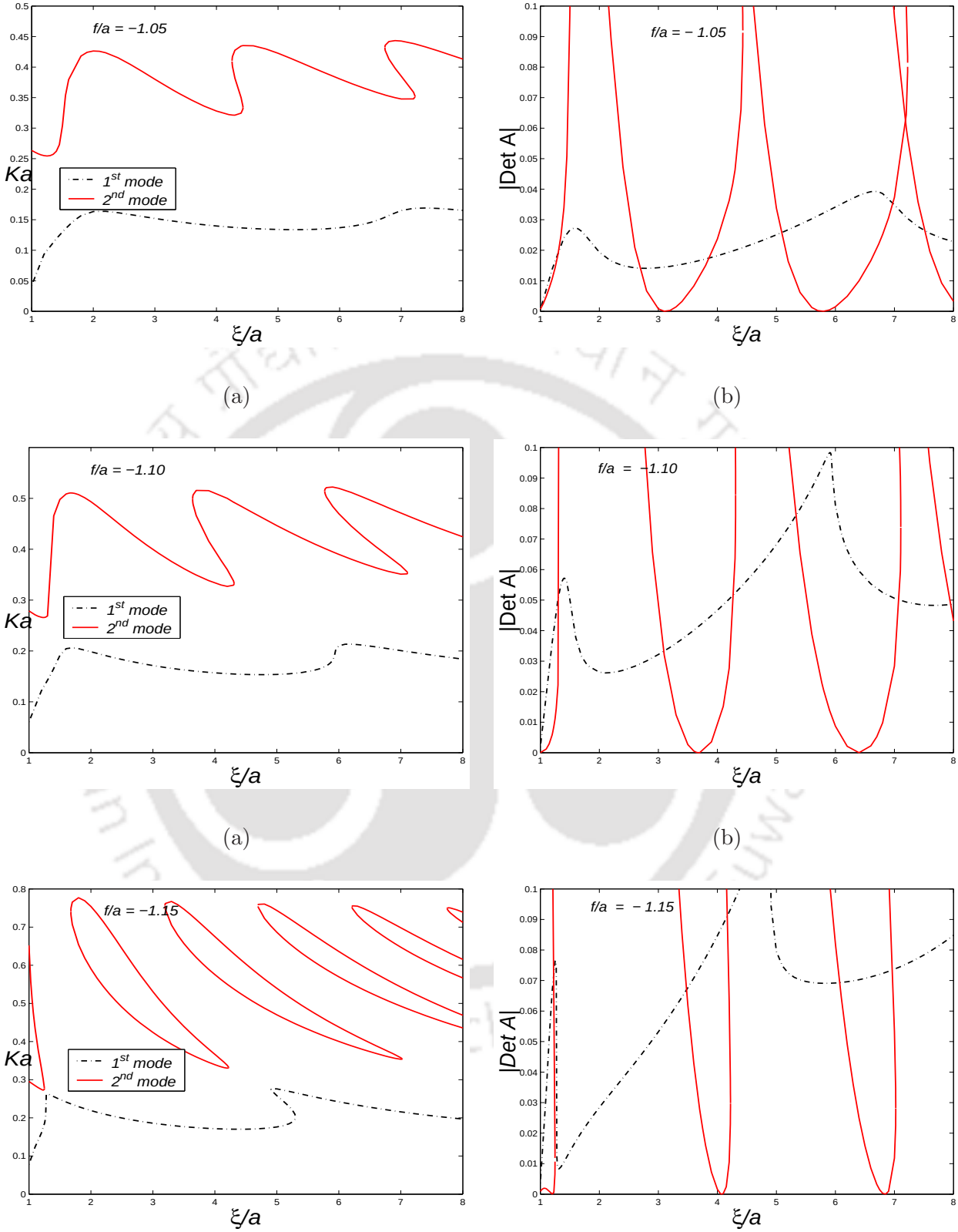

Figure 6.7: (a) Values of Ka at which the real part of the determinant vanishes and (b) the absolute values of the determinant of the complex matrix for three different values of submergence depth f/a for two cylinders of equal radius a submerged in the lower layer; $d/a = 2.0$, $\rho = 0.5$, $\alpha_{inc} = 0.34$, $D/a^4 = 0.001$ and $\varepsilon/a = 0.001$.

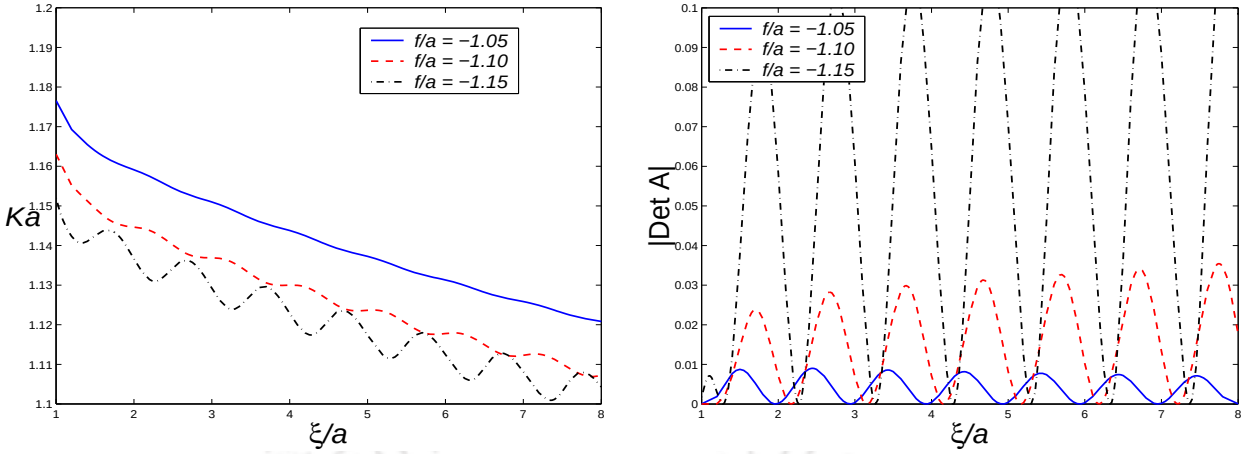

Figure 6.8: Variation of third mode for three different values of submergence depth f/a for two cylinders of equal radius a submerged in the lower layer; $d/a = 2.0$, $\rho = 0.5$, $\alpha_{inc} = 0.34$, $D/a^4 = 0.001$ and $\varepsilon/a = 0.001$.

$$T^{U}_{nm} = \frac{\varepsilon_m}{2}\Big(K_{n-m}(2l\xi) + (-1)^{m+1}K_{n+m}(2l\xi)\Big)\cos(n+m)\frac{\pi}{2} + \varepsilon_m \int_0^\infty \sinh nu \, \sinh mu \, \Big(\cos(2l\xi\sinh u - 1)\Big)\Big[(-1)^{m+1}A^{(1)}_{Un}(v)e^{vf} + B^{(1)}_{Un}(v)e^{-vf}\Big]\, du. \tag{6.45}$$

Here also, as was done in the previous case, by varying the frequency Ka and fixing the other parameters, we conveniently locate the real zeros of the truncated determinant and then check for the existence of trapped waves by observing the absolute value of the determinant since zeros of the absolute value of the determinant correspond to the trapped modes.

Numerical Results

With both the cylinders placed in the upper layer, we investigate the existence of trapped waves with ξ/a varying in the range 1.0 to 6.0. In this case, only the variation of trapped waves is considered by varying the values of the ice parameters. This consideration is mainly due to the fact that large computational expense occurs while computing the integrals in (6.42)–(6.45) which are more in number as compared to the lower layer case. Ka is varied up to the value 3.0 to locate the zeros of the real part of the truncated determinant. Here three sets of ice parameters are considered: $D/a^4 = 0, \varepsilon/a = 0$; $D/a^4 = 0.0001, \varepsilon/a = 0.0001$; $D/a^4 = 0.001, \varepsilon/a = 0.001$. The first set corresponds to the result for the upper layer covered by a free surface. In all figures, the depth d/a of the upper layer is taken as 2.5 and the submergence depth f/a as 1.25.

Figure 6.9(a) shows that there exist two modes for which the real part of the determinant vanishes. Corresponding to those values of Ka, we present the plot of the absolute values of the determinant in Fig. 6.9(b). It is observed that for both modes, there exist values of ξ/a for which trapped waves exist. However, if those values of ξ/a are changed even by a small amount, the embedded trapped waves will cease to exist.

Figure 6.10 shows that a very small thickness of the ice parameter ε/a will give rise to one extra mode - the third one, as compared to the case with a free surface. For this third mode,

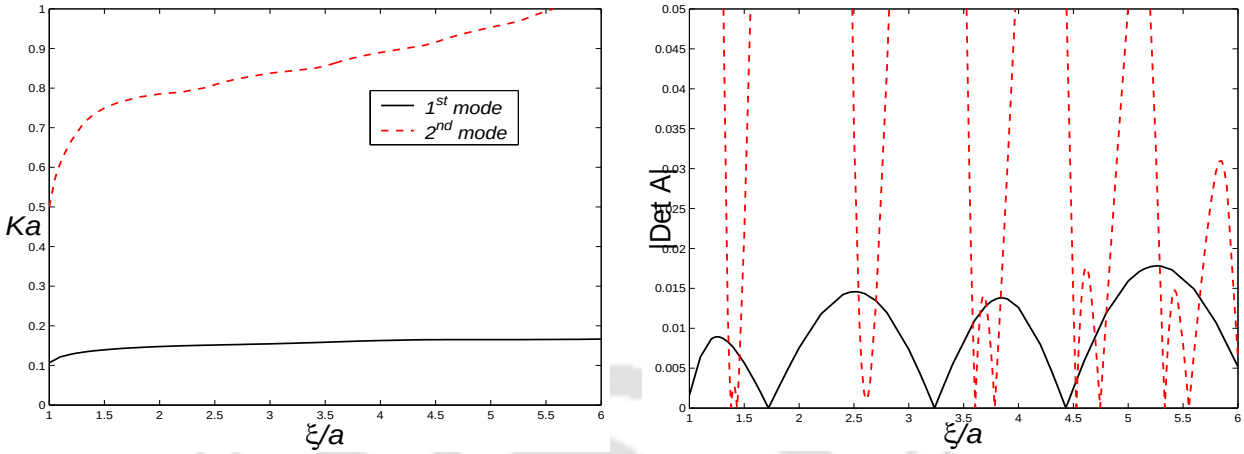

(a) (b)

Figure 6.9: (a) Values of Ka at which the real part of the determinant vanishes and (b) the absolute values of the determinant of the complex matrix for two cylinders of equal radius a submerged in the upper layer; $d/a = 2.50$, $f/a = 1.25$, $\rho = 0.5$, $\alpha_{inc} = 0.34$, $D/a^4 = 0$ and $\varepsilon/a = 0$.

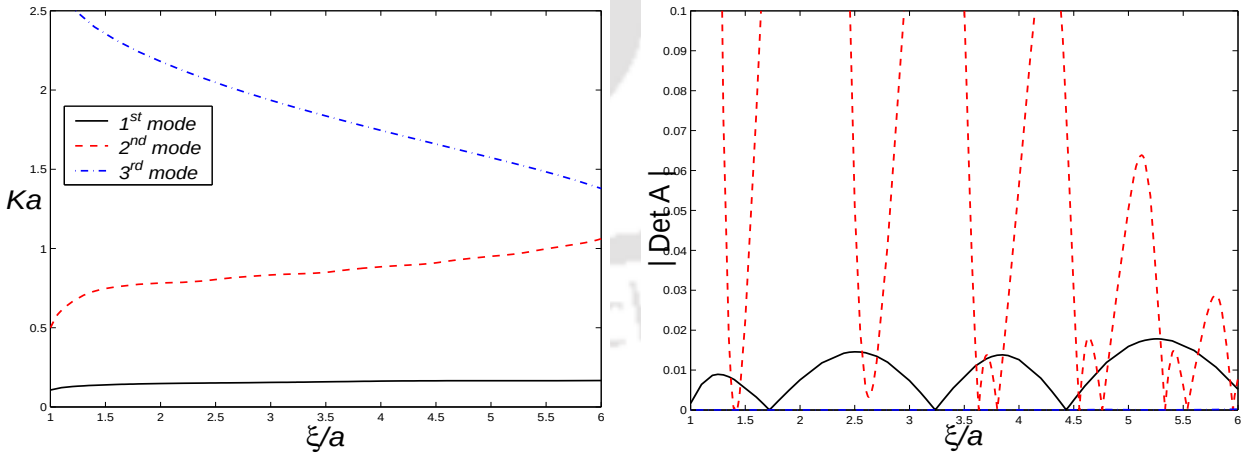

(a) (b)

Figure 6.10: (a) Values of Ka at which the real part of the determinant vanishes and (b) the absolute values of the determinant of the complex matrix for two cylinders of equal radius a submerged in the upper layer; $d/a = 2.50$, $f/a = 1.25$, $\rho = 0.5$, $\alpha_{inc} = 0.34$, $D/a^4 = 0.0001$ and $\varepsilon/a = 0.0001$.

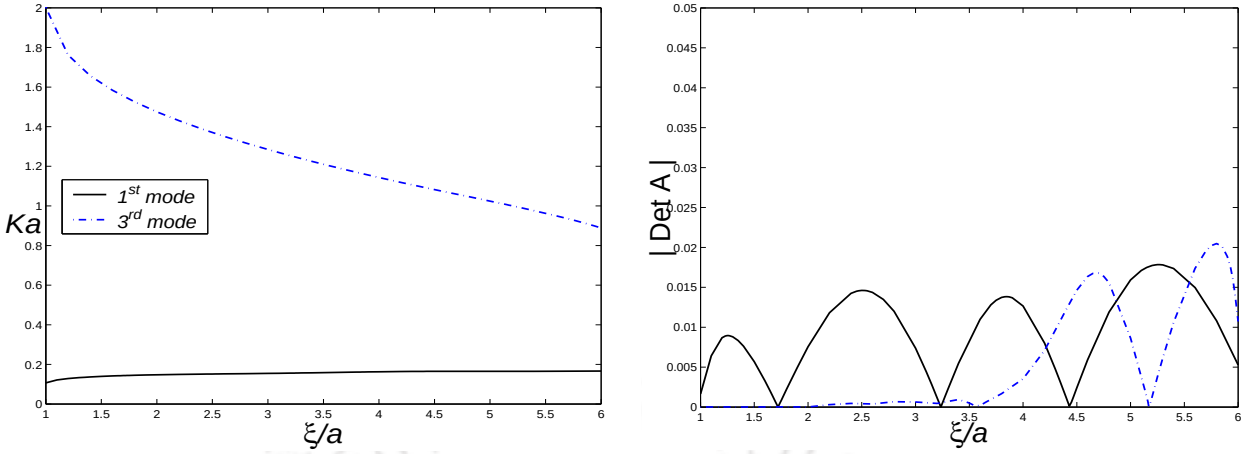

(a) (b)

Figure 6.11: (a) Values of Ka at which the real part of the determinant vanishes and (b) the absolute values of the determinant of the complex matrix for two cylinders of equal radius a submerged in the upper layer; $d/a = 2.50$, $f/a = 1.25$, $\rho = 0.5$, $\alpha_{inc} = 0.34$, $D/a^4 = 0.001$ and $\varepsilon/a = 0.001$.

there exist trapped waves for all values of ξ/a within the range considered. For Fig. 6.11, the values of the ice parameter set are considered to be 10 times more than those considered for Fig. 6.10. In this case, the first mode remains the same but the second mode does not exist while the third mode exists with its values getting lowered as compared to those in Fig. 6.10. For the third mode, trapped waves will always exist for values of ξ/a approximately up to 3.60.

6.5 Conclusions

The work described in this chapter is an investigation of trapped water waves supported by a pair of horizontal circular cylinders submerged in either layer of a two-layer fluid in an ocean, where the upper layer is of finite depth and is bounded above by a thin ice-cover modeled as a thin elastic plate, which replaces the free surface, and the lower layer is of infinite depth. In such a situation, propagating waves exist at two different wavenumbers for any given frequency: the one with the smaller wavenumber corresponds to an ice-surface disturbance and the other to an interfacial wave motion. Since only the embedded trapped waves confined to the area between the cylinders are considered, so propagating waves exist only near the interface, not near the ice-cover. For the case when the cylinders are placed entirely in the lower layer, we present numerical evidence that trapped modes do exist above the cut-off frequency for oblique waves for such a geometry. For the parameter values chosen, the number of trapped modes embedded in the continuous spectrum decreases with an increase in the flexural rigidity of the ice-cover. The trapped mode frequency decreases when either the depth of the upper layer or the submergence depth increases. When the cylinders are placed entirely in the upper layer, we consider both cases of the layer covered by a free surface or by a thin ice-cover. Here also it is observed that with a small change in the values of the separation parameter, embedded trapped mode ceases to exist for the free surface and also for very small thickness of the ice-

cover. It is to be noted that the existence of trapped modes throughout the present work is based on numerical evidence only, i.e., we numerically locate the values of those frequencies for which the truncated determinant vanishes. Though numerical computation is carried out for a pair of cylinders, we also develope the theoretical background for the problem in which N cylinders follow a specific arrangement. The consideration of two cylinders in either layer in an ice-covered two-layer fluid makes the problem more acceptable from a physical point of view. The present case of a pair of cylinders can be repeated for symmetrical arrangements involving larger number of cylinders.

Chapter 7

Effects of surface tension on trapped modes in a two-layer fluid

7.1 Introduction

In all the problems that we have considered till now in the thesis, the effects of surface tension at the free surface as well as the interface(s) have been neglected. In this chapter we include surface tension effect both at the free surface and the interface of the two-layer fluid of finite depth. Then we numerically locate the frequencies for which trapped modes exist by locating the zeros of the suitably truncated determinant of an infinite system of homogenous linear equation. Finally we examine the effect of variation of both surface tension parameters on the values and the pattern of trapped mode and then conclude whether the exclusion of surface tension in formulating the problems is justifiable or not.

7.2 Mathematical formulation of the problem

As the first step towards the investigation of trapped modes, we formulate the physical problem as a boundary value problem associated with Modified Helmholtz equation. Cartesian coordinates are chosen such that the xy-plane coincides with the undisturbed interface between the two fluids. Each fluid is assumed to be of infinite horizontal extent in the x- and y-directions while the depth is along the z-direction which is considered positive vertically upwards. The upper fluid layer $(-\infty < x < \infty;\ -\infty < y < \infty;\ 0 < z < d)$ is of constant density ρ_I in the presence of surface tension T_1 with $z = d$ as the mean free surface. The lower fluid $(-\infty < x < \infty;\ -\infty < y < \infty;\ -h < z < 0)$ is assumed to be of constant density ρ_{II} in the presence of surface tension T_2 with the mean interface at $z = 0$ and bottom surface is considered at $z = -h$ (Fig. 7.1). Assuming that the fluid is inviscid, incompressible and immiscible, and the motion irrotational, the fluid motion is described by the two velocity potentials $\Phi^j(x, y, z, t)$, $j = I, II$. Let $\eta(x, y, t)$ and $\zeta(x, y, t)$ be the small displacements at the upper surface and the interface, respectively. The governing equation for the boundary value problem involving the potential $\Phi^j(x, y, z, t)$, $j = I, II$, is the Laplace's equation

$$\nabla^2\Phi^j = 0 \qquad \text{in the respective fluid region.} \tag{7.1}$$

The linearized kinematic conditions at the mean free surface and the mean interface are,

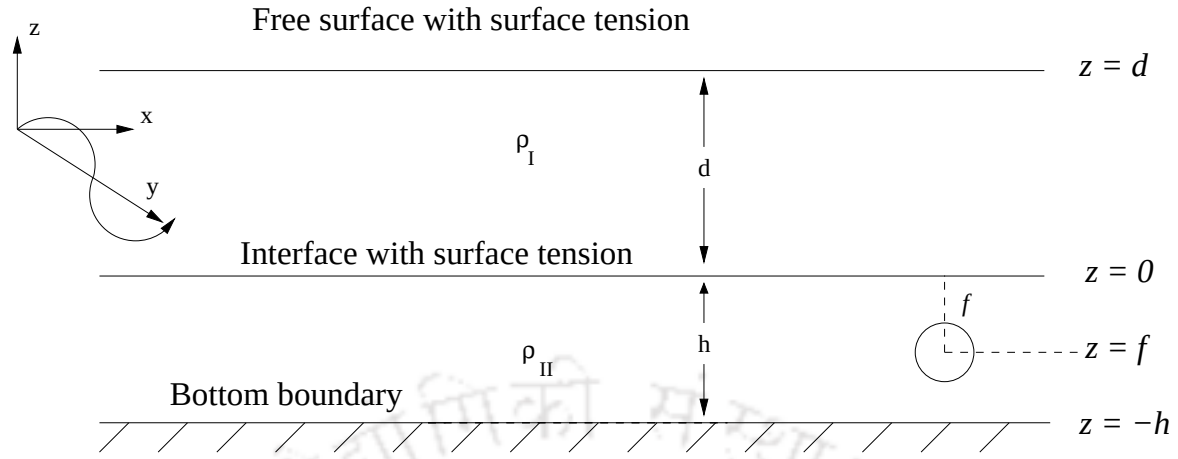

Figure 7.1: Schematic diagram for a two-layer fluid with surface tension at free surface and interface.

respectively, given by

$$\frac{\partial \eta}{\partial t} = \frac{\partial \Phi^{I}}{\partial z} \qquad \text{on} \qquad z = d, \tag{7.2}$$

$$\frac{\partial \zeta}{\partial t} = \frac{\partial \Phi^{I}}{\partial z} = \frac{\partial \Phi^{II}}{\partial z} \qquad \text{on} \qquad z = 0. \tag{7.3}$$

In the presence of surface tension, the general relations connecting surface tension and pressure gradient are given by (Mohapatra and Sahoo (2011))

$$P_0 - p_1 = \frac{T_1}{R} \qquad \text{in the case of free surface,} \tag{7.4}$$

$$p_2 - p_1 = \frac{T_2}{R} \qquad \text{in the case of interface,} \tag{7.5}$$

where $1/R$ is the mean curvature, P_0 is the constant atmospheric pressure and p_j is the hydrodynamic pressure in fluid region j. The mean curvature $1/R$ in Cartesian coordinates is given by

$$\frac{1}{R} = \begin{cases} \dfrac{\eta_{xx} + \eta_{yy}}{(1 + \eta_x^2 + \eta_y^2)^{3/2}} & \text{in the case of free surface,} \\ \dfrac{\zeta_{xx} + \zeta_{yy}}{(1 + \zeta_x^2 + \zeta_y^2)^{3/2}} & \text{in the case of interface.} \end{cases} \tag{7.6}$$

According to the linearized theory of water waves, the hydrodynamic pressure p_j in the corresponding fluid region is given by

$$p_j = -\rho_j g\Big(z + \frac{1}{g}\frac{\partial \Phi^{j}}{\partial t}\Big), \tag{7.7}$$

where ρ_j is the fluid density. Hence, from Eqs. (7.6) and (7.7), the linearized dynamic free-surface boundary condition in the presence of surface tension T_1 at the mean free surface $z = d$ is given by

$$\rho_I\Big(g\eta + \frac{\partial \Phi^{I}}{\partial t}\Big) - T_1\Big(\frac{\partial^2 \eta}{\partial x^2} + \frac{\partial^2 \eta}{\partial y^2}\Big) = 0. \tag{7.8}$$

Further, from Eqs. (7.6) and (7.7), the linearized dynamic condition at the mean interface $z = 0$ in the presence of interfacial surface tension T_2 is given by

$$\rho_{II}\Big(g\zeta + \frac{\partial \Phi^{II}}{\partial t}\Big) - T_2\Big(\frac{\partial^2 \zeta}{\partial x^2} + \frac{\partial^2 \zeta}{\partial y^2}\Big) = \rho_I\Big(g\eta + \frac{\partial \Phi^{I}}{\partial t}\Big). \tag{7.9}$$

When it is assumed that the fluid motion is simple harmonic in time with radian frequency ω, the velocity potential, free surface and interface elevations can be written in the form

$$\begin{aligned} \Phi^j(x,y,z,t) &= \mathrm{Re}[\phi^j(x,z)e^{ily}e^{-i\omega t}], \\ \eta(x,y,t) &= \mathrm{Re}[\bar{\eta}(x)e^{ily}e^{-i\omega t}] \\ \zeta(x,y,t) &= \mathrm{Re}[\bar{\zeta}(x)e^{ily}e^{-i\omega t}]. \end{aligned}$$

Thus, the spatial velocity potentials ϕ^j for $j = I, II$ satisfy (7.1). By combining the kinematic and dynamic boundary conditions (7.2), (7.3), (7.8) and (7.9), the linearized boundary conditions at the mean free surface and mean interface can be written as

$$\frac{\partial \phi^{I}}{\partial z} - K\phi^{I} - M_1\frac{\partial}{\partial z}\Big(\frac{\partial^2}{\partial x^2} - l^2\Big)\phi^{I} = 0 \qquad \text{on} \qquad z = d, \tag{7.10}$$

$$\frac{\partial \phi^{II}}{\partial z} - K\phi^{II} - \widetilde{M}_2\frac{\partial}{\partial z}\Big(\frac{\partial^2}{\partial x^2} - l^2\Big)\phi^{II} = \rho\Big(\frac{\partial \phi^{I}}{\partial z} - K\phi^{I}\Big) \qquad \text{on} \qquad z = 0, \tag{7.11}$$

where $M_1 = T_1/(\rho_I g)$, $\widetilde{M}_2 = T_2/(\rho_{II} g)$, $\rho = \rho_I/\rho_{II}$ with $0 < \rho < 1$. An equivalent form of the interface condition (7.11) is given by

$$\frac{\partial \phi^{II}}{\partial z} - K\phi^{II} - M_2\frac{\partial}{\partial z}\Big(\frac{\partial^2}{\partial x^2} - l^2\Big)\phi^{II} = \rho\Big\{\frac{\partial \phi^{I}}{\partial z} - K\phi^{I} - M_2\frac{\partial}{\partial z}\Big(\frac{\partial^2}{\partial x^2} - l^2\Big)\phi^{I}\Big\}, \tag{7.12}$$

where $M_2 = T_2/\{(\rho_{II} - \rho_I)g\}$.

The impermeable bottom boundary condition is given by

$$\frac{\partial \phi^{II}}{\partial z} = 0 \qquad \text{on} \qquad z = -h. \tag{7.13}$$

Within this framework, progressive waves or incident waves take the form (up to an arbitrary multiplicative constant)

$$\phi^{I} = \exp(\pm ix\sqrt{u^2 - l^2})\Big(F_+(u)e^{u(z-d)} + F_-(u)e^{-u(z-d)}\Big), \tag{7.14}$$

$$\phi^{II} = \exp(\pm ix\sqrt{u^2 - l^2})\cosh u(z+h)F(u), \tag{7.15}$$

where

$$F(u) = \frac{F_+(u)e^{-ud} - F_-(u)e^{ud}}{\sinh uh}, \tag{7.16}$$

$$F_\pm(u) = (1 + M_1u^2)u \pm K, \tag{7.17}$$

and u satisfies the dispersion relation

$$\begin{aligned} &\Big\{u(1 + M_2u^2) + K\sigma\Big\}F_+(u)e^{-2u(d+h)} + \Big\{u(1 + M_2u^2) - K\sigma\Big\}F_-(u) \quad - \\ &\Big\{u(1 + M_2u^2) - K\Big\}F_+(u)e^{-2ud} - \Big\{u(1 + M_2u^2) - K\Big\}F_+(u)e^{-2ud} = 0. \end{aligned} \tag{7.18}$$

This equation has exactly two positive real roots u_1 and u_2 ($u_1 < u_2$, say). For the existence of trapped modes, it is required that

$$\phi^{I}, \phi^{II}, |\nabla\phi^{I}|, |\nabla\phi^{II}| \to 0 \quad \text{as} \quad |x| \to \infty \tag{7.19}$$

and hence l is restricted to be in the range $l > u_2 > u_1$ which ensures that no wave propagation to infinity takes place at the interface or near the free surface.

7.3 Solutions by multipoles

In this section, we discuss the effect of surface tension on trapped waves. The structure considered here is an impermeable horizontal circular cylinder of radius a, having its axis along $z = f$ and its generator running parallel to the y-axis, and is placed in the two-layer fluid. If $f > 0$, the cylinder is in the upper fluid, whereas for $f < 0$ the cylinder is in the lower fluid. Polar coordinates (r, θ) are defined in the xz-plane centred on $(0, f)$ as

$$x = r\sin\theta \text{ and } z = f - r\cos\theta.$$

Kassem (1986) elaborated different types of multipoles describing the velocity potentials when each layer of a two-layer fluid is of finite constant depth. Following his method, multipoles, which are singular at $(0, f)$ and symmetric about $x = 0$, are constructed. The trapped mode potential is then constructed from a linear combination of all possible multipoles. Application of the body boundary condition results in an infinite system of homogenous linear equations.

7.3.1 Cylinder submerged in the upper layer

Since the singularity is in the upper fluid, it follows that

$$\phi_n^{I} \sim K_n(lr)\cos(n\theta) \qquad \text{as} \qquad r = \sqrt{x^2 + (z-f)^2} \to 0;\ n = 1, 2, 3, \ldots \tag{7.20}$$

We try the following as solutions:

$$\phi_n^{I} = K_n(lr)\cos n\theta + \int_0^\infty \cosh nu \cos(lx\sinh u)\Big[A_{U}(v)e^{vz} + B_{U}(v)e^{-vz}\Big]du, \tag{7.21}$$

$$\phi_n^{II} = \int_0^\infty \cosh nu \cos(lx\sinh u)C_{U}(v)\cosh v(z+h)du, \tag{7.22}$$

where $v = l\cosh u$.

With the help of the boundary conditions at the free surface, the interface and the bottom, the coefficients $A_{U}(v)$, $B_{U}(v)$ and $C_{U}(v)$ appearing in Eqs. (7.21) and (7.22) are obtained as

$$A_{U}(v) = \frac{F_+(v)e^{-2vd}}{F_-(v)}\Big[B_{U}(v) + (-1)^n e^{vf}\Big],$$

$$B_{U}(v) = \frac{\Big[(-1)^n F_+(v)e^{v(f-2d)} + F_-(v)e^{-vf}\Big]}{G(v)}\Big[v(1+M_2v^2) - K - e^{-2vh}\{v(1+M_2v^2) + K\sigma\}\Big],$$

$$C_{U}(v) = \frac{2K(1-\sigma)B_{U}(v)}{\{v(1+M_2v^2) - K\}e^{vh} - \{v(1+M_2v^2) + K\sigma\}e^{-vh}},$$

where

$$G(v) = \Big\{v(1+M_2v^2) - K\Big\}F_+(v)e^{-2vd} + \Big\{v(1+M_2v^2) + K\Big\}F_-(v)e^{-2vh} \quad - \\ \Big\{v(1+M_2v^2) + K\sigma\Big\}F_+(v)e^{-2v(d+h)} - \Big\{v(1+M_2v^2) - K\sigma\Big\}F_-(v). \tag{7.23}$$

The total velocity potential ϕ can now be written as

$$\phi = \sum_{n=0}^{\infty} \alpha_n \phi_n^I, \tag{7.24}$$

with

$$\phi_n^I = K_n(lr)\cos n\theta + \sum_{m=0}^{\infty} A_{mn} I_m(lr)\cos m\theta, \tag{7.25}$$

and

$$A_{mn} = \epsilon_n \int_0^{\infty} \cosh mu \cosh nu \Big[(-1)^n A_{U}(v)e^{vf} + B_{U}(v)e^{-vf}\Big]du. \tag{7.26}$$

Applying the body boundary condition $\frac{\partial \phi}{\partial r} = 0$ on $r = a$, we obtain an infinite system of homogenous linear equations in the unknowns α_n:

$$\alpha_n + \frac{I_n'(la)}{K_n'(la)} \sum_{m=0}^{\infty} \alpha_m A_{mn} = 0, \qquad n = 0, 1, 2, \ldots \tag{7.27}$$

where $'$ denotes differentiation with respect to r.

For a given set of parameter values, the problem of finding the trapped mode frequencies is completely specified by the two non-dimensional parameters Ka and la. By fixing one and varying the other, we locate the zeros of the truncated determinant. For the numerical evaluation of the zeros of the determinant, we truncate the system to a 32×32 system and the result presented below are obtained correct up to three decimal places. The effect of submergence depth, depths of either fluid layer is already covered by the work in Linton and Cadby (2003). We now investigate the effects of both the surface tension on the dispersion plots and density plots of trapped modes (if any).

Numerical results

Figures 7.2–7.4 show the results obtained for trapped modes above a horizontal circular cylinder of radius a submerged in the upper layer of a two-layer fluid bounded above by a free surface with the inclusion of surface tension at both the free surface and the interface. For all the cases, the depth h/a of the lower layer is taken as 6.0. For the dispersion curve (Fig. 7.2), with the given set of parameter values, we observe that when there was no surface tension at the interface there did exist two trapped modes (Linton and Cadby (2003)) but with the consideration of even smaller values of surface tension at the interface, there exists only one trapped mode. Now this mode does not get so much affected by an increase in the non-dimensionalized surface tension parameter M_2/a^2.

Trapped mode wavenumbers are plotted against density ratio in Figs. 7.3–7.4 for different values of surface tension parameters M_1/a^2 and M_2/a^2 assuming one parameter to be zero and other varying. The submergence depth f/a is taken as 1.05 and the depth of the upper layer

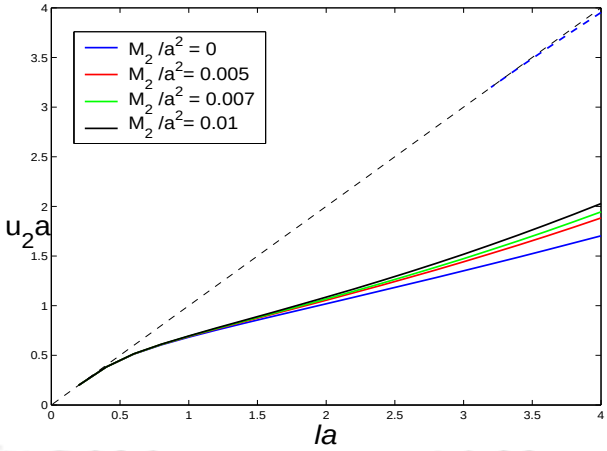

Figure 7.2: Dispersion curves for a cylinder of radius a in the upper layer for different values of M_2/a^2; $\rho = 0.5$, $d/a = 3$, $f/a = 1.01$, $h/a = 6$ and $M_1/a^2 = 0$.

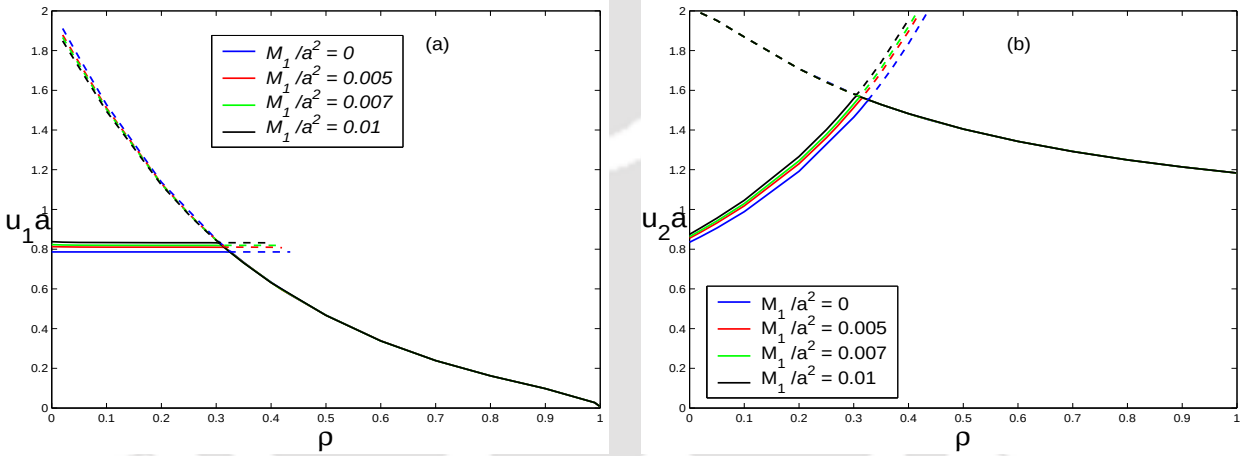

Figure 7.3: Trapped mode wavenumbers plotted against ρ for a cylinder of radius a in the upper fluid layer for different values of M_1/a^2; $la = 2$, $d/a = 2.1$, $h/a = 6$, $f/a = 1.05$ and $M_2/a^2 = 0$.

as 2.10 since we note the existence of near crossing points between two modes corresponding to these values in Linton and Cadby (2003). In the present case also, existence of two modes along with near crossing points is shown but in addition to that not much effect is observed with the inclusion of surface tension at the free surface and the interface.

7.3.2 Cylinder submerged in the lower layer

Now the problem is considered with the cylinder placed in the lower layer. The multipoles singular at $z = f(< 0)$ are required to be modified. This can be done in the same manner as was done previously for the case of the cylinder placed in the upper layer ($f > 0$). The suitable symmetric multipoles are

$$\phi_n^I = \int_0^\infty \cosh nu \cos(lx \sinh u) \Big[A_L(v) e^{vz} + B_L(v) e^{-vz} \Big] du, \tag{7.28}$$

$$\phi_n^{II} = K_n(lr) \cos n\theta + \int_0^\infty \cosh nu \cos(lx \sinh u) \Big[C_L(v) e^{vz} + D_L(v) e^{-vz} \Big] du, \tag{7.29}$$

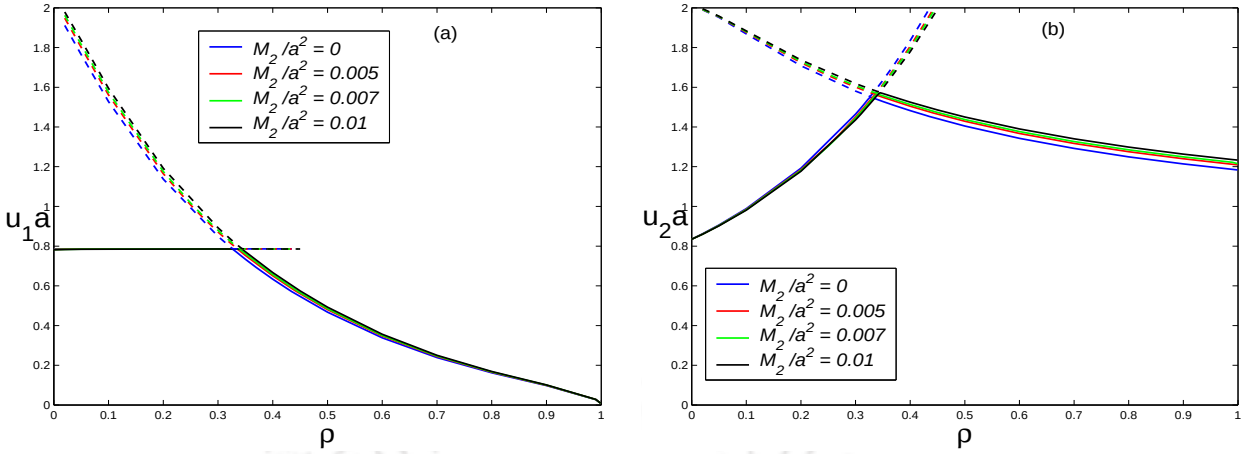

Figure 7.4: Trapped mode wavenumbers plotted against ρ for a cylinder of radius a in the upper fluid layer for different values of M_2/a^2; $la = 2$, $d/a = 2.1$, $h/a = 6$, $f/a = 1.05$ and $M_1/a^2 = 0$.

where the integrals are Cauchy Principal Value integrals with

$$\begin{aligned}
A_{_L}(v) &= \frac{F_+(v)}{F_-(v)} B_{_L}(v) e^{-2vd}, \\
B_{_L}(v) &= \frac{K(1+\sigma)F_-(v)}{G(v)} \Big((-1)^{n+1} e^{vf} - e^{-v(f+2h)} \Big), \\
C_{_L}(v) &= \frac{B_{_L}(v)}{K(1+\sigma)F_-(v)} [\{v(1+M_2v^2) + K\sigma\} F_+(v) e^{-2vd} - \{v(1+M_2v^2) + K\} F_-(v)], \\
D_{_L}(v) &= \Big(C_{_L}(v) + e^{-vf} \Big) e^{-2vh},
\end{aligned}$$

where $G(v)$ is given by Eq. (7.23). Due to the trapped mode condition, there will be no singularities on the real axis. The polar expansion of the multipoles, following the previous procedure, is

$$\phi_n^{II} = K_n(lr)\cos n\theta + \sum_{m=0}^{\infty} B_{mn} I_m(lr) \cos m\theta, \tag{7.30}$$

where

$$B_{mn} = \epsilon_n \int_0^{\infty} \cosh mu \cosh nu \Big[(-1)^n C_{_L}(v) e^{vf} + D_{_L}(v) e^{-vf} \Big] du. \tag{7.31}$$

By applying the body boundary condition, a similar kind of system of equations like (7.27) is obtained for β_n:

$$\beta_n + \frac{I_n'(la)}{K_n'(la)} \sum_{m=0}^{\infty} \beta_m B_{mn} = 0, \qquad n = 0, 1, 2, \ldots \tag{7.32}$$

Here also, as in the previous case, by varying the frequencies Ka and fixing the other parameters, the zeros of the truncated determinant are conveniently located. The results presented next are obtained correct up to three decimal places where a 32×32 system has been used after truncating the system arising out of Eq. (7.32).

Numerical results

Figures 7.5–7.7 show the plots of the non-dimensional trapped mode frequencies for a circular cylinder of radius a immersed in the lower layer of the two-layer fluid. In all cases, the depth d/a of the upper layer is taken as 3.0, the submergence depth f/a is taken as -1.01 which means that the cylinder is very close to the interface and the depth h/a of the lower layer is taken as 6.0. Figure 7.5 shows the dispersion curves for four different values of M_2/a^2: $M_2/a^2 = 0$, 0.005, 0.007 and 0.01. For each set of parameter values, there are two curves corresponding to two modes which are displayed in the graphs. We clearly observe that the trapped mode wavenumber $u_2 a$ increases when the surface tension value at the interface increases, the second mode being affected more than the first mode.

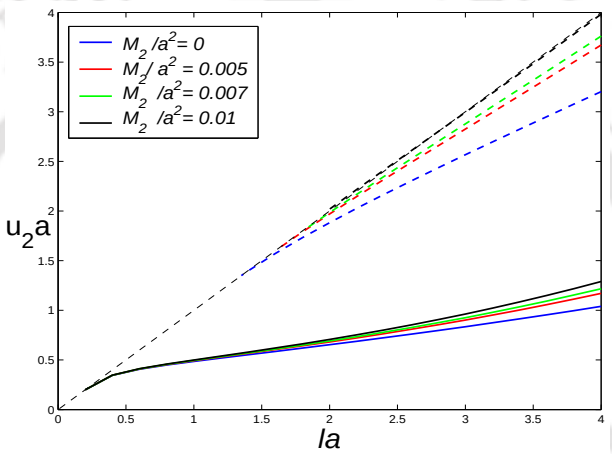

Figure 7.5: Dispersion curves for a cylinder of radius a in the lower layer for different values of M_2/a^2; $\rho = 0.5$, $d/a = 3$, $f/a = -1.01$, $h/a = 6$ and $M_1/a^2 = 0$.

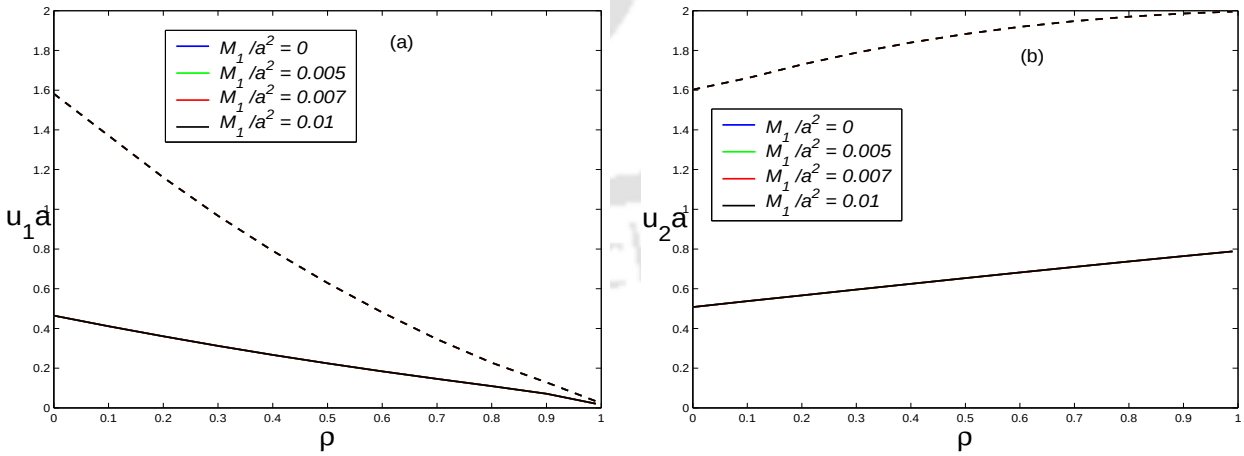

Figure 7.6: Trapped mode wavenumbers plotted against ρ for a cylinder of radius a in the lower fluid layer for different values of M_1/a^2; $la = 2$, $d/a = 3.0$, $h/a = 6.0$, $f/a = -1.01$ and $M_2/a^2 = 0$.

When trapped mode wavenumbers are plotted against density ratio for different values of surface tension parameter M_1/a^2 at the free surface, we observe that the modes do not get affected by the variation of the same. But with the variation of surface tension parameter

M_2/a^2, as seen from Fig. 7.7, trapped modes for both the wavenumbers get affected. With an increase in M_2/a^2, the second trapped mode for both the wavenumbers u_1a and u_2a increases more as compared to the first mode.

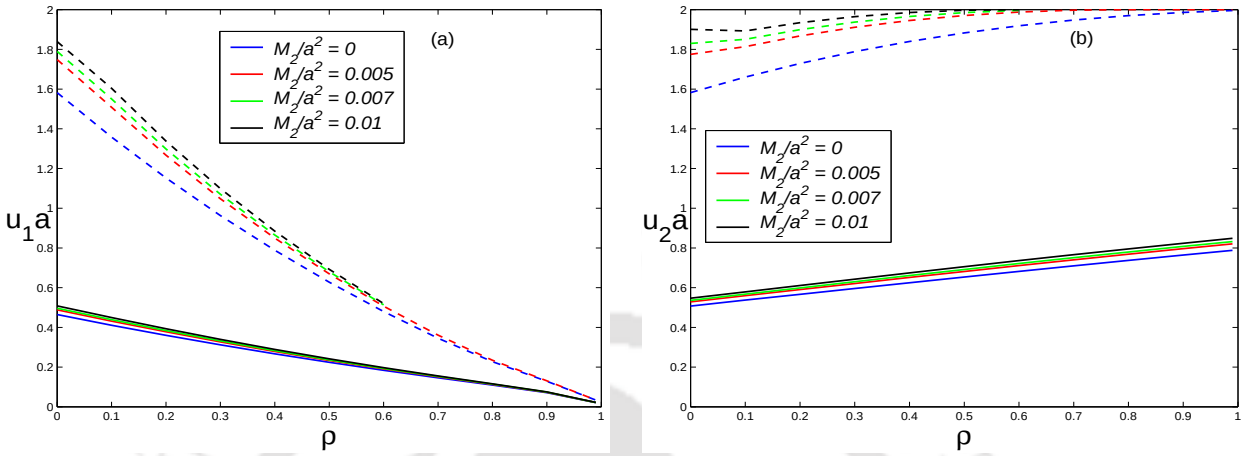

Figure 7.7: Trapped mode wavenumbers plotted against ρ for a cylinder of radius a in the lower fluid layer for different values of M_2/a^2; $la = 2$, $d/a = 3.0$, $h/a = 6.0$, $f/a = -1.01$ and $M_1/a^2 = 0$.

7.4 Conclusions

In the present chapter we examine the effect of inclusion of surface tension on the trapped mode. The dispersion curves for the cylinder placed in either of the layers are analyzed for different values of the interfacial surface tension. For both the cases, second mode gets affected more compared to the first mode. When the cylinder is placed in the upper layer, the second mode does not exist with an increase in interfacial surface tension. For the cylinder placed in the lower layer, the value of wavenumbers for the second mode decreases corresponding to an increase in the same surface tension parameter. Trapped mode wavenumbers are also plotted against density ratio for different values of free surface and interfacial surface tension for the cases of cylinder placed in either of the layers. For both cases, we observe that by varying both surface tension parameters, the pattern or value of wavenumbers does not change in a significant manner.

Hence it can be concluded that it is very much justifiable to ignore the effect of surface tension from the free surface or the interface as we have done for all the problems that have been considered in the previous chapters. Its inclusion will give rise to a third order boundary condition and hence will make the computation time-consuming. Even then no significant change is observed on the pattern of trapped modes and values of the frequency.

Our observation is that inclusion of surface tension at the free surface and/or the interfaces, as dictated by the problem, brings no significant change in the trapped modes. Though the problem carried out in this chapter is for a two-layer fluid flow with a free surface, similar observation is expected when the free surface be replaced by a rigid lid or an ice-cover.

Chapter 8

Summary and future work

This chapter is devoted to a brief summary of the results highlighting the contributions made by this thesis. It also provides information for the scope of possible extensions of the present work and future investigations.

8.1 Summary

In this thesis the trapping of a small amplitude harmonic surface water waves by submerged horizontal circular cylinder (cylinders) in two-layer and three-layer fluids has been investigated by using linear water wave theory.

In Chapter 2, we consider the trapped mode problem concerning a submerged cylinder entirely located within one of the layers of a two-layer fluid with both layers being of finite depth. The layers are bounded by upper and lower rigid surfaces, which are approximations of the free surface and the bottom surface, respectively, in a channel. Multipole potentials are constructed which, for frequencies less than the cut-off value, do not radiate energy away from the submerged body. These potentials, each of which satisfies all conditions except the body boundary condition, are singular on the axis of the cylinder but not in the fluid region. The trapped mode potential is then constructed from a linear combination of all possible multipoles. Application of the body boundary condition results in an infinite system of homogenous linear equations. Then the trapped mode frequencies are obtained numerically by locating the zeros of the truncated determinant. Different modes are found by fixing the depth of both the layers (d/a and h/a for lower and upper layer respectively) and also the density ratio ρ, and then by varying the submergence depth f/a. When the cylinder is placed in either of the layers, trapped mode frequency decreases with an increase in the depth of the other layer. With an increase in density ratio, trapped mode frequency increases when the cylinder is placed in the lower layer but decreases when the cylinder is placed in the upper layer.

In Chapter 3, the previous work in Chapter 2 is extended to a problem where the upper fluid is bounded above by a thin ice-cover modeled as a thin elastic plate, which replaces the free surface and the lower fluid is bounded by a rigid horizontal bottom surface. The trapped mode supported by a submerged horizontal circular cylinder placed in such type of fluid region is handled by the same multipole expansion technique. Earlier, Linton and Cadby (2003) computed the trapped mode frequencies for a cylinder placed in either layer of a two-layer fluid, in which the upper layer had a free surface and the lower layer extended to infinite

depth. It is reasonable to compare the results obtained in this chapter with the work of Linton and Cadby (2003) as both the problems bear similarities to a large extent. For a cylinder placed in the upper layer, the trapped motion is confined only to the vicinity of the ice-cover and the interface. The trapped mode wavenumbers increase due to the presence of the ice-cover on the upper surface. For the case when the cylinder is placed in the lower layer, the motion is confined to the vicinity of the interface only. As the cylinder moves towards the horizontal rigid bottom away from the interface, the trapped mode ceases to exist.

Both problems mentioned above consist of a finite depth lower layer which is bounded below by a flat, horizontal, rigid bed. But the flexibility of the bed is also a very important aspect of study which has not been accounted for in these previous investigations. The understanding of the free vibration characteristics of the fluid-structure interaction plays a significant role in various branches of engineering, for example, the propellant in space vehicles can be free from resonance, large-capacity oil containers in the petrochemical industry can survive earthquakes, very large floating oil storage tanks, ships and submarines can avoid or be subjected to reduced localized vibrations. Therefore in Chapter 4 we examine the trapped modes supported by a submerged horizontal circular cylinder placed in either layer of a two-layer fluid flowing over an elastic bottom at a finite depth. By the same procedure as was followed in Chapter 2, we look into the effect of the variations of elastic plate parameters on the existence of trapped modes. For the case of the cylinder placed in the lower layer, the presence of elastic bottom suppresses the existence of the second mode (among the two modes that exist for each wavenumber) which is a different conclusion as compared to the infinite depth lower layer. Both trapped mode wavenumbers increase due to the consideration of the elasticity of the sea-bed as compared to a flat and rigid bed.

Chapter 5 is concerned with the effect of width of the middle layer on the trapped modes due to the presence of a totally submerged cylinder placed in either the bottom layer or the uppermost layer of a three-layer fluid of infinite depth. It is observed that with an increase in the width of the middle layer, the trapped mode frequencies decrease for the case when the cylinder is placed in the lower layer. When either of the density ratios or both tend to 1, then it is not possible to recover either the two-layer or the single-layer case as is evident from the present investigation - contrary to what was concluded in Chakrabarti et al. (2005). That is, however small the width of the pycnocline may be, it still influences the trapped modes and the three-layer case cannot be considered as equivalent to the two-layer case in the limit. The presence of the middle layer in between two layers can be compared with the presence of a smooth pycnocline of constant density. The problem formulated here has the possibility of getting extended to other forms of upper surface conditions also.

Chapter 6 is concerned with the investigation of trapped water waves supported by a pair of horizontal circular cylinders submerged in either layer of a two-layer fluid in an ocean, where the upper layer is of finite depth and is bounded above by a thin ice-cover modeled as a thin elastic plate, which replaces the free surface, and the lower layer is of infinite depth. In this chapter we do not consider the trapped waves below the cut-off value but rather we consider the trapped waves which are embedded in a continuous spectrum. Hence, in addition to the multipole expansion method, the knowledge of contour integration is required to locate numerically the distance between these cylinders for which trapped wave exists. Although numerical

computation is carried out for the case of a pair of cylinders only, theoretical development is presented for the case of multiple cylinders also. Using multipole expansion method, an infinite system of homogenous linear equations is obtained with all its coefficients complex-valued. For a fixed geometrical configuration and density ratio, the existence of trapped mode frequencies is examined by numerically computing the separation parameter for which the truncated complex determinant vanishes. The variation of this separation parameter is observed by varying the values of the ice parameters, the depth of the upper layer and the submergence depth when the pair of cylinders is placed in the lower layer. The case in which the cylinders are placed in the upper layer is also considered and the distances are located for which trapped waves exist. The effect of the variation of the ice parameters on the existence of trapped modes is also looked into. For the case when the cylinders are placed entirely in the lower layer, we present numerical evidence that trapped modes do exist above the cut-off frequency for oblique waves for such a geometry. For the parameter values chosen, the number of trapped modes embedded in the continuous spectrum decreases with an increase in the flexural rigidity of the ice-cover. The trapped mode frequency decreases when either the depth of the upper layer or the submergence depth increases. This problem has the possibility of getting modified by replacing the thin ice-cover by a rigid lid.

In Chapter 7 we include surface tension at both the free surface and the interface of a two-layer fluid of finite depth. The inclusion of surface tension parameters gives rise to a third order boundary condition at the free surface and the interface. The computation of trapped mode frequencies becomes more laborious. We examine the variation of trapped modes by assuming one of the surface tension parameters to be zero and other varying. It is observed that trapped mode frequencies, when plotted against density ratio for the case of cylinder placed in either of the layers, does not get so much affected with the variation of any of the surface tension parameters. Due to the inclusion of the effect of surface tension, more computational expense occurs while locating the trapped mode frequencies and no significant change is observed. Hence, the exclusion of the effects of surface tension for all the previous problems considered in this thesis is justified.

Our findings for all problems are supported by a reasonable number of graphs depicting various modes. The present study is expected to facilitate the analysis of various physical problems in ocean engineering concerning scattering and trapping of waves besides some related areas of mathematical physics where higher-order boundary conditions arise in a natural way.

8.2 Future work

The problem pertaining to trapped waves in a two-layer fluid over horizontal bottom may further be extended to one over an uneven bed or over a porous bed. It can be assumed that the upper layer is covered by a free surface. Therefore the possible extensions for this type of problems are:

1. Oblique gravity trapped waves in a two-layer fluid due to variation in bottom topography.

2. Oblique flexural trapped waves in a two-layer fluid due to an uneven bottom.

3. The trapped water waves in a two-layer fluid in an ice-covered ocean of finite depth with a porous bottom.

For the problem mentioned in the first one, the bottom topographical variation can be modeled as two steps of different water depths with finite and infinite regions. The problem can be formulated using matched eigenfunction expansions and then a homogeneous integral equation may be used to derive the horizontal fluid velocity across the line joining the finite and infinite regions. Then by using Fourier expansion method, an infinite system of homogenous linear equations can be obtained, the vanishing of the determinant of which provides trapped mode eigenvalues if they exist. For the second one, the trapped mode can be investigated over a small bottom undulation in particular. Sinusoidal ripples on the sea-bed are of considerable significance due to the ability of an undulating bed to reflect incident wave energy which is important in respect of possible ripple growth if the bed is erodible.

In our thesis we examine the trapped modes in an infinite depth three-layer fluid with layer-wise different densities where we restrict the uppermost layer to be covered by a free surface only. Its extension to an ice-cover or a rigid lid can also be considered. The middle layer considered in this case is of constant density but it can also be extended to the case where the middle layer is linearly stratified. Hence the possible extensions in a three-layer fluid are:

1. Oblique gravity trapped waves in a three-layer fluid bounded above by a rigid lid.

2. Oblique flexural trapped waves in a three-layer fluid of finite depth.

3. The trapped water waves in a three-layer fluid in which density of the middle layer varies linearly with the width of the layer.

We consider the trapped modes arising due to the presence of the impermeable horizontal circular cylinder placed in either layer of a two-layer and a three-layer fluids. The same cylinder may be replaced by a totally submerged horizontal symmetric thin bodies or vertical cliffs placed in either of the layers. Hence the possible extensions in this regard can be:

1. Oblique gravity trapped waves in a finite depth two-layer fluid supported by a symmetric thin body.

2. Trapped waves in a two-layer fluid of finite depth supported by vertical cliffs.

We are fairly confident that these above mentioned problems can be attempted and solved with the knowledge garnered while investigating the problems in this thesis.

Bibliography

H. F. Bauer. Hydroelastic vibrations in a rectangular container. *Int. J. Solids Struct.*, 17: 639–652, 1981.

H. F. Bauer. Frequencies of a hydroelastic rectangular system. *Forsch Ingenieurwes*, 59:8–28, 1993.

J. Bhattacharjee and T. Sahoo. Flexural gravity wave problems in two-layer fluids. *Wave Motion*, 45:133–153, 2008.

J. R. Cadby and C. M. Linton. Three-dimensional water-wave scattering in two-layer fluids. *J. Fluid Mech.*, 423:155–173, 2000.

M. A. Callan, C. M. Linton, and D. V. Evans. Trapped waves in two-dimensional waveguides. *J. Fluid Mech.*, 229:51–64, 1991.

A. Chakrabarti, P. Daripa, and Hamsapriye. Trapped modes in a channel containing three layers of fluids and a submerged cylinder. *Z. Angew. Math. Phys.*, 56:1084–1097, 2005.

M. Chiba, H. Watanabe, and H. F. Bauer. Hydroelastic coupled vibrations in a cylindrical container with a membrane bottom containing liquid with surface tension. *J. Sound Vib.*, 251(4):717–740, 2002.

H. Chung and C. Fox. Calculation of wave-ice interaction using Weiner-Hopf technique. *N. Z. J. Math.*, 31(1):1–18., 2002.

D. Das and B. N. Mandal. Wave scattering by a horizontal circular cylinder in a two-layer fluid with an ice-cover. *Int. J. Eng. Sci.*, 45:842–872, 2007.

E. B. Davies and L. Parnovski. Trapped modes in acoustic waveguides. *Q. J. Mech. Appl. Math.*, 51(3):477–492, 1998.

D. V. Evans and C. M. Linton. Trapped modes in open channels. *J. Fluid Mech.*, 225:153–175, 1991.

D. V. Evans and P. McIver. Edge waves over a shelf: full linear theory. *J. Fluid Mech.*, 142: 79–95, 1984.

D. V. Evans and R. Porter. Trapped modes about cylinders in a channel. *J. Fluid Mech.*, 339: 331–356, 1997.

D. V. Evans, M. Levitin, and D. Vassiliev. Existence theorem for trapped modes. *J. Fluid Mech.*, 261:21–31, 1994.

D.V. Evans and R. Porter. Wave scattering by narrow cracks in ice sheets floating on water of finite depth. *J. Fluid Mech.*, 484:143–165, 2003.

C. Fox and V. A. Squire. On the oblique reflection and transmission of ocean waves at shore fast sea ice. *Philos. Trans. R. Soc. Lond. A*, 347:185–218, 1994.

A. Friis, J. Grue, and E. Palm. Application of Fourier transform to the second order 2D wave diffraction problem. In *M. P. Tulin's Festschrift: Mathematical Approaches in Hydrodynamics (ed. T. Miloh)*, pages 209–227. SIAM, 1991.

R. Harter, I. D. Abrahams, and M. J. Simon. The effect of surface tension on trapped modes in water-wave problem. *Proc. R. Soc. A*, 463:3131–3149, 2007.

R. Harter, M. J. Simon, and I. D. Abrahams. The effect of surface tension on localized free-surface oscillations about surface-piercing bodies. *Proc. R. Soc. A*, 464:3039–3054, 2008.

F. John. On the motion of floating bodies II. *Commun. Pure Appl. Math.*, 3:45–101, 1950.

D. S. Jones. The eigen values of $\nabla^2 u + \lambda u = 0$ when the boundary conditions are given on semi-infinite domains. *Math. Proc. Camb. Phil. Soc.*, 49:668–684, 1953.

S. E. Kassem. Multipole expansions for two superposed fluids, each of finite depth. *Math. Proc. Camb. Phil. Soc.*, 91:323–329, 1982.

S. E. Kassem. Wave source potentials for two superposed fluids, each of finite depth. *Math. Proc. Camb. Phil. Soc.*, 100:595–599, 1986.

N. Kuznetsov. Trapping modes of internal waves in a channel spanned by a submerged cylinder. *J. Fluid Mech.*, 254:113–126, 1993.

N. Kuznetsov, M. McIver, and P. McIver. Wave interaction with two-dimensional bodies floating in a two-layer fluid: uniqueness and trapped modes. *J. Fluid Mech.*, 490:321–331, 2003.

C. M. Linton and J. R. Cadby. Scattering of oblique waves in a two-layer fluid. *J. Fluid Mech.*, 461:343–364, 2002.

C. M. Linton and J. R. Cadby. Trapped modes in a two-layer fluid. *J. Fluid Mech.*, 481: 215–234, 2003.

C. M. Linton and D. V. Evans. Integral equations for a class of problems concerning obstacles in waveguides. *J. Fluid Mech.*, 245:349–365, 1992a.

C. M. Linton and D. V. Evans. The radiation and scattering of surface waves by a vertical circular cylinder in a channel. *Phil. Trans. R. Soc. Lond. A*, 338:325–357, 1992b.

A. E. H. Love. *A Treatise on the Mathematical Theory of Elasticity.* Dover Publication, New York, 2007.

W. W. Mallard and R. A. Dalrymple. Water waves propagating over a deformable bottom. In *Proceedings 9th Annual Offshore Technology Conference, Houston*, pages 141–145, 1977.

H. D. Maniar and J. N. Newman. Wave diffraction by a long array of cylinders. *J. Fluid Mech.*, 339:309–330, 1997.

M. McIver. An example of non-uniqueness in the two-dimensional linear water wave problem. *J. Fluid Mech.*, 315:257–266, 1996.

M. McIver. Trapped modes supported by submerged obstacles. *Proc. R. Soc. Lond. A*, 456: 1851–1860, 2000.

P. McIver. Complex resonances in the water-wave problem for a floating structure. *J. Fluid Mech.*, 536:423–443, 2005.

P. McIver and D. V. Evans. The trapping of surface waves above a submerged horizontal cylinder. *J. Fluid Mech.*, 151:243–255, 1985.

P. McIver and M. McIver. Trapped modes in an axisymmetric water-wave problem. *Q. J. Mech. Appl. Math.*, 50:165–178, 1997.

P. McIver and M. McIver. Trapped modes in the water-wave problem for a freely-floating structure. *J. Fluid Mech.*, 558:53–67, 2006.

P. McIver and M. McIver. Motion trapping structures in the three-dimensional water-wave problem. *J. Eng. Math.*, 58:67–75, 2007.

P. McIver, M. McIver, and J. Zhang. Excitation of trapped modes by the forced motion of structures. *J. Fluid Mech.*, 494:141–162, 2003.

S. Mohapatra and S. N. Bora. Water wave interaction with a sphere in a two-layer fluid flowing through a channel of finite depth. *Arch. Appl. Mech.*, 79:725–740, 2009a.

S. Mohapatra and S. N. Bora. Propagation of oblique waves over small bottom undulation in an ice-covered two-layer fluid. *Geophys. Astro. Fluid*, 103(5):347–374, 2009b.

S. Mohapatra and S. N. Bora. Exciting forces due to interaction of water waves with a submerged sphere in an ice-covered two-layer fluid of finite depth. *Appl. Ocean Res.*, 34:187–197, 2012.

S. C. Mohapatra and T. Sahoo. Surface gravity wave interaction with elastic bottom. *Appl. Ocean Res.*, 33:31–40, 2011.

R. Mondal and T. Sahoo. Wave structure interaction problems for two-layer fluids in three dimensions. *Wave Motion*, 49:501–524, 2012.

S. A. Nazarov and J. H. Videman. A sufficient condition for the existence of trapped modes for oblique waves in a two-layer fluid. *Proc. R. Soc. A*, 465:3799–3816, 2009.

S. A. Nazarov, J. Taskinen, and J. H. Videman. Asymptotic behavior of trapped modes in two-layer fluids. *Wave Motion*, 50:321–331, 2012.

R. Porter. Trapping of water waves by pairs of submerged cylinders. *Proc. R. Soc. Lond. A*, 458:607–624, 2002.

M. J. Simon and F. Ursell. Uniqueness in linearized two-dimensional water-wave problems. *J. Fluid Mech.*, 148:137–154, 1984.

I. V. Sturova. Problems of radiation and diffraction for a circular cylinder in a stratified fluid. *Fluid Dyn.*, 34(4):521–533, 1999.

R. Eatock Taylor and C. S. Hu. Multipole expansions for wave diffraction and radiation in deep water. *Ocean Engng.*, 18:191–224, 1991.

R. C. Thorne. Multipole expansions in the theory of surface waves. *Proc. Camb. Phil. Soc.*, 49:707–716, 1953.

F. Ursell. On the heaving motion of a circular cylinder on the surface of a fluid. *Q. J. Mech. Appl. Math.*, 2:218–231, 1949.

F. Ursell. Surface waves on deep water in the presence of a submerged circular cylinder. *Proc. Camb. Phil. Soc.*, 46:141–158, 1950.

F. Ursell. Trapping modes in the theory of surface waves. *Proc. Camb. Phil. Soc.*, 47:347–358, 1951.

F. Ursell. Mathematical aspects of trapping modes in the theory of surface waves. *J. Fluid Mech.*, 183:421–437, 1987.

G. N. Watson. *A Treatise on the Theory of Bessel Functions*. Merchant Books, New York, 2008.

Appendix A

Euler–Bernoulli equation for a thin ice-cover

Let η be the displacement of a point located at the centre of a plane in the direction of the normal to this plane, and we write

$$\kappa_1 = \frac{\partial^2 \eta}{\partial x^2}, \qquad \kappa_2 = \frac{\partial^2 \eta}{\partial y^2}, \qquad \tau = \frac{\partial^2 \eta}{\partial x \partial y}.$$

The strain–energy–function takes the form (Love (2007), Pg. 503, Eq. (6))

$$\frac{Ez^2}{2(1-\nu^2)}\Big[(\kappa_1+\kappa_2)^2 - 2(1-\nu)(\kappa_1\kappa_2 - \tau^2)\Big], \tag{A.1}$$

where E and ν, respectively, denote the effective average Young's modulus and Poisson's ratio for ice. The potential energy of bending, estimated per unit area, is obtained by integrating the above expression with respect to z from 0 to h_0, with h_0 being the thickness of the ice-cover. The integration results in the following:

$$\frac{\mathfrak{D}}{2}\Big[(\kappa_1+\kappa_2)^2 - 2(1-\nu)(\kappa_1\kappa_2 - \tau^2)\Big], \tag{A.2}$$

where $\mathfrak{D}$ is the "flexural rigidity" given by $\dfrac{E{h_0}^3}{12(1-\nu^2)}$.

The kinetic energy per unit area is $T(x,y,t) = \frac{1}{2}m\eta_t^2$, where m is the mass per unit surface area of the ice-cover. Total potential energy per unit area, $V(x,y,t)$, is the sum of the strain energy due to the curvature of the plate and the potential energy due to the transverse pressure, i.e.,

$$V(x,y,t) = \frac{1}{2}\mathfrak{D}\Big[(\nabla^2_{x,y}\eta)^2 - 2(1-\nu)(\eta_{xx}\eta_{yy} - \eta_{xy}^2)\Big] - q\eta, \tag{A.3}$$

where q is the net external force on the plate per unit area.

Let us consider a rectangular domain $R : \{(x,y) \mid 0 < x < x_0,\ y_0 < y < y_1\}$ on the plate and $T = (t_0, t_1)$ be an interval in time. Then the Lagrangian operator is

$$L(\eta) = \int_T \int_R (T - V)dx\ dy\ dt. \tag{A.4}$$

Hence the Lagrangian is

$$\mathcal{L} := \frac{1}{2}\mathfrak{D}\Big[(\nabla^2_{x,y}\eta)^2 - 2(1-\nu)(\eta_{xx}\eta_{yy} - \eta^2_{xy})\Big] - q\eta - \frac{1}{2}m\eta_t^2 \equiv \mathcal{L}(x, z, t, \eta, \eta_t, \eta_{xx}, \eta_{yy}, \eta_{xy}). \quad \text{(A.5)}$$

The corresponding Euler–Lagrange equation is

$$\frac{\partial\mathcal{L}}{\partial\eta} - \frac{\partial}{\partial x}\left(\frac{\partial\mathcal{L}}{\partial\eta_t}\right) + \frac{\partial^2}{\partial x^2}\left(\frac{\partial\mathcal{L}}{\partial\eta_{xx}}\right) + \frac{\partial^2}{\partial y^2}\left(\frac{\partial\mathcal{L}}{\partial\eta_{yy}}\right) + \frac{\partial^2}{\partial x\partial y}\left(\frac{\partial\mathcal{L}}{\partial\eta_{xy}}\right) = 0. \quad \text{(A.6)}$$

Now,

$$\begin{aligned} \frac{\partial\mathcal{L}}{\partial\eta} &= -q; \qquad \frac{\partial\mathcal{L}}{\partial\eta_t} = -m\eta_t; \qquad \frac{\partial\mathcal{L}}{\partial\eta_{xx}} = \mathfrak{D}[\eta_{xx} + \eta_{yy} - (1-\nu)\eta_{yy}]; \\ \frac{\partial\mathcal{L}}{\partial\eta_{yy}} &= \mathfrak{D}[\eta_{xx} + \eta_{yy} - (1-\nu)\eta_{xx}]; \qquad \frac{\partial\mathcal{L}}{\partial\eta_{xy}} = 2\mathfrak{D}(1-\nu)\eta_{xy}. \end{aligned}$$

Putting these values into Eq. (A.6) gives

$$\mathfrak{D}\nabla^4_{x,y}\eta + m\eta_{tt} = q, \quad \text{(A.7)}$$

where $\nabla^4_{x,y} = (\partial^4/\partial x^4) + 2(\partial^2/\partial x^2)(\partial^2/\partial y^2) + (\partial^4/\partial y^4)$ is the biharmonic operator in the plane of the ice-cover. In our case η is the displacement normal to the xy-plane at the upper surface. It is clear that Eq. (A.7) is equivalent to Eq. (3.5).

Appendix B

Coordinate shift

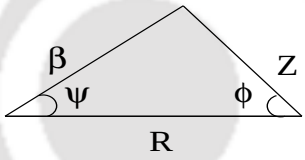

Figure B.1: Coordinate shift for Graf's addition theorem

We are required to transform $K_n(lr_j)\cos n\theta_j$, $j = 1, 2, ..., N$, where the coordinates (r_j, θ_j) associated with the j-th cylinder are measured from (h_j, f) to the coordinates (r_p, θ_p) associated with the p-th cylinder placed at (h_p, f) and vice versa. We use Graf's Addition Theorem for modified Bessel functions (Watson (2008)) given by

$$K_n(\beta)\cos n\psi = \sum_{m=-\infty}^{\infty} K_{n+m}(R)I_m(Z)\cos m\phi, \tag{B.1a}$$

$$K_n(\beta)\sin n\psi = \sum_{m=-\infty}^{\infty} K_{n+m}(R)I_m(Z)\sin m\phi, \tag{B.1b}$$

where R, β, Z are the sides of the triangle given in Fig. B.1. In the present case, the triangle has sides r_j, r_p and $|h_j - h_p|$ and so upon the following substitutions

$$\beta = lr_j; \quad \psi = \frac{\pi}{2} - \theta_j; \quad Z = lr_k; \quad \phi = \theta_k - \frac{3\pi}{2}; \quad R = l|h_j - h_p|, \tag{B.2}$$

and considering the cases $h_j > h_p$, $h_p > h_j$ separately, we have

$$K_n(lr_j)\cos n\theta_j = \sum_{m=0}^{\infty}\Big(C_{nm}^{jp}\cos m\theta_p + D_{nm}^{jp}\sin m\theta_p\Big)I_m(lr_p), \tag{B.3}$$

$$K_n(lr_j)\sin n\theta_j = \sum_{m=0}^{\infty}\Big(A_{nm}^{jp}\cos m\theta_p + B_{nm}^{jp}\sin m\theta_p\Big)I_m(lr_p), \tag{B.4}$$

where

$$A^{jp}_{nm} = \frac{\varepsilon_m}{2}\Big((-1)^m K_{n+m}(l|h_j-h_p|)+K_{n-m}(l|h_j-h_p|)\Big)\sin(n+m)\frac{\pi}{2}, \quad \text{(B.5)}$$

$$B^{jp}_{nm} = \frac{\varepsilon_m}{2}\Big((-1)^{m+1} K_{n+m}(l|h_j-h_p|)+K_{n-m}(l|h_j-h_p|)\Big)\cos(n+m)\frac{\pi}{2}, \quad \text{(B.6)}$$

$$C^{jp}_{nm} = \frac{\varepsilon_m}{2}\Big((-1)^m K_{n+m}(l|h_j-h_p|)+K_{n-m}(l|h_j-h_p|)\Big)\cos(n+m)\frac{\pi}{2}, \quad \text{(B.7)}$$

$$D^{jp}_{nm} = -\frac{\varepsilon_m}{2}\Big((-1)^{m+1} K_{n+m}(l|h_j-h_p|)+K_{n-m}(l|h_j-h_p|)\Big)\sin(n+m)\frac{\pi}{2}. \quad \text{(B.8)}$$

Using the relations $x_j = h_p - h_j + x_k$ and $z_j = z_p$ in the integral in (6.12), we obtain

$$\begin{aligned}(-1)^n & \int_0^\infty \cosh nu\ \cos(lx_j\sinh u)\ e^{vz_j}\ C_L(v)\ du \\ = & \quad (-1)^n\int_0^\infty \cosh nu\ \cos(l|h_p-h_j|\sinh u)\ \cos(lx_p\sinh u)\ e^{vz_p}\ C_L(v)\ du \\ + & \quad (-1)^{n+1}\int_0^\infty \cosh nu\ \sin(l|h_p-h_j|\sinh u)\ \sin(lx_p\sinh u)\ e^{vz_p}\ C_L(v)\ du. \quad \text{(B.9)}\end{aligned}$$

The well known generating function of modified Bessel functions is utilized (Watson (2008)):

$$\exp\Big[\frac{1}{2}X(T+T^{-1})\Big] = \sum_{m=0}^{\infty}\frac{1}{2}\varepsilon_m\Big(T^m+T^{-m}\Big)I_m(X), \quad \text{(B.10)}$$

where $\varepsilon_0 = 1$, $\varepsilon_m = 2, m \geq 1$. Substituting $X = -lr_p$, $T = \exp[i(\theta_p + iu)]$ in it and equating real and imaginary parts, the following results are obtained:

$$e^{vz_p}\ \cos(lx_p\sinh u) = e^{vf}\sum_{m=0}^{\infty}(-1)^m\ \varepsilon_m\ \cosh mu\ I_m(lr_p)\ \cos m\theta_p, \quad \text{(B.11)}$$

$$e^{vz_p}\ \sin(lx_p\sinh u) = e^{vf}\sum_{m=0}^{\infty}(-1)^{m+1}\ \varepsilon_m\ \sinh mu\ I_m(lr_p)\ \sin m\theta_p. \quad \text{(B.12)}$$

Using the above relations in (B.9), we obtain

$$(-1)^n\int_0^\infty \cosh nu\cos(lx_j\sinh u)e^{vz_j}C_L(v)\ du = \sum_{m=0}^{\infty}\Big[\alpha^{jp}_{nm}\cos m\theta_p + \beta^{jp}_{nm}\sin m\theta_p\Big]I_m(lr_p), \quad \text{(B.13)}$$

with

$$\alpha^{jp}_{nm} = (-1)^{m+n}\varepsilon_m\int_0^\infty \cosh nu\ \cosh mu\ \cos(l|h_p-h_j|\sinh u)\ e^{vf}\ C_L(v)\ du, \quad \text{(B.14)}$$

$$\beta^{jp}_{nm} = (-1)^{m+n}\varepsilon_m\int_0^\infty \cosh nu\ \sinh mu\ \sin(l|h_p-h_j|\sinh u)e^{vf}\ C_L(v)\ du. \quad \text{(B.15)}$$

Similarly, for the integral in (6.14), we get

$$(-1)^{n+1}\int_0^\infty \sinh nu\ \sin(lx_j\sinh u)\ e^{vz_j}\ C_L(v)\ du = \sum_{m=0}^{\infty}\Big[a^{jp}_{nm}\cos m\theta_p + b^{jp}_{nm}\sin m\theta_p\Big]I_m(lr_p), \quad \text{(B.16)}$$

with

$$a_{nm}^{jp} = (-1)^{m+n+1}\varepsilon_m \int_0^\infty \sinh nu \, \cosh mu \, \sin(l|h_p - h_j| \sinh u) \, e^{vf} \, C_L(v) \, du, \quad \text{(B.17)}$$

$$b_{nm}^{jp} = (-1)^{m+n}\varepsilon_m \int_0^\infty \sinh nu \, \sinh mu \, \cos(l|h_p - h_j| \sinh u) \, e^{vf} \, C_L(v) \, du. \quad \text{(B.18)}$$

These are the results used in Chapter 6 for shifting local coordinates from any arbitrary cylinder j to a fixed cylinder p.

List of published and communicated papers

Based on the work carried out in this thesis, the following published and communicated papers have resulted:

1. S. Saha and S.N. Bora, "Trapped modes in a two-layer fluid of finite depth bounded above by a rigid lid", *Wave Motion*, 50, (2013), 1050–1060, (DOI: 10.1016/j.wavemoti.2013.04.009).

2. S. Saha and S.N. Bora, "Flexural gravity waves trapped in a two-layer fluid of finite depth", *Applied Ocean Research*, 44, (2014), 1–12, (DOI:10.1016/j.apor.2013.08.005).

3. S. Saha and S.N. Bora, "Trapped waves supported by a pair of cylinders in an ice-covered two-layer fluid", *Communicated*.

4. S. Saha and S.N. Bora, "Trapped modes in a three-layer fluid", *Revised version submitted to IMA Journal of Applied Mathematics*.

5. S. Saha and S.N. Bora, "Elastic bottom effect on trapped waves in a two-layer fluid", *Communicated*.

6. S. Saha and S.N. Bora, "Surface tension effect on trapped modes in a finite depth two-layer fluid", *Revised version under preparation for submission to ANZIAM Journal*.